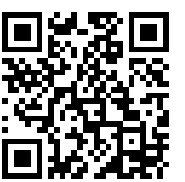

Massachusetts institute of technology. Dept. of electrical engineering. Contributions. no.15-19

Apparent Dielectric Strength of Varnished Cambric

A. E. KENNELLY and R. J. WISEMAN

Reprinted from Electrical World
December 15, 1917

Research Division
Electrical Engineering Department
Massachusetts Institute of Technology
Bulletin No. 15 January 1918

Apparent Dielectric Strength of Varnished Cambric

By

A. E. Kennelly and R. J. Wiseman

Reprinted from

Elcctrical World, December 15, 1917

Reprinted from Electrical World, December 15, 1917

Apparent Dielectric Strength of Varnished Cambric

Its Diminution with Increase of Electrode Diameter Associated with Metallic Structure of Electrode and Possibly Due to High-Frequency Oscillations—Necessity of Standardizing Size of Test Electrodes

BY A. E. KENNELLY AND R. J. WISEMAN

USING varnished cambric 0.3 mm. (0.012 in.) thick between flat metallic-disk electrodes, F. M. Farmer[1] has found that the apparent dielectric strength, in volts per unit thickness, diminishes more than 50 per cent in changing from disks of very small diameter to disks of 15 in. (38 cm.) diameter. In other words, increasing the area of the applied disk electrodes without altering the thickness of the insulating material diminishes greatly the apparent dielectric strength. The same phenomenon was also shown to be present, in varying degrees, with insulating films of hard rubber, oil and air.

In the discussion of Mr. Farmer's paper on this subject the consensus of opinion was in favor of attributing the apparent relative weakness of large plates to the probability of weak spots in the cambric. That is, admitting that a cambric sheet cannot have exactly the same dielectric strength at all points, if only on account of accidental variations in thickness, it must follow that a large-disk electrode is more likely to cover a weak spot than a small electrode and thus will break down the dielectric at a lower impressed voltage.

Although the above weak-spot argument cannot be denied, it is difficult to say how much of the observed falling off in the dielectric strength of large sheets is attributable to it. If all of the diminution with increase in electrode size were due to weak spots, then similar tests of oil films or air films should reveal no such diminution, because weak spots can hardly occur in homogeneous fluid media. However, Mr. Farmer's paper showed marked diminutions toward large diameters both with oil and air films.

[1] "The Dielectric Strength of Thin Insulating Materials," *Transactions A. I. E. E.*, Vol. 32, p. 2097, December, 1913.

The problem of diminution in the apparent dielectric strength of cambric between flat-disk electrodes of increasing size was also studied at the Massachusetts Institute of Technology in 1913-14 by L. H. Webber, who repeated a number of Mr. Farmer's observations and confirmed them in essential particulars.

Influence of Oil Immersion on Cambric

The subject was further investigated at the Massachusetts Institute of Technology in 1914-15 by G. Y. Fong, who again confirmed Mr. Farmer's observations on varnished cambric. It was further found that when the cambric was first immersed in transformer oil and then placed between opposed parallel disk electrodes, the falling off in dielectric strength between 1.3-cm. (½-in.) and 10-cm. (4-in.) electrodes was distinctly less than when the cambric was immersed in atmospheric air. When the tests were made on linseed-oil-soaked cambric, the apparent dielectric strength was substantially uniform for all sizes of disk electrodes between 1.3 cm. and 25 cm. (½ in. and 9.8 in.). When the tests were made on castor-oil-soaked cambric the apparent dielectric strength actually increased slightly when the disk diameter was increased.

Later it was found that the results with linseed oil, and especially with castor-oil-soaked cambric, were not reliable, owing to the viscosity of these oils. That is, when specimens were tested between large disks it was very difficult to squeeze out the excess oil, and the thickness of the test substance was actually increased by the layers of unexpelled oil. All that can be claimed, therefore, is that when air is replaced by oil as the medium immersing the cambric, there is less falling off in apparent dielectric strength where larger sizes of electrodes are used.

Investigations of Dielectric Strength with Multiple Electrodes

More extensive investigation of the whole subject was permitted in the research division of the M. I. T. electrical engineering department in July, 1915, by an appropriation from the American Telephone & Telegraph Company, the experimental work being conducted by Dr. R. J. Wiseman.

After checking the results obtained by Mr. Farmer with cambric, tests were made with a number of small-disk electrodes of equal size, electrically connected into a "multiple electrode," as is indicated in Fig. 3. The lower electrode consisted of a single metallic disk,

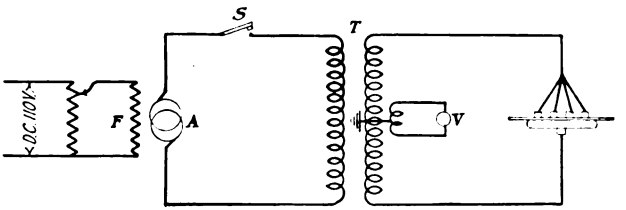

FIG. 1—CONNECTIONS USED IN TESTING DIELECTRIC STRENGTH OF VARNISHED CAMBRIC

A is a motor-driven 220-volt, 20-kva. alternator, operated at constant speed and frequency (60 cycles) by a direct-connected motor not shown. The voltage at the armature terminals is controlled by a drop-wire rheostat connected to 110-volt direct-current mains on one side and to the alternator field magnets on the other. In all of the tests the drop-wire rheostat was so operated as to raise the voltage at the rate of approximately 1000 r.m.s. volts per second. The high-tension transformer *T* has a rating of 10 kva., at 50,000 r.m.s. volts on the secondary. A tertiary coil in the transformer is connected to a voltmeter calibrated to show the voltage at secondary terminals. The centers of both secondary and tertiary coils are grounded. Short leads extend from the secondary terminals to the horizontal electrodes on the test specimen. The voltmeter *V* is fairly dead-beat in its indications and is read at the instant of first discharge, which is revealed not only by the sound of the rupture spark but also by the sudden falling of the voltage. A foot switch *S*, in the primary circuit, is then immediately opened so as to extinguish the arc. The voltages supplied by the generator were almost purely sinusoidal throughout all the tests.

as before, and this supported the cambric test sheet. On the test sheet rested the multiple electrode of small metallic disks, all connected by flexible fine copper wires about 40 cm. (15.7 in.) long. Each individual small disk had a length of 1.2 cm. (0.47 in.) and a diameter of 1.2 cm. (0.47 in.), and its edge was slightly rounded. The number of these little disks forming the multiple electrode was varied in different tests from one up to sixteen, corresponding in total active area to that of a single-disk electrode from 1.2 cm. up to 4.8 cm. (0.47 in. to 1.9 in.) in diameter.

The connections used in the tests are shown in Fig. 1. Ten observations, made in rapid succession and occupying about ten minutes, constitute a test. After the series is completed the thickness of each sample is measured, by a micrometer, close to the point of rupture. The arithmetical mean of the ten thicknesses so

measured is taken as the mean thickness of the cambric. The arithmetical mean of the ten breakdown voltages, after each has been corrected for the thickness of the corresponding test piece, is taken as the mean breakdown voltage for the mean thickness of

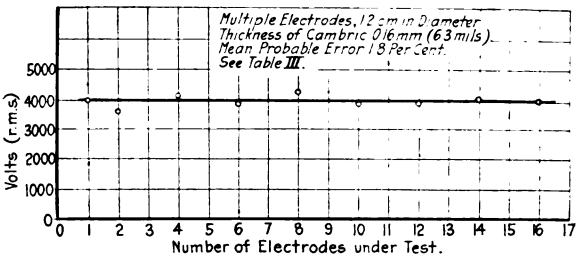

FIG. 2—CHANGE IN PUNCTURING VOLTAGE OF VARNISHED CAMBRIC, WITH NUMBER OF ELECTRODES USED IN MULTIPLE

the series. The probable error of both the mean voltage and the mean thickness is recorded[1] with the test. It is customary to find the probable error of mean voltage to be about 1.5 per cent, and the probable error of mean thickness to be about 1 per cent.

TABLE I—TEN OBSERVATIONS OF THE PUNCTURING VOLTAGE OF VARNISHED CAMBRIC BETWEEN A PARTICULAR SET OF METALLIC ELECTRODES*

No.	Observed R.M.S. Puncturing Emf. (Volts)	Thickness of Sample (Mm.)	Voltage Corrected to Mean Thickness
1	6110	0.155	6360
2	5860	0.162	5840
3	5990	0.163	5920
4	6360	0.155	6610
5	5990	0.161	5990
6	6110	0.164	6030
7	5740	0.169	5450
8	6240	0.162	6210
9	6360	0.153	6720
10	6360	0.169	6050
		Mean 0.1613 (1 ±0.0075)	6118 (1 ±0.013)

*Conditions of test: Lower electrode, a solid steel disk 10.2 cm. in diamete r upper electrode, thirteen small brass cylinders each 1.1 cm. in diameter and 1.1 cm. long, held in same plane by a perforated hard-rubber base. Medium surrounding the cambric, air. Temperature, 26 deg. C. Frequency, 60 cycles

[1]See Tables II and III.

In order to maintain a substantially uniform electric field between opposite disk electrodes, it was found that it was necessary to have the gap not exceed 5 per cent of the electrode diameter. This ratio was determined experimentally with films of air by observing the marks left by the discharges on the electrode disks. The marks began to concentrate perceptibly toward the centers of the disks when the gap exceeded 5 per cent of the diameter. Consequently, in order to eliminate effects due to non-uniformity of electric field, all of the observations here presented are limited to electrode diameters which are more than twenty times the thick-

TABLE II—COMPARATIVE MEAN PUNCTURING VOLTAGES WITH SINGLE DISK ELECTRODES

(Diameters between 1.2 cm. and 25.4 cm.; varnished cambric 0.16 mm. thick; surrounding medium, air; ten observations to each series)

Diameter		Surface Area (Sq. Cm.)	Mean R.M.S. Puncturing Voltage (V)	Apparent Dielectric Strength Volts per Mm. V/S
(In.)	(Cm.)			
0.47	1.2	1.13	7,350 (1 ± 0.016)	45,900
2.0	5.1	20.4	6,570 (1 ± 0.0074)	41,100
4.0	10.2	81.6	5,620 (1 ± 0.0079)	35,100
6.0	15.2	181.4	5,350 (1 ± 0.020)	33,400
8.0	20.3	324.0	5,500 (1 ± 0.015)	34,400
10.0	25.4	506.0	5,090 (1 ± 0.027)	31,800

ness of cambric. In fact, diameters of less than 1 cm. (0.39 in.) have not been used. Limiting the minimum diameter to 1 cm. (0.39 in.) has the further advantage of obtaining a more representative sample of the test sheet. Mr. Farmer, as pointed out in his 1913 paper, carried the minimum electrode diameter to much lower values, and even to needle points, for the purpose of more comprehensive comparison. Reducing the limits of diameters in Mr. Farmer's paper to, say, 1.1 cm. and 5.1 cm. (0.47 in. and 2 in.), to permit comparison with results reported here, it appears that the diminution in apparent dielectric strength reported by Mr. Farmer was from 1120 volts per mil to 970 volts per mil, or 13.4 per cent, which agrees very closely with recent results.

Results with Multiple Electrodes

When multiple electrodes, like the one shown in Fig. 3, replaced solid single-disk electrodes, the diminution of apparent dielectric strength with increasing area largely disappeared. That is to say, if the increase in area of the electrodes was from 1.13 sq. cm. to 18.1 sq. cm. (0.175 sq. in. to 2.81 sq. in.), by changing the diameter from 1.2 cm. to 4.8 cm. (0.47 in. to 1.8 in.), the puncturing voltage fell off more than 13 per cent; whereas when the same increase in area was effected

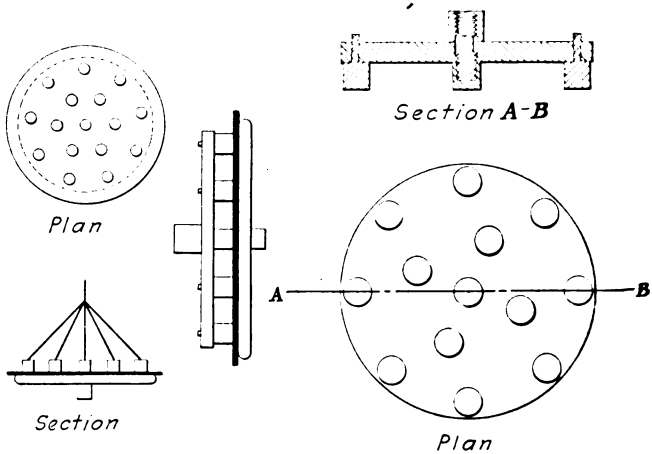

FIGS. 3, 4 AND 5—SECTIONS THROUGH TWO TYPES OF MULTIPLE-DISK ELECTRODES USED IN TESTS

by multiple electrodes (sixteen electrodes each of 1.13 sq. cm.) the puncturing voltage fell off only about 1 per cent. This remarkable result was independently checked both at the M. I. T. laboratory in Cambridge and at the Electrical Testing Laboratories of New York. This result was checked in various ways, and it controverts the weak-spot theory of the diminution, because there should be as great a probability of encountering a weak spot under 18 sq. cm. (2.79 sq. in.) of a solid disk as under 18 sq. cm. of a multiple electrode.

The results obtained with a multiple electrode of varying number of disks are shown in Fig. 2, each circle representing the arithmetical mean value of a series of ten observations of puncture on different

samples of the same cambric sheet. Similar results were obtained with multiple electrodes on both sides of the test sheet.

The reasons for the above remarkable disparity between the results with single and multiple electrodes baffled investigation for a long time. A hint toward the solution was found, however, when tests were made

TABLE III—COMPARATIVE MEAN PUNCTURING VOLTAGES*

(Lower disk electrode, 25.4 cm. in diameter, and upper electrode, consisting of a selected number of 1.2-cm. disk electrodes in multiple,† for varnished cambric 0.16 mm. thick; surrounding medium, air; ten observations to each series)

Number of Electrodes	Equivalent Diameter of Single Electrode Cm.	Total Surface Area of Multiple Electrode Sq. Cm.	Mean R.M.S. Puncturing Voltage (V)	Apparent Dielectric Strength, Volts per Mm. V/S
1	1.2	1.13	3,920 (1 ± 0.015)	24,500
2	1.7	2.26	3,580 (1 ± 0.033)	22,400
4	2.4	4.52	4,100 (1 ± 0.025)	25,600
6	2.94	6.78	3,810 (1 ± 0.018)	23,800
8	3.39	9.04	4,130 (1 ± 0.010)	25,800
10	3.8	11.3	3,810 (1 ± 0.021)	23,800
12	4.15	13.56	3,860 (1 ± 0.0089)	24,100
14	4.48	15.82	3,920 (1 ± 0.0086)	24,500
16	4.8	18.08	3,890 (1 ± 0.020)	24,300

*See Fig. 2. †See Fig. 3.

with a multiple electrode of thirteen disks, each 1.2 cm. in diameter and 1.2 cm. long (0.47 in. by 0.47 in.) clamped in a perforated brass frame, 10 cm. (3.9 in.) in diameter, so as to form virtual projections from its surface. A section of this electrode, through the axis, is given in Fig. 4. The diminution in puncturing voltage in passing from one disk to sixteen with this multiple electrode was found to be greater than for the single disk of equivalent active surface. This showed that the diminution in apparent dielectric strength with increasing area was associated in some way with the metallic structure of the electrode. The same increase in surface with separated small disks gave very little diminution, whereas when obtained either in a solid disk or in a metallically framed set of small disks the diminution was large. Special series of tests showed that the weight or mechanical pressure on the upper electrode did not appreciably affect the results.

A hard-rubber base or connecting frame was then substituted for the brass base, as shown in section by Fig. 5. The small-disk electrodes were screwed into the rubber base and then ground to a flat testing surface. The disks were connected electrically to a common main terminal by a corresponding number of fine enameled copper wires of 0.25 mm. (0.00985 in.) diameter, each 40 cm. (15.7 in.) long. The tests with this electrode showed a diminution of 5.8 per cent in apparent puncture voltage between one and sixteen electrodes (1.13 sq. cm. to 18.1 sq. cm.).

When the tests were repeated with the disks directly connected by very short copper wires of the same diameter, the diminution mounted to 10.8 per cent. In other words, changing the length of the fine connecting wires between the elements of the multiple electrode from 40 + 40 cm. to 2 cm. changed the diminution from 5.8 to 10.8 per cent. These results, which are presented in the first column of Table IV, were communicated to the Electrical Testing Laboratories, where Mr. Farmer repeated the tests, using the same electrodes. The varnished cambric used for the check tests was, however, not just the same as that which had been employed originally. The results of the check tests are given in columns 2, 3 and 4 of Table IV, and their arithmetical means in the last column. Each entry represents the mean of twenty observations at successive breakdowns made in the same way.

It will be seen that although the numerical values of the percentage reductions of breakdown voltage for the different conditions enumerated are by no means the same, yet there is a general qualitative agreement and check between the results in the two laboratories. Furthermore, there is no difference of opinion as to the main facts, namely, that when the electrode forms an electrically solid mass the dielectric-strength diminution is large, while, on the contrary, as the elements of the multiple electrode are separated electrically, without altering the total active surface, the diminution tends to disappear.

The results suggest that the diminution in apparent dielectric strength may possibly be due to high-frequency electric oscillations set up across the dielectric, with the electrodes forming a pair of parallel

oscillators. When the diameter of the disk electrodes is increased the oscillating system becomes enlarged, so that its free oscillations would be lowered in frequency but would be increased in amplitude. Under the influence of such oscillations, the air pocketed between

TABLE IV—COMPARATIVE DIMINUTION IN MEAN PUNCTURING VOLTAGE FOR VARNISHED CAMBRIC

(Upper electrode areas from 1.1 sq. cm. to 18 sq. cm. in different arrangements; surrounding medium, air)

	M.I.T.	Electrical Testing Laboratories			Mean E.T.L
	1	2	3	4	5
Thickness of cambric, mm	0.16	0.15	0.15	0.3	....
Thickness of cambric, mils	6.3	6	6	12	....
Mean breakdown voltage, approximate kv.	7	3	3	13	....
Types of Upper Electrode	Percentage Diminution				
1. Solid disk	13.3	12.2	21.5	10.7	14.8
2. Multiple electrodes held in metallic base. (Fig. 4)	15.4	4.7	20.0	9.4	11.3
3. Multiple electrodes held in hard-rubber base with short connecting wires	10.8	14.2	2.5	8.7	8.5
4. Multiple electrodes held in hard-rubber base with thin connecting wires 40 cm. long. (Fig. 5)	5.8	3.1	7.7	5.4	5.4
5. Separated multiple electrodes with long, thin connecting wires and without a connecting frame. (Fig. 3)	1.0	0	....	....	0

the electrodes and the surfaces of the cambric sheet may be ionized and forcibly impelled against the dielectric in such a manner as to weaken it rapidly. Moreover, the larger the area of the single-disk electrodes the more likely are these air pockets to present themselves, owing to slight irregularities in the thickness of the cambric. When multiple electrodes are used, with the elements spread out and interconnected by long fine wires, less opportunity is offered for the formation of air pockets and for the high-frequency oscillations to develop an appreciable intensity. The disruptive power of high-frequency oscillations in dielectrics, under the influence of ionized air, is well known.

When oil was used as the medium surrounding the electrodes and test cambric, the diminution in apparent dielectric strength with increase in area was always less than with air.

Investigations with Other Than Brass Electrodes

A further trial was made with electrodes of leadfoil 0.013 mm. (0.000512 in.) thick, both single and multiple. When a single leadfoil sheet was laid on the cambric test piece and pressed down by a glass plate, the diminution in apparent dielectric strength with increase in area was considerable, although not so marked as when a single electrode disk of metal 4 mm. (0.157 in.) thick was employed. Slits were then cut in the leadfoil electrode so as to subdivide its surface into parallel strips connected at one end. This subdivision lowered the diminution to about 2 per cent between the limits 1.1 sq. cm. and 18.1 sq. cm. (0.17 and 2.81 sq. in.) total area, thus corroborating the multiple-electrode test. Incidentally, the application of the high-voltage test caused the leadfoil electrode, or electrodes, to adhere to the test sheet of cambric so closely as to make separation without injury difficult. This adhesive property of leadfoil electrodes may have practical applications.

Fluid mercury electrodes about 2 mm. (0.0788 in.) thick have been tried over the cambric test sheet in place of solid single metallic disks, but without material change in the observed results. That is to say, the diminution in break-down voltage with area was substantially the same as with brass disks. The mercury electrodes were kept in the form of circular disks by means of encircling wooden frames.

Although the above-mentioned observations seem to suggest the existence of very high-frequency oscillations, of the order perhaps of many millions per second, as the principal cause of the diminution in the apparent dielectric strength of cambric sheets with increasing area, yet it must be noted that there has been no direct evidence available to indicate the existence of such high-frequency oscillations.

As an inference from the experiments, whatever opinion may be entertained concerning the ultimate cause of the diminution of apparent dielectric strength with increase in size of metallic-disk electrodes, it is evident that the size used should be standardized. If the electrodes are too small, the electric field between them will not be uniform and the sample of the dielectric test piece will not be sufficiently representative.

If the electrodes are too large, the apparent dielectric strength will be unduly small. For practical purposes it is suggested that electrode disks 1 cm. (0.4 in.) in diameter may be used, if the thickness of cambric does not exceed 0.5 mm. (0.0197 in.).

The authors desire to acknowledge their indebtedness to the American Telephone & Telegraph Company for the appropriations under which the research has been carried on, and also to Profs. D. C. Jackson and C. A. Adams, as well as to W. I. Middleton, for valued suggestions. They are especially under obligations to the Electrical Testing Laboratories of New York and F. M. Farmer, the chief engineer, for the execution of the check tests, to which reference has already been made, and for permission to incorporate the results of those tests in this paper.

EDITORIAL COMMENT.

WHEN a condenser is formed by two parallel opposed conducting surfaces, such as a pair of flat brass disks separated by a film of air, the electric field between them, when the disks are electrically displaced in potential, is theoretically strongest at the center and diminishes radially outward toward the edges. If, however, the air gap or air-film thickness is less than 5 per cent of the disk diameter, and also if the edges of the disks are slightly rounded, the electric field becomes substantially uniform at all points between the disks. Experiment shows that with the disk faces set fairly parallel to each other in air, the disruptive discharges of successive electric breakdowns are then distributed substantially according to the ordinary laws of accidental errors, the pattern formed by the marks, on the disk surfaces, of the successive spark discharges showing no tendency to crowd at any point.

If, then, a uniform electric field is produced, its intensity should be directly proportional to the impressed voltage between the disks and inversely proportional to the air gap, while the area of the disk electrodes should have no appreciable effect on the dielectric

strength of the air film, so long as the thickness of the film is less than 5 per cent of the disk diameter. In other words, the dielectric breakdown voltage of an air film of given thickness, say 0.3 mm., should be the same whether the disk diameters are 2 cm. or 5 cm. The same proposition of dielectric strength independent of the area should likewise apply to flat films of other dielectrics such as oil and varnished cambric.

It was pointed out, however, in a paper by F. M. Farmer, read before the A. I. E. E. in 1913, that the apparent dielectric strength of flat films of air, oil and varnished cambric differed very appreciably with the diameter of the disk electrodes used in the test. The larger the disk the lower the breakdown voltage. There was some difference of opinion expressed, in the discussion following the paper, as to the origin of these variations in apparent dielectric strength; but it was supposed that, at least in the case of varnished cambric, which is necessarily composite in structure and liable to vary somewhat in thickness, the experimental facts might be explained on the basis of accidental weaker spots in the dielectric, so that a large area of electrode would probably cover and include more weak spots and so permit of a lower breakdown voltage.

We are printing this week an interesting article by A. E. Kennelly and R. J. Wiseman on this subject. Their experimental results indicate that in varnished cambric the breakdown voltage diminishes with the diameter in substantially the same manner as Mr. Farmer's original paper showed, but that the diminution in breakdown voltage does not depend upon the area of the electrodes. It appears that the area can be increased over a considerable range without any material diminution in apparent breakdown voltage, provided that the area is electrically broken up into elements separated by wires. This very remarkable experimental result has been checked through tests by other observers, and with other instruments, at the Electrical Testing Laboratories of New York.

The reasons for this experimental result have not

yet been cleared up. It is suggested that under the application of an alternating emf., free electric oscillations in the condenser may perhaps be set up from one part to another. If so, the oscillations must have extremely high frequency, with a wave length perhaps measured in decimeters. High-frequency currents are indeed known to possess highly destructive powers on insulating materials, especially in the presence of ionizable gas. However, direct experimental evidence of the presence of such oscillations will be required before we can safely accept this explanation. There is a fine opportunity here for the work of experimental physicists —one of which we hope to see them take advantage.

Reprinted from Electrical World, December 15, 1917

LIST OF RESEARCH BULLETINS

Bulletin Number

*1. The Economical Transportation of Merchandise in Metropolitan Districts. H. Pender and H. F. Thomson; March, 1912.

*2. Notes on the Cost of Motor Trucking. H. Pender and H. F. Thomson; October, 1912.

*3. Observations on Horse and Motor Trucking. H. Pender and H. F. Thomson; March, 1913.

*4. Relative Fields of Horse, Electric and Gasoline Trucks. H. F. Thomson; August, 1914.

*5. The Delivery and Handling of Miscellaneous Freight at the Boston Freight Terminals. H. Pender, H. F. Thomson, and C. P. Eldred; February, 1914.

6. The Delivery System of R. H. Macy & Co. of New York. H. F. Thomson, H. L. Manley, and A. L. Pashek; September, 1914.

7. Explorations over the Vibrating Surfaces of Telephonic Diaphragms under Simple Impressed Tones. A. E. Kennelly and H. O. Taylor; April, 1915.

8. The Mechanics of Telephone-Receiver Diaphragms as Derived from their Motional-Impedance Circles. A. E. Kennelly and H. A. Affel; November, 1915.

9. Experimental Researches on Skin Effect in Conductors. A. E. Kennelly, F. A. Laws, and P. H. Pierce; September, 1915.

10. Tractive Resistances to a Motor Delivery Wagon on Different Roads and at Different Speeds. A. E. Kennelly and O. R. Schurig; June, 1916.

11. Some Properties of Vibrating Telephone Diaphragms. A. E. Kennelly and H. O. Taylor; April, 1916.

12. Experimental Researches on the Skin Effect in Steel Rails. A. E. Kennelly, F. H. Achard, and A. S. Dana; August, 1916.

13. Skin-Effect Resistance Measurements of Conductors at Radio-Frequencies up to 100 000 Cycles per Second. A. E. Kennelly and H. A. Affel; December, 1916.

* Out of print.

Bulletin Number

14. Street Railway Fares; their relation to length of haul and cost of service. D. C. Jackson and D. J. McGrath; August, 1917.

15. Apparent Dielectric Strength of Varnished Cambric. A. E. Kennelly and R. J. Wiseman; January, 1918.

Magnetic Flux Distribution in Annular Steel Laminae

A. E. KENNELLY and P. L. ALGER

Report of an Investigation Read before the American Institute of Electrical Engineers at their 335th Meeting, at New York, December 14, 1917

Research Division
Electrical Engineering Department
Massachusetts Institute of Technology
Bulletin No. 16 March 1918

To be presented at the 335th Meeting of the American Institute of Electrical Engineers, New York, December 14, 1917.

(Subject to final revision for the Transactions.)

MAGNETIC FLUX DISTRIBUTION IN ANNULAR STEEL LAMINAE

BY A. E. KENNELLY AND P. L. ALGER

ABSTRACT OF PAPER

The distribution of alternating magnetic flux density in ring laminae is studied experimentally. It is found to differ materially at different radii, not only in root-mean-square magnitude, but also in wave form. The reasons for this distortion are discussed.

IT IS well known that when a circular steel lamina, of the simple geometrical form shown in Figs. 1 and 4, is subjected to a circumferential alternating m.m.f., by the application of a ring winding, the magnetic flux density in the lamina is not constant over the cross section, but varies with the distance from the midplane. The flux density is greatest at the surfaces and is a minimum at the midplane, owing to what is commonly called "skin effect," or magnetic screening due to superficial eddy currents. This variation of flux density may be called "depth variation." The experiments here reported were undertaken to ascertain whether the flux density in the plane of the lamina likewise varied. If "edge effect" were present, the flux density would be greatest at the inner and outer edges, and would reach a minimum at the mid radius. Such variations of flux density may be called "radial variations." The experiments have shown that there is a very marked radial variation of flux density in such laminae, and also a very marked difference in the wave form of alternating magnetic flux density at different radial belts; but these variations are to be attributed, for the most part, to variations in the permeability μ of the metal under the different values of $\mathfrak{H}$ at the different radii, the "edge effect" or lateral magnetic screening being small in comparison therewith.

The m.m.f. of the ring winding has of course one and the same value in all of the circumferential belts. The same ampere turns or gilberts act on the outer edge as on the inner edge. The gilberts per cm. are therefore less at the outer than at the inner edge. This excess of magnetic intensity $\mathfrak{H}$ towards the inner edge

Manuscript of this paper was received October 25, 1917.

tends to create a greater flux density at that edge. But the permeability varies with $\mathfrak{H}$ in such a manner that the crowding at the inner edge is exaggerated for low magnetic densities. Moreover, the wave form of the alternating magnetic flux is considerably distorted at the edges from that of the total flux in the lamina.

These distortions of radial flux density, although very striking, are not entirely new. Kapp has called attention to the fact that the mean flux density in the laminated core of a dynamo armature, obtained by dividing the total flux by the armature cross section, is not the same as the arithmetical mean of the flux densities at the inner and outer radii.[1] Niethammer[2] has also computed the flux densities at different radii of a laminated ring transformer, and has pointed out that at low average densities, the distribution, with a permeability assumed constant, must be

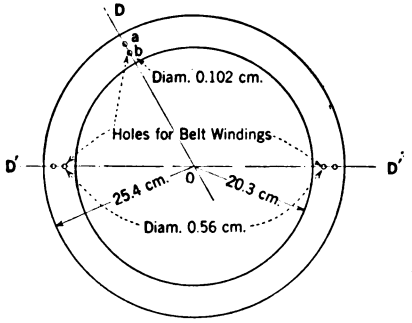

FIG. 1—SILICON STEEL LAMINA

markedly different from that with permeability varying with $\mathfrak{H}$ in the ordinary way. So far as we are aware, however, the matter has not been investigated experimentally, and the necessarily accompanying distortion in magnetic wave form has not been noticed or referred to.

Laminae Tested. The laminae were annular stampings of high-silicon steel. The external diameter of these stampings was 50.8 cm. (20 in.), the internal diameter was 40.6 cm. (16 in.) and their thickness 0.355 mm. (0.014 in.). These were standard blank stampings of best grade transformer steel. The material is characterized by high resistivity (52000 absohm-cm.), with a

1. Dynamomaschinen für Gleich-und Wechselstrom, 3rd Edition, p. 254, by G. Kapp.

2. Sammlung Elektrotechnischer Vorträge, Vol. II, Part 11-12. Magnetism, pp. 10-12, by F. Niethammer.

low temperature coefficient of the same, and a high initial permeability.

A laminated core was made up of 25 of the above stampings, using an insulating layer of paper 0.076 mm. (0.003 in.) between laminae. The resulting core had an average thickness of 1.2 cm. (0.47 in.) The weight of steel in the core was 4.78 kg. (10.5 lb.)

As is indicated in Fig. 1, small holes *a*, *b*, were drilled through the core, in a diametral line *O D*, and perpendicular to the plane of the laminae. The diameter of each hole was 1.02 mm. (0.040 in.) Figure 2 gives in greater detail the distances between these holes, and the edges of the core. The object of the holes was to divide the core radially into three concentric annular belts,

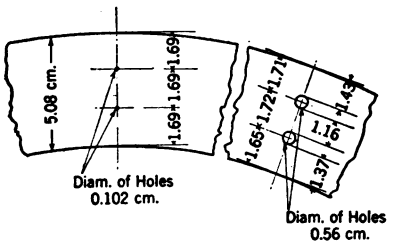

FIG. 2—SHOWING POSITIONS OF HOLES FOR BELT WINDINGS

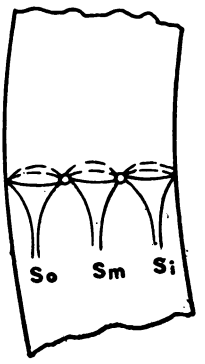

FIG. 3—BELT WINDINGS

the magnetic flux in each of which could be separately determined by the aid of suitable windings through the holes. Four fine insulated copper wires were passed through each hole to form a winding of two turns (Fig. 3) around each annular belt. By the use of a Drysdale-Tinsley potentiometer, the voltage induced in these two-turn windings could be measured at all the frequencies employed. In order, however, to obtain oscillograms of the induced alternating-voltage wave forms, it was found necessary to employ windings of more numerous turns, and two sets of larger holes (diam. 5.6 mm. or 0.22 in.) to receive these windings, were drilled on another diametral line *D' D'*, as shown in Fig. 1. Twenty turns were used in these larger belt windings.

A primary single-layer winding was distributed around the core, consisting of 450 turns of d.c.c. copper wire No. 19 A. W. G.

(bare diam. 0.91 mm.) divided into six coils *aa'*, *bb'*, Fig. 4, averaging 75 turns each. In addition, two secondary coils *cc'*, *cc'*, of 75 turns each, were applied at diametrically opposite sectors, around all the laminae forming the core.

The sources of primary impressed voltage were two three-phase alternators, specially designed by Prof. C. A. Adams, to deliver a close approximation to a sinusoidal wave. One of these generators was used up to a frequency of 100 ~, and the other for frequencies from 100 ~ to 800 ~. The electrical connections are indicated in Fig. 4.

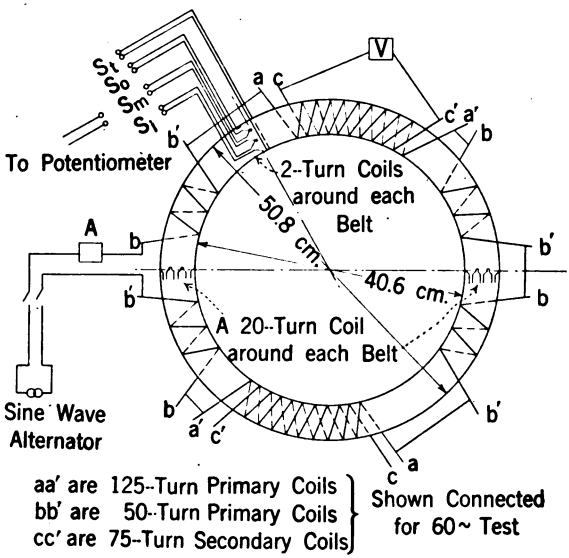

FIG. 4

METHODS OF TESTING

A-C. Tests. The method of testing by alternating currents consisted in impressing a sinusoidal e.m.f. on the primary winding *bb'* Fig. 4, of the desired frequency, so as to produce a total flux in the core of sinusoidal wave form. The average maximum cyclic flux density generated in the core was then deduced from observations of the voltmeter, and also from Drysdale potentiometer readings on a single secondary turn S_t around the core. The total flux in the core was found to be substantially sinusoidal, as shown in Fig. 5, which is an oscillogram of the e.m.f. induced in S_t. It was soon found, however, that the fluxes in the three annular belts were nonsinusoidal. The three fundamental com-

ponents of the inner, middle and outer belt e.m.fs from the inner, middle, and outer secondary coils S_i, S_m and S_o respectively, were measured on the Drysdale potentiometer, as is indicated in Tables I, II, and III for the frequencies of 60, 340 and 696 ~.

Belt Potentiometer Tests. The results arrived at in the foregoing tables show that the maximum fundamental flux densities in the three belt paths are very different, especially towards low densities. The cross sections of the three belt paths, as determined by the positions of the two small holes through the core, were equal within 3 per cent; but the outside belt carried at $B_{max.} = 1000$, 340~, only 24 per cent of the total flux instead of 30.9 per cent on the basis of constant permeability. On the other hand, the inside belt carried 45 per cent. The middle belt carried 31 per cent. The results for three different frequen-

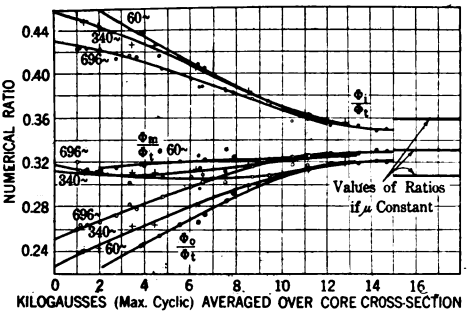

FIG. 6—VARIATION OF FLUX DISTRIBUTION WITH DENSITY

cies are shown at various flux densities averaged over the entire core, in Fig. 6. The curves show that the greatest distortion from uniformity in the three annular belt fluxes occurs at the lowest flux density, and it diminishes as the density increases. At the highest flux density of 13 kilogausses (maximum cyclic averaged over the entire cross section) the three belt flux densities are more nearly in inverse proportion to the lengths of the respective annular flux paths. The reasons for this non uniform distribution at low flux densities will be considered later on.

Belt Oscillograms. Figs. 7, 8 and 9 are oscillograms of the secondary e.m.f. induced in windings of 20 turns each on the inner, middle, and outer belts, S_i, S_m and S_o respectively, taken at the same time as Fig. 5. The oscillograph was a Duddell vibration galvanometer tuned to about 2000 ~. This

TABLE I.

RESULTS OF TESTS AT THE FREQUENCY OF 60 CYCLES PER SECOND.

Volts	Potentiometer Readings				$\mathfrak{B}_{max}$						$\frac{\mathfrak{B}o}{\Sigma\mathfrak{B}}$	$\frac{\mathfrak{B}m}{\Sigma\mathfrak{B}}$	$\frac{\mathfrak{B}i}{\Sigma\mathfrak{B}}$	$\frac{\Sigma\mathfrak{B}}{3\mathfrak{B}_i}$
i_{75}	o_2	m_2	i_2	$i_1/0°$	o	m	i	i_1	i_{75}	i				
I	II	III	IV	V	VI	VII	VIII	IX	X	XI	XII	XIII	XIV	XV
3.61	0.0234\0°.9	0.0302\0°.5	0.0418\1°.3	0.0477	2920	3770	5210	3970	4000	3980	0.246	0.317	0.437	0.998
4.23	0.0290\1° 3	0.0377/0° 1	0.0474/1°.4	0.0558	3620	4700	5910	4640	4690	4660	0.254	0.330	0.416	1.019
5.65	0.0405\4°.9	0.0497/0°.3	0.0623/1°.9	0.0771	5050	6200	7760	6420	6260	6370	0.266	0.326	0.408	0.996
7.15	0.0555\3°.5	0.0617/0°.2	0.0729/3°.0	0.0950	6920	7700	9100	7900	7930	7910	0.292	0.325	0.383	1.000
8.50	0.0685\3°.5	0.0726/0°.8	0.0844/2°.1	1.139	8540	9050	10530	9470	9430	9460	0.303	0.322	0.375	0.990
10.25	0.0854\4°.5	0.0886/0°.2	0.0981/3°.2	1.348	10660	11060	12250	11200	11370	11260	0.313	0.326	0.361	1.006
11.1	0.094 \3°.7	0.0969/0°.2	0.1041/3°.0	1.461	11780	12100	13000	12150	12310	12200	0.319	0.328	0.353	1.007
12.‘7	0.1015\3°.0	0.1045/0°.5	0.1125/2°.0	1.612	12650	13030	14020	13410	13610	13450	0.319	0.328	0.353	0.985
13.05	0.1104\1°.8	0.1140/0°.7	0.1199/2°.4	1.709	13780	14220	14950	14210	14480	14250	0.321	0.331	0.348	1.003
13.9	0.1123\2°.0	0.1159\1°.9	0.1232\1°.4	1.765	14010	14460	15380	14680	15400	14700	0.320	0.330	0.350	0.994
3.42	0.0228/0°.3	0.0296/0°.5	0.0406\0°.2	0.0460	2845	3695	5070	3820	3790	3810	0.245	0.318	0.437	1.017
5.95	0.0435\2°.4	0.0512\0°.3	0.0644/1°.9	0.0803	5430	6390	8040	6670	6600	6650	0.273	0.322	0.405	0.998
6.80	0.0524\3°.0	0.0608\1°.8	0.0704/1°.7	0.0916	6540	7590	8790	7620	7550	7600	0.285	0.331	0.384	1.006
4.92	0.0351\1°.7	0.0425/0°.2	0.0551/1°.4	0.0666	4370	5300	6860	5540	5460	5510	0.264	0.321	0.415	1.001

Col. I indicates the induced secondary e.m.f., by voltmeter in the 75-turn over-all winding.
Cols. II, III, IV, give the two-turn belt winding e.m.fs. by a-c. potentiometer, on outer, middle and inner belts respectively.
Col. V gives the single-turn over-all e.m.f. by potentiometer.
Cols. VI, VII, VIII give the corresponding computed values of flux density, max. cyclic gausses, in the outer, middle, and inner belts.
Col. IX gives the computed average flux density by potentiometer, X that by voltmeter in Col. I.
Col. XI gives the accepted average flux density (max. cyc. gausses) allowing weights to IX and X.
Cols. XII, XIII, and XIV give the respective ratios of outer, middle, and inner belt fluxes to the total flux.
Col. XV gives the ratio of the sum of the belt fluxes to the total flux as a check. It should be unity throughout.

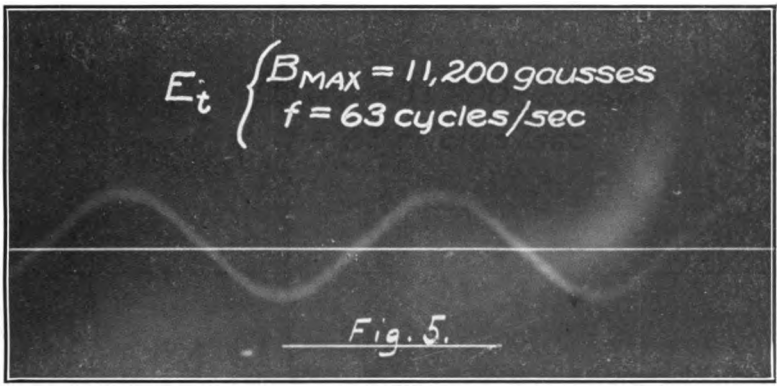

Fig. 5.

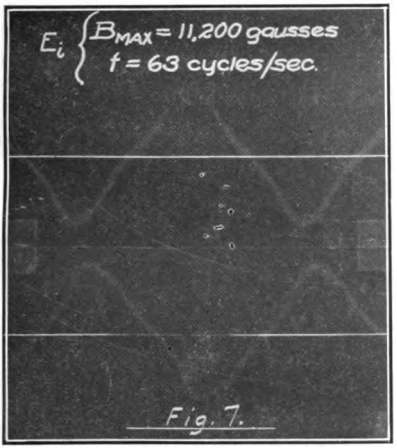

Fig. 7.

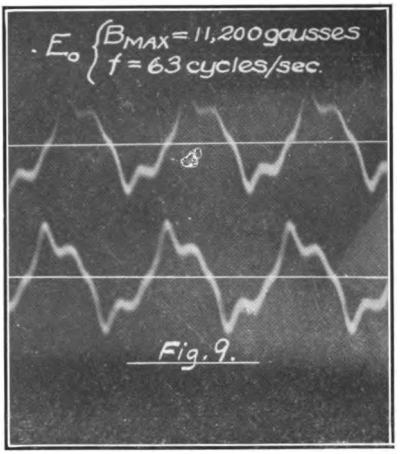

Fig. 9.

[KENNELLY]

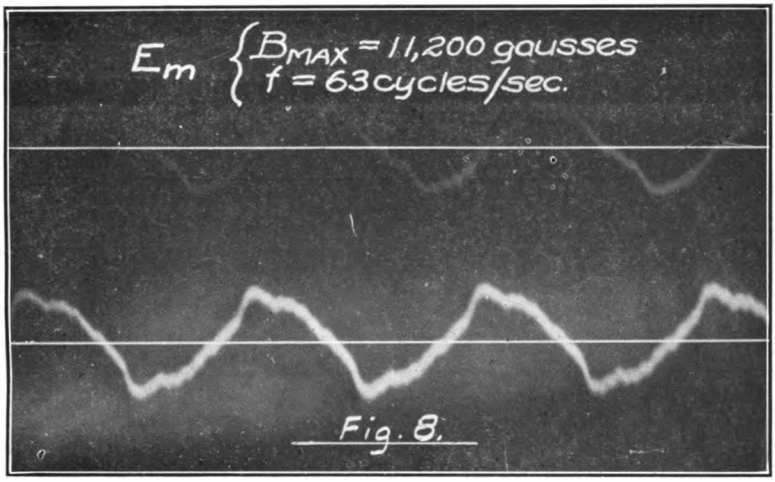

Fig. 8.

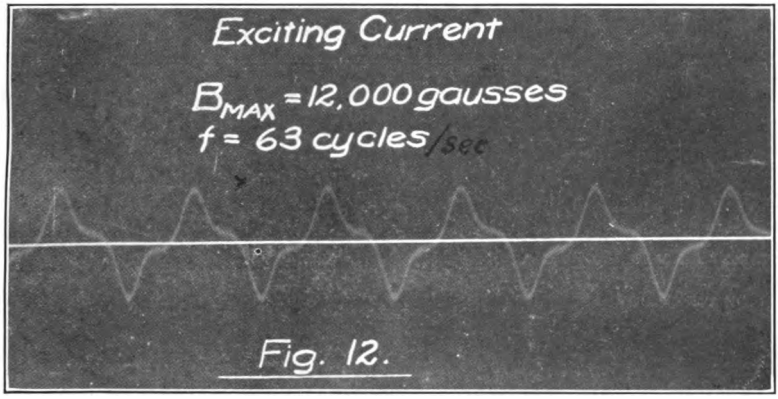

Fig. 12.

[KENNELLY]

TABLE II.

RESULTS OF TESTS AT THE FREQUENCY OF 340 ~

E. m. f. by voltmeter	E. M. F. by Potentiometer				$\mathfrak{B}_{max}$						$\frac{\mathfrak{B}o}{\Sigma\mathfrak{B}}$	$\frac{\mathfrak{B}_m}{\Sigma\mathfrak{B}}$	$\frac{\mathfrak{B}t}{\Sigma\mathfrak{B}}$	$\frac{\Sigma\mathfrak{B}}{3\mathfrak{B}_t}$
t_{75}	o_2	m_2	i_2	$i_1/0°$	o	m	i_1	i_1	t_{75}	t				
6.5	0.0463/7°.0	0.0594/2°.0	0.0858\2°.1	0.0916	1020	1310	1885	1345	1270	1320	0.242	0.311	0.447	1.068
10.0	0.066 /5°.4	0.085 /0°.9	0.121 \3°.2	0.135	1455	1875	2660	1980	1960	1973	0.243	0.313	0.444	1.012
18.0	0.123 /3°.5	0.146 \0°.8	0.200 \2°.7	0.234	2710	3210	4400	3440	3520	3465	0.263	0.311	0.426	0.994
23.0	0.160 /4°.2	0.188 /0°	0.257 \1°.8	0.301	3520	4140	5660	4420	4500	4445	0.264	0.311	0.425	1.000
32.2	0.246 /2°.6	0.275 /1°.0	0.352 /1°.2	0.425	5410	6050	7800	6240	6310	6270	0.281	0.314	0.405	1.023
43.8	0.351 /0°.1	0.371 \3°.0	0.451 /2°.4	0.586	7720	8160	9920	8600	8580	8590	0.299	0.317	0.384	1.001
57.8	0.479 \0°.8	0.494 \3°.0	0.552 /2°.9	0.760	10570	10900	12180	11180	11300	11220	0.314	0.324	0.362	0.999
66.0	0.550 \0°.6	0.560 \2°.9	0.614 /3°.0	0.872	12120	12340	13530	12830	12900	12850	0.319	0.325	0.356	0.985

TABLE III

RESULTS OF TESTS AT THE FREQUENCY OF 696 ~

E. M. F. by voltmeter	E. M. F. by Potentiometer				$\mathfrak{B}_{max}$						$\frac{\mathfrak{B}_o}{\Sigma\mathfrak{B}}$	$\frac{\mathfrak{B}_m}{\Sigma\mathfrak{B}}$	$\frac{\mathfrak{B}_t}{\Sigma\mathfrak{B}}$	$\frac{\Sigma\mathfrak{B}}{3\mathfrak{B}_t}$
e_{75}	o_2	m_2	i_2	$t_1/0°$	o	m	i	t_1	t_{75}	t				
10.7	0.071/2°.8	0.087\0°.7	0.115\3°.0	0.144	765	935	1240	1030	1020	1025	0.260	0.318	0.422	0.956
12.2	0.083/3°.3	0.098\0°.8	0.133\3°.7	0.159	890	1060	1430	1140	1170	1140	0.264	0.313	0.423	0.988
15.3	0.102/3°.2	0.122\1°.0	0.164\4°.4	0.200	1100	1310	1760	1435	1460	1440	0.264	0.314	0.422	0.966
21.4	0.148/2°.3	0.174\1°.1	0.235\3°.1	0.284	1590	1870	2530	2030	2040	2035	0.266	0.312	0.422	0.982
29.0	0.209/2°.3	0.242\1°.5	0.317\2°.6	0.390	2250	2600	3410	2780	2770	2780	0.272	0.315	0.413	0.991
....	0.262/3°.2	0.280\0°.6	0.386\1°.8	0.466	2820	3010	4150	3340	....	3340	0.282	0.302	0.416	0.996
38.4	0.279/2°.9	0.309\0°.9	0.417\2°.1	0.508	3000	3320	4490	3650	3670	3660	0.278	0.307	0.415	0.984
50.4	0.386/2°.4	0.410\1°.2	0.541\1°.4	0.670	4150	4410	5810	4800	4810	4800	0.289	0.307	0.404	0.998
60.9	0.504/1°.4	0.518\1°.2	0.668/0°.2	0.846	5420	5570	7190	6070	5810	6070	0.298	0.307	0.395	0.999
66.4	0.568/0°.8	0.535\2°.0	0.698/1°.0	0.901	6110	5750	7510	6440	6350	6440	0.297	0.315	0.388	1.002
67.7	0.568/1°.0	0.656\2°.0	0.711/0°.8	0.917	6110	5980	7650	6570	6470	6570	0.309	0.303	0.388	1.001
77.6	0.656/0°.9	0.635\2°.7	0.809/2°.2	1.058	7050	6830	8700	7550	7420	7550	0.302	0.312	0.386	0.998
90.6	0.772\0°.1	0.749\2°.2	0.919/2°.1	1.230	8300	8050	9880	8780	8660	8780	0.316	0.307	0.377	0.998
97.2	0.858\0°.2	0.823\4°.6	0.990/3°.1	1.334	9220	8850	10640	9530	9290	9530	0.321	0.308	0.371	1.004
107.8	0.944\0°.6	0.926\3°.6	1.070/3°.2	1.469	10150	9950	11150	10520	10300	10520	0.325	0.318	0.357	0.990
114.7	1.009\0°.5	0.985\4°.3	1.120/3°.6	1.568	10840	10600	12040	11200	10960	11200	0.324	0.317	0.359	0.997

instrument was selected for the purpose, instead of the ordinary oil-damped oscillograph because of its sensitiveness, the current required to operate it being only about 10 milliamperes r. m. s. It was desirable to keep the oscillographic current and ampere turns as low as possible, so as not to distort the voltages and flux distributions among the three belts. With 20 secondary belt turns, and 10 milliamperes, this secondary m.m.f. would be only 0.2 r. m. s. ampere-turn per belt. The resistance of the instrument itself was 130 ohms, and an extra resistance of 57 ohms was included in its circuit. The effect of this counter m.m.f. of 0.2 ampere-turn was to distort somewhat the wave

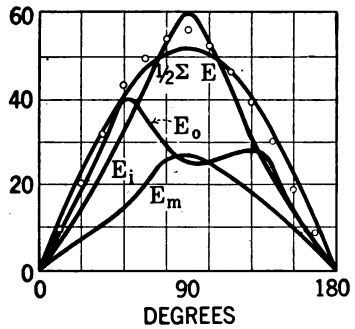

FIG. 10—REPRODUCTION OF BELT OSCILLOGRAMS TO A UNIFORM SCALE AND THE EQUIVALENT SINUSOIDAL TOTAL E.M.F. SUMMATION ORDINATES ARE SHOWN BY THE CIRCLES

Fourier analaysis of flux waves in Fig. 10.

$$E_0 = 34.5 \sin \theta + 5.3 \sin 3\theta - 4.2 \sin 5\theta +$$
$$+ 3.1 \cos \theta - 2.9 \cos 3\theta + 0.4 \cos 5\theta +$$
$$E_m = 23.8 \sin \theta - 2.4 \sin 3\theta + 0.9 \sin 5\theta +$$
$$- 1.5 \cos \theta + 1.0 \cos 3\theta + 0.6 \cos 5\theta +$$
$$E_i = 47.7 \sin \theta - 8.6 \sin 3\theta + 2.0 \sin 5\theta +$$
$$+ 0.2 \cos \theta + 0.1 \cos 3\theta - 0.4 \cos 5\theta +$$

$$E_0 + E_m + E_i = 106.0 \sin \theta - 5.7 \sin 3\theta - 1.3 \sin 5\theta +$$
$$+ 1.8 \cos \theta - 1.8 \cos 3\theta + 0.6 \cos 5\theta +$$

shape of flux in each of the three belts. This distortion should however be of the same character for each belt, and if the three belt fluxes were the same, the three belt oscillograms should be substantially the same.

The oscillograms in Figs. 5, 7, 8 and 9 are, however, markedly different, showing that the three belt fluxes differ not only in their maxima, but also in their wave form. Moreover, in order to estimate the amount of distortion in the belt oscillograms due to counter m.m.f., all of the oscillograms were repeated with only one-third of the resistance in the secondary circuit, so as to increase the distorting counter m.m.f. about three times. The upper curves in Figs. 7, 8 and 9 were taken with 0.2 ampere turn

of counter m.m.f., while the lower curves were thus taken with 0.6 ampere turn of counter m.m.f. It will be seen that since the differences between the upper and lower curves in each case are not large, the differences between the upper curves and corresponding curves unaffected by counter m.m.f. would be still less.

As a further check on the belt oscillograms, they have been copied to a uniform scale, as shown in Fig. 10, and then combined by addition, as indicated by the small circles. The best representative sine wave is drawn on the same figure for comparison, the

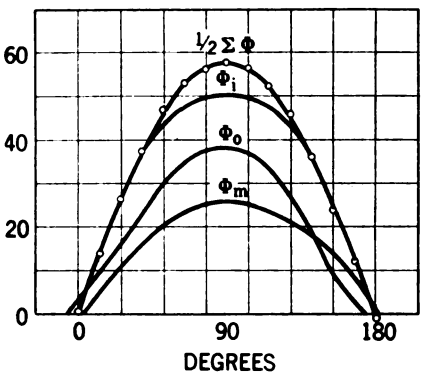

FIG. 11—FLUX WAVES DERIVED FROM INTEGRATION OF THE BELT E.M.F. WAVES IN FIG. 10—ALSO THE SINUSOIDAL TOTAL FLUX INTO WHICH THEY COMBINE.

Fourier analysis of flux waves in Fig. 11.

$$\phi_0 = 36.6 \sin\theta - 2.4 \sin 3\theta - 0.8 \sin 5\theta + \\ + 3.2 \cos\theta + 0.3 \cos 3\theta - 0.4 \cos 5\theta +$$

$$\phi_m = 26.6 \sin\theta + 0.8 \sin 3\theta + 0.1 \sin 5\theta + \\ - 1.6 \cos\theta - 0.4 \cos 3\theta + 0.2 \cos 5\theta +$$

$$\phi_i = 53.2 \sin\theta + 2.6 \sin 3\theta + 0.5 \sin 5\theta + \\ + 0.1 \cos\theta - 0.04 \cos 3\theta - 0.1 \cos 5\theta +$$

$$\varphi_0 + \varphi_m + \varphi_i = 116.4 \sin\theta + 1.0 \sin 3\theta - 0.2 \sin 5\theta + \\ + 1.7 \cos\theta - 0.14 \cos 3\theta - 0.3 \cos 5\theta +$$

total flux being substantially sinusoidal as in Fig. 5. The deviations of the circles from this sine wave are sufficiently small to be attributable to errors in reproducing the oscillograms of Figs. 7, 8 and 9, the amplitudes of which were actually only 1 to 2 cm.

The Fourier analysis of the curves E_o, E_m and E_i are indicated in Fig. 10. The harmonics beyond the fifth are negligible throughout. It will be seen that E_o contains a 17 per cent triple and a 12 per cent quintuple component. E_m has a 11 per cent triple component. E_i has an 18 per cent triple component.

In the summation of the three waves, the harmonics almost disappear except for a residual 6 per cent triple component.

On integrating the curves of Fig. 10, so as to reduce the induced e.m.f.s. to their equivalent magnetic fluxes, the curves of Fig. 11 are obtained. As naturally follows such a process of integration, the resulting flux curves are smoother than the original oscillographic e.m.f. curves. The agreement of their sum with a sine wave is accordingly better. The largest belt flux is clearly the inner one ϕ_i. It would be expected that the outer belt flux should be the smallest; but as is shown in Fig. 2, the width of the middle belt was somewhat unduly small. Figs. 10 and 11 are thus in substantial accordance with Fig. 5, in showing that the total flux through the core was sinusoidal, although the individual belt fluxes were far from sinusoidal.

The corresponding Fourier analysis of the curves in Fig. 11 appear beneath it. They are in substantial conformity with the e.m.f. wave analysis of Fig. 10.

The results, appearing in the tables and presented graphically in Fig. 6, also indicate that the numerical sums of the fundamentals of the three belt e.m.fs. are equal to the e.m.fs. of the turns around the entire core. Moreover in Fig. 6 the sums of the ordinates on the belt curves remain equal to unity throughout the entire range of averaged flux density.

Reasons for the Distortions in the Belt Flux Densities

It is well known that in the primary winding of an excited transformer under no load, the exciting current is nonsinusoidal when the impressed e.m.f. is sinusoidal; firstly because of the varying permeability, and secondly because of hysteresis. The current wave under ordinary conditions is peaked. An oscillogram of the primary current at 63 $\sim$ and 12,000 gausses (max. cyc.) appears in Fig. 12. The peak is to be ascribed to the change of permeability of the iron during the cycle. Assuming a total flux that is sinusoidal, the exciting current at each moment must conform to the $\mathfrak{H}$-$\mathfrak{G}$ cycle for the entire core. If the various belt paths in the laminae had equal lengths, they would share the flux equally, neglecting skin effects. Actually, however, the inner belt paths are shorter, and these therefore tend to carry a larger share of the flux. This in turn alters the reluctance, because the permeability depends upon the density. At low densities, the tendency is to increase the flux of the inner belt paths yet more, because the permeability at first increases

with flux density. At high densities, on the contrary, the tendency is in the opposite direction. Consequently, at low densities, the flux in the inner belts tends to be very different from that in the outer belts, as is shown by Fig. 6. At high densities, however, the permeances of the different belts are more nearly uniform, and the belt fluxes are nearly inversely proportional to the belt lengths.

Effect on Belt-Flux Wave Form

An examination of Fig. 11 shows that the wave form of ϕ_i, the inner belt of flux, is flat by comparison with a sinusoid; whereas ϕ_o is peaked and ϕ_m is intermediate. It is evident

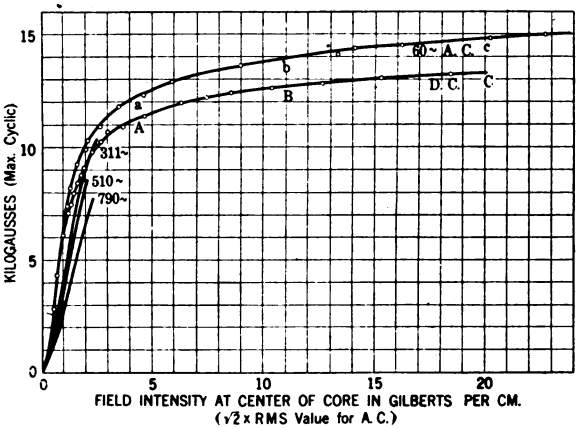

Fig. 13—Saturation Curves for x 5 Silicon Steel Obtained from a Laminated Annular Core—Inside Diameter 40.6 cm.—Outside Diameter 50.8 cm.—Laminations 0.0356 cm. Thick

that ϕ_i must be relatively flat from the curves of Fig. 6, which show that at low densities the inner belt carries an extra large share of flux, whereas towards higher densities this extra share is reduced. On the other hand, ϕ_o must be relatively peaked because the share of the outer belt increases as the density increases. In Fig. 10 the conditions are inverted, the relatively flat belt flux ϕ_i give rise to a relatively peaked e.m.f. E_i; while the peaked ϕ_o gives rises to the flattened E_o. Moreover, the exciting current has its wave form determined by the total flux in the core, or the sum of all the belt fluxes. At the lower densities existing in the outer belt, this current will be too peaked and distorted to produce a sine wave of flux; so that the outer

belt flux wave will be correspondingly peaked and distorted. The conditions are just reversed in the inner belt. This accounts for the e.m.f. wave in the outer belt being so much more irregular than in the others. Again, the inner flux, being the largest of the three, has the greatest share in determining the exciting current, and so remains the smoothest.

Saturation Curves

Fig. 13 shows the saturation curve *A B C* for the whole core of 25 laminae, as deduced from d-c. observations with a flux meter connected to an enveloping coil of six secondary turns. The upper curve *a b c* represents the corresponding saturation

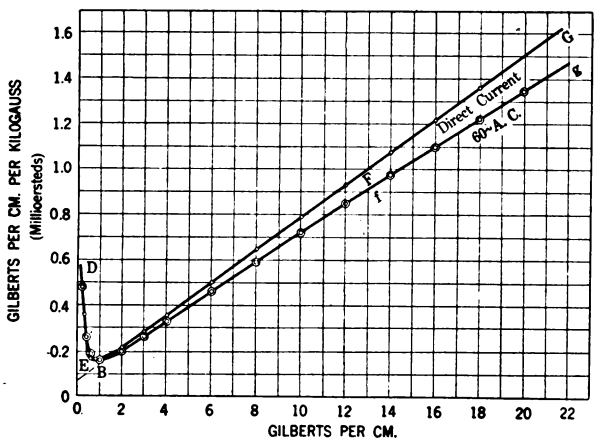

FIG. 14

with 60 ~ alternating current, multiplying the observed r.m.s. primary current by $\sqrt{2}$, to obtain the maximum cyclic magnetic intensity $\mathfrak{H}$. The observed e.m.f. per secondary turn was also multiplied by $\sqrt{2}$ to obtain the maximum cyclic kilogausses $\mathfrak{B}$. Owing to distortion of the impressed e.m.f. waves from the sinusoidal form at high flux densities, the factor $\sqrt{2}$ is evidently too low for $\mathfrak{H}$ and too high for $\mathfrak{B}$. It is supposed that if these errors did not exist, and that both $\mathfrak{H}$ and $\mathfrak{B}$ were sinusoidal quantities throughout, the curve *a b c*, would coincide with the direct-current excitation curve *A B C*.

Similar a-c. saturation curves at higher frequencies are also shown up to 7 and 9 kilogausses. It is supposed that these fall below the low-frequency curve because of skin effect.

The corresponding curves of reluctivity in the laminae, for different values of $\mathfrak{H}$, appear in Fig. 14. The reluctivity for direct currents is a rapidly descending line from 0 to 0.5 gilbert per[3] cm. It then becomes a steadily ascending straight line $F\,G$ defined by the equation $\nu = 0.000\ 07 + 0.000\ 0723\ \mathfrak{H}$ oersted-cm. The apparent reluctivity for a-c. excitation, as similarly obtained from the saturation curve $a\ b\ c$ of Fig. 13, is the curve $D\ E\ f\ g$. As before, it is supposed that if there were no errors of distortion in impressed wave form, this curve would coincide with $D\ E\ F\ G$.

It must be remembered that the reluctivity straight line $B\ E\ F\ G$ is a mean value obtained for the core as a whole.

Outline Theory of the Radial Variation

If each lamina has internal radius R_1 cm., and external radius R_2 cm. and a thickness of h cm., then the reluctance $\mathfrak{R}$ of the lamina will be, in any belt of radius r and width $d\,r$, in terms of the reluctivity ν,

$$\mathfrak{R} = \frac{\nu \cdot 2\,\pi\,r}{h \cdot d\,r} \qquad \text{oersteds (1)}$$

Under a total direct-current m.m.f. of $\mathfrak{F}$ gilberts, the flux in this belt will be

$$d\,\varphi = \frac{\mathfrak{F}}{\mathfrak{R}} = \frac{\mathfrak{F} \cdot h \cdot d\,r}{\nu \cdot 2\,\pi\,r} \qquad \text{maxwells (2)}$$

But

$$\mathfrak{F} = 2\,\pi\,r\,\mathfrak{H} \qquad \text{gilberts (3)}$$

so that

$$d\,\varphi = \frac{\mathfrak{H}}{\nu} \cdot h \cdot d\,r \qquad \text{maxwells (4)}$$

The total flux in the lamina will then be the integral of this, or

$$\phi = h \int_{R_1}^{R_2} \frac{\mathfrak{H}}{\nu}\, d\,r \qquad \text{maxwells (5)}$$

3. "Magnetic Reluctance," TRANS., A.I.E.E., Vol. 8, Oct. 27th, 1891, pp. 486-533. Also "Investigation of Magnetic Laws for Steel and other Materials," by J. D. Ball, *Journal of the Franklin Institute*, Vol. 181, April, 1916, pp. 459-504.

If ν were directly proportional to $\mathfrak{H}$, or if $\nu = b\,\mathfrak{H}$ oersted-cm,

$$\text{then} \qquad \phi = h \int_{R_1}^{R_2} \frac{d\,r}{b} = \frac{h}{b}\,(R_2 - R_1) \qquad \text{maxwells (6)}$$

This would mean uniform flux densities in all of the belt paths and the absence of all radial distortion. But the reluctivity is not directly proportional to $\mathfrak{H}$. As we have seen for this particular quality of steel, below $\mathfrak{H} = 0.5$, $\nu = 0.0007 - 0.001\,\mathfrak{H} = a_1 - b_1\,\mathfrak{H}$, and above $\mathfrak{H} = 0.5$

$$\nu = 0.000\,07 + 0.000\,0723\,\mathfrak{H} = a + b\,\mathfrak{H} \qquad \text{oersted-cm. (7)}$$

The effect of this constant term a or a_1 in the reluctivity is therefore to make the belt flux $d\,\varphi_r$ at radius r in terms of the local magnetic intensity $\mathfrak{H}_r$ and flux density $\mathfrak{B}_R$

$$d\,\varphi_r = \frac{\mathfrak{H}_r \cdot h \cdot dr}{a + b\,\mathfrak{H}_r} = h \cdot \mathfrak{B}_r \cdot d\,r = \frac{\mathfrak{F} \cdot h \cdot d\,r}{2\,\pi\,r\,a + b\,\mathfrak{F}} \qquad \text{maxwells (8)}$$

The d-c. distribution of flux density for a given value of $\mathfrak{F}$, will thus necessarily vary with r, and will tend to be greater on the inside.

We may define the flux-density distortion in a lamina as the difference between the innermost and outermost densities $\mathfrak{B}_1 - \mathfrak{B}_2$ divided by the flux density $\mathfrak{B}_R$ at the geometric mean radius R That is, if R is the geometric mean radius,

$$R = \sqrt{R_1\,R_2} = n\,R_1 = R_2/n \qquad \text{cm. (9)}$$

where n is a numerical ratio, such that $R_2 = n^2\,R_1$
It then follows from (8) that

$$\frac{\mathfrak{B}_1 - \mathfrak{B}_2}{\mathfrak{B}_R} = a\left(n - \frac{1}{n}\right) \frac{a + b\,\mathfrak{H}_R}{(a + b\,n\,\mathfrak{H}_R)\left(a + \frac{b}{n}\,\mathfrak{H}_R\right)}$$

$$= a\left(n - \frac{1}{n}\right) \frac{\nu_R}{\nu_1\,\nu_2} \qquad \text{numeric (10)}$$

Since approximately $\qquad \nu_1\,\nu_2 = \nu^2_R \qquad$ (oersted-cm.)^2 (11)

the distortion is approximately

$$\frac{\mathfrak{B}_1 - \mathfrak{B}_2}{\mathfrak{B}_R} = \frac{a}{\nu_R}\left(n - \frac{1}{n}\right) \qquad \text{numeric (12)}$$

The quantity

$$n - \frac{1}{n} = \frac{R_2 - R_1}{R} \qquad \text{numeric (13)}$$

or is the ratio of the width to the geometric mean radius of the lamina. We may call it the width-radius ratio. In the laminae tested, the width-radius ratio was $\frac{2}{\sqrt{80}} = 0.2236$. Consequently to the degree of approximation represented by (**12**), the flux-density distortion in a lamina subjected to any continuous-current m.m.f. is equal to the width-radius ratio times the ratio of the reluctivity constant a to the total reluctivity at the geometric mean belt R

If $a = 0$, the flux-density distortion disappears, as we have already seen.

If $b = 0$, so that the reluctivity is independent of the excitation, (**12**) becomes $\frac{\mathfrak{B}_1 - \mathfrak{B}_2}{\mathfrak{B}_R} = \left(n - \frac{1}{n}\right)$, or the distortion is numerically equal to the width-radius ratio.

As ν_R increases, with increasing flux density, towards saturation, the ratio a/ν_R becomes very small, and the distortion nearly disappears.

On the ascending straight line of reluctivity, above $\mathfrak{H} = 0.5$, in the case considered, a/ν_R is always less than unity, or the distortion to continuous m.m.f. is always less than the width-radius ratio.

On the initial descending straight line of reluctivity, below $\mathfrak{H} = 0.5$ in the case considered, a/ν_R is likely to exceed unity, so that over this range of $\mathfrak{H}$, the distortion is likely to be greater than the width-radius ratio, and, in particular cases, may be several times greater.

In order to prevent the existence of all distortion, the width-radius ratio must be reduced to zero, which means that the lamina must be cut from a cylinder, instead of from a flat sheet of metal. In the ordinary case of a flat annular stamping, the distortion diminishes as the mean radius is increased. When it

is desired to measure the magnetic properties of the steel with considerable precision, the width-radius ratio should be kept as small as possible, otherwise the mean apparent permeability of the steel at any given intensity $\mathfrak{H}$, as derived from the joint behavior of all the belts in parallel, will differ from the true permeability in any one belt. The error tends to be greatest at low densities referred to the descending branch of the $\nu - \mathfrak{H}$ graph, and diminishes towards high densities.

The authors are indebted to the American Telephone and Telegraph Co., under an appropriation from which the investigation was carried on. They are also indebted to Prof. C. A. Adams and to Mr. R. Eksergian, for valuable suggestions during the work.

Conclusions

(1) As has already been noted by several writers, the flux density differs in different belts of an annular steel lamina, under a circumferential impressed m.m.f. from a distributed toroidal winding. The phenomenon may be described as radial distortion of flux density.

(2) The distortion occurs both with continuous and alternating m.m.fs. It may be very marked at low densities. At high frequencies, flux-density distortion is complicated by skin effects.

(3) With alternating m.m.fs., a distortion is effected in the alternating magnetic wave form, as well as in the maximum cyclic flux density. Each belt has its own density, and its own wave form. The total flux in the lamina being, say, sinusoidal, the individual belt fluxes will be nonsinusoidal. The external belt fluxes have, in general, the most distorted wave forms.

(4) The magnitude of flux-density distortion may be defined as the difference between the inside and outside flux densities, divided by the flux density at the geometrical mean radius. In the case reported, the observed a-c. flux-density distortion was approximately $\frac{0.45 - 0.24}{0.31} = 0.68$, at low densities.

(5) The magnitude of flux-density distortion depends upon the width-radius ratio of the lamina, or the width of the lamina divided by its geometrical mean radius. In the case reported, this ratio was 0.224. The smaller this ratio, other things being equal, the less the distortion.

(6) For a given width-radius ratio, the flux-density distortion depends, to a first approximation, on the ratio a/ν of the constant

reluctivity term a to the total reluctivity ν in the geometric mean belt. Over the ascending straight range of the reluctivity-intensity $\nu - \mathfrak{H}$ graph, this ratio is less than unity, so that, at least in the continuous-current case, the distortion will be less than the width-radius ratio over this range (above $\mathfrak{H} = 1$ in the case reported.) On the descending branch of the $\nu - \mathfrak{H}$ graph, the ratio a/ν will be greater than unity, so that at low values of $\mathfrak{H}$ and $\mathfrak{B}$, the distortion is likely to exceed the width-radius ratio (below $\mathfrak{H} = 1$, $\mathfrak{B} = 6000$ in the case reported).

(7) When the magnetic characteristics of steel laminae are to be measured with precision, small width-radius ratios should be used, in order to avoid errors due to flux-density distortion. Strictly speaking, curves derived from annular laminae are all subject to distortion errors, especially at low densities.

(8) The eddy-current losses occurring in annular laminae under sinusoidal a-c. excitation are exaggerated by the presence of harmonics in the various belt fluxes.

List of Symbols Employed

a, b	Reluctivity constants for a sample of steel.
$\mathfrak{B}$	flux density in steel, (gausses, or maxwells per sq. cm.)
$\mathfrak{B}_{max}$	maximum cyclic flux density in steel (gausses).
$\mathfrak{B}_i$ $\mathfrak{B}_m$ $\mathfrak{B}_o$	flux densities in inner, middle, and outer belts of a lamina (gausses) and in alternating-current cases maximum cyclic gausses.
$\mathfrak{B}_t$	flux density in a lamina averaged over the entire cross section (gausses and in alternating-current cases maximum cyclic gausses).
$\mathfrak{B}_1$ $\mathfrak{B}_2$ $\mathfrak{B}_R$	flux density at inner edge, at outer edge, and at geometric mean belt of a lamina, respectively (gausses, and in a-c. cases, maximum cyclic gausses).
E	electromotive force induced in a winding (volts).
$\mathfrak{F}$	magnetomotive force applied to a lamina circumferentially (gilberts or c. g. s. magnetic units).
$\mathfrak{H}$	magnetic intensity or magnetic force in steel (gilberts per cm.)
$\mathfrak{H}_r$	magnetic intensity in a lamina at belt of radius r (gilberts per cm.)
h	width of a lamina measured along any radius (cm.)

n ratio of geometric mean radius to inner radius of an annular lamina (numeric).

$\nu = a + b\mathfrak{H}$ reluctivity of steel (oersted-cm.)

ν_1, ν_2, ν_R reluctivity at inner, outer, and geometric mean belts of a lamina, respectively (oersted-cm.)

ϕ total magnetic flux in a lamina (maxwells).

ϕ_r magnetic flux in a belt of a lamina at radius r (maxwells).

ϕ_i, ϕ_m, ϕ_o magnetic fluxes in the inner, middle, and outer belts of an annular lamina, respectively (maxwells).

$\mathfrak{R}$ reluctance of a belt path (oersteds.)

r radius of an annular belt (cm.)

R_1, R_2 internal and external radii of an annular lamina (cm.)

$R = \sqrt{R_1 R_i}$ geometric mean radius of an annular lamina (cm.)

Σ summation sign, $\angle$ angle sign, $\sim$ sign for cycles per second.

LIST OF RESEARCH BULLETINS

Bulletin Number

*1. The Economical Transportation of Merchandise in Metropolitan Districts. H. Pender and H. F. Thomson; March, 1912.

*2. Notes on the Cost of Motor Trucking. H. Pender and H. F. Thomson; October, 1912.

*3. Observations on Horse and Motor Trucking. H. Pender and H. F. Thomson; March, 1913.

*4. Relative Fields of Horse, Electric and Gasoline Trucks. H. F. Thomson; August, 1914.

*5. The Delivery and Handling of Miscellaneous Freight at the Boston Freight Terminals. H. Pender, H. F. Thomson, and C. P. Eldred; February, 1914.

6. The Delivery System of R. H. Macy & Co. of New York. H. F. Thomson, H. L. Manley, and A. L. Pashek; September, 1914.

7. Explorations over the Vibrating Surfaces of Telephonic Diaphragms under Simple Impressed Tones. A. E. Kennelly and H. O. Taylor; April, 1915.

8. The Mechanics of Telephone-Receiver Diaphragms as Derived from their Motional-Impedance Circles. A. E. Kennelly and H. A. Affel; November, 1915.

9. Experimental Researches on Skin Effect in Conductors. A. E. Kennelly, F. A. Laws, and P. H. Pierce; September, 1915.

10. Tractive Resistances to a Motor Delivery Wagon on Different Roads and at Different Speeds. A. E. Kennelly and O. R. Schurig; June, 1916.

11. Some Properties of Vibrating Telephone Diaphragms. A. E. Kennelly and H. O. Taylor; April, 1916.

12. Experimental Researches on the Skin Effect in Steel Rails. A. E. Kennelly, F. H. Achard, and A. S. Dana; August, 1916.

13. Skin-Effect Resistance Measurements of Conductors at Radio-Frequencies up to 100 000 Cycles per Second. A. E. Kennelly and H. A. Affel; December, 1916.

* Out of print.

Bulletin Number

14. Street Railway Fares; their relation to length of haul and cost of service. D. C. Jackson and D. J. McGrath; August, 1917.

15. Apparent Dielectric Strength of Varnished Cambric. A. E. Kennelly and R. J. Wiseman; January, 1918.

16. Magnetic Flux Distribution in Annular Steel Laminae. A. E. Kennelly and P. L. Alger; March, 1918.

Electromagnetic Theory of the Telephone Receiver

A. E. KENNELLY and H. NUKIYAMA

Report of an Investigation Read before the American Institute of Electrical Engineers at their 348th Meeting, at Boston, Mass, March 14, 1919

Research Division
Electrical Engineering Department
Massachusetts Institute of Technology
Bulletin No. 17 March, 1919

A paper presented at the 348th meeting of the American Institute of Electrical Engineers, Boston, Mass., March 14th, 1919.

(Subject to final revision for the Transactions.)

ELECTROMAGNETIC THEORY OF THE TELEPHONE RECEIVER

With Special Reference to Motional Impedance

BY A. E. KENNELLY AND H. NUKIYAMA

ABSTRACT OF PAPER

The theory of the telephone receiver here offered is based upon the motional impedance circle which has been published in various chapters during the last few years. The new theory, which is stated under definite limitations, is a further development; taking into account the m.m.f. produced by the vibration of the diaphragm in the permanent magnetic field. The motional power is thus shown to be derived partly from the testing alternating current and partly from changes in power expended in the magnetic circuit. The motional impedance circle may therefore also be regarded as a power circle, with components along three different axes of reference.

Object of the Paper. It is well known that every telephone receiver possesses a certain difference of vector impedance between the "damped" and "free" conditions, such that, when plotted in polar coordinates, over a suitable range of alternating-current frequency, gives rise to a "motional-impedance locus", which locus is approximately circular, and is known as its "motional-impedance circle".

The motional impedance circle of a telephone receiver affords valuable material for determining the principal mechanical and electrical constants of the instrument.*

In the theory of the motional-impedance circle, as hitherto published, certain phenomena have been left out of consideration for the sake of simplicity; and especially that component of alternating magnetic flux passing through the coils which is due to the displacement of the diaphragm from its zero position when freely vibrating. The result has been that the motional-impedance circle failed to reveal the power expended parasitically (by both hysteresis and eddy currents) in the magnetic circuit. This defect in the theory has already been pointed out by Eccles.†

Manuscript of this paper was received on January 29, 1919.

*Bibliography, No. 9.

†Bibliography, No. 24.

It is the object of this paper to supply the above-mentioned omission, and thus to offer a closer approximation between the theory and the observed behavior of the telephone receiver as an electromagnetic motor. It should be pointed out, however, that the theory here presented is still far from being complete, and that much more work, both theoretical and experimental remains to be executed, analysed and reported, before the theory can be regarded as satisfactorily established.

Limitations of the New Theory. The following limitations should be noted in regard to the stage of attainment aimed at in the theory here presented.

1. The alternating current supplied to the receiver is of small amplitude, and of single frequency; so that the magnetic flux passing through the coils and polar surfaces may be regarded as a normal permanent flux, plus a small sinusoidal variation. All the alternating mechanical, magnetic and electric quantities, are therefore assumed to be simple harmonic functions of the time.

2. Throughout the range of frequency considered, the flux in the magnetic circuit of the coils retains the same magnitude and phase with respect to the constant exciting alternating current. This means that the influences of magnetic skin effect and hysteresis in the magnetic circuit remain substantially constant.

3. The proportional effect of a small increment of m.m.f. in the magnetic circuit, due either to a small increase in exciting current, or to a small diminution in air gap at the poles, shall be the same, both in magnitude and in phase.

4. That over the range of frequencies considered, the "force-factor" A, the "equivalent mass" m of the diaphragm, the "mechanical resistance" r of the same, and the "stiffness coefficient" s, remain substantially constant.

The theory is presented with relation to a series of impedance measurements already published* on a particular bipolar Bell receiver "C"; so that these measurements offer, in a particular case, a check upon the application of the theory.

Magnetic Circuit and Vibrating System. In Fig. 1, it is assumed that the two poles N and S are permanently magnetized, as though under the action of a constant-current magnetomotive force $\mathfrak{F}_0$ gilberts. Under the influence of the

*Bibliography 17, pp. 422–428 and 449–450.

permanent magnetic flux Φ_0 maxwells in the magnetic circuit, the diaphragm becomes flexed from its horizontal plane position and comes to rest at a certain zero position at the same distance from each pole. Since vibrational displacements occur on each side alternately of this reference position of rest, we may reckon a displacement therefrom of x cm. towards the poles as positive, and away from the poles as negative. The total number of turns on both coils together, is taken as N. The active surface of each pole, or of the diaphragm opposite thereto, is taken as S sq. cm., and since the polar gap is small

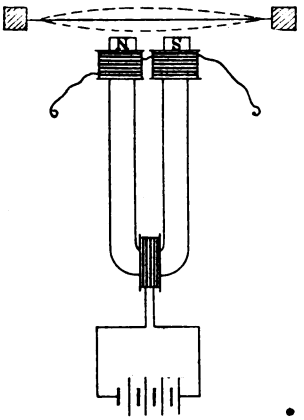

FIG. 1—SIMPLIFIED MAGNETIC CIRCUIT OF BIPOLAR RECEIVER

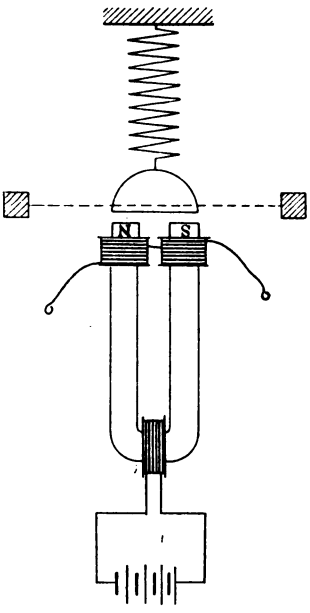

FIG. 2—SIMPLIFIED MECHANICAL SYSTEM OF BIPOLAR RECEIVER

by comparison with the linear dimensions of this surface, we may neglect the magnetic fringe at the polar edges.

In Fig. 2, the mechanical vibration system is indicated as simplified into an equivalent mass m grams, under the retractive influence, so far as concerns alternating stresses, of s dynes per cm. of displacement. The frictional resistance force of this system to motion is taken as simply proportional to the velocity of displacement; so that if $\dot{x}$ represents the velocity $\frac{dx}{dt}$ of the mass m, the retarding force is $-r\dot{x}$ dynes, where r is the

mechanical resistance of the mass in dynes per unit velocity, or dynes per kine.

The simplification in the vibrational system represented in the transition from Fig. 1 to Fig. 2 seems justified from experimental results.

Magnetomotive Force Damped and Free. When the diaphragm is damped, or prevented from vibrating, a simple alternating current of I r. m. s. absamperes will develop a corresponding simple alternating m.m.f. of $\mathfrak{F}_i$ r. m. s. gilberts, in phase with I. This may be represented as in Fig. 3, by the plane vector f_i in the horizontal or reference-phase position. In the receiver analysed, the testing current I was 0.000204

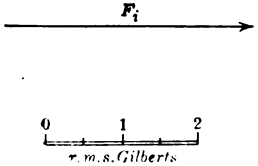

FIG. 3—M. M. F. DIAGRAM AT CONSTANT CURRENT—DIAPHRAGM DAMPED

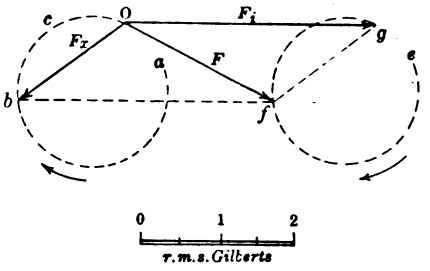

FIG. 4—M. M. F. DIAGRAM AT CONSTANT CURRENT AND 1028 CYCLES PER SEC. DIAPHRAGM FREE

absamperes r. m. s., and taking the number of turns on the two coils together as 1300, the m.m.f. thereby produced would be

$$4\pi \times 1300 \times 0.000204 = 3.334 \text{ gilberts r. m. s.}$$

This is represented, to a scale of 1.0 gilbert per linear cm. in Fig. 1, as a vector 3.33 cm. in length.

When the diaphragm is free, or allowed to vibrate, the same exciting current will produce the same m. m. f. as before; but a new periodic m. m. f. will be developed in the magnetic circuit, owing to the periodic change in diaphragm displacement, and length of airgap; so that the reluctance in the circuit of the permanent magnet will be periodically varied accordingly.

Let $\mathfrak{F}_0$ = the m. m. f. of the permanent magnet (gilberts)
$\mathfrak{R}_0$ = the reluctance in the permanent magnetic circuit (oersteds)
Φ_0 = the magnetic flux across the airgaps in the circuit (maxwells)

Then in the magnetic circuit of the permanent magnet, there will be a permanent magnetic flux which, neglecting magnetic leakage through the surrounding air, will be

$$\Phi_0 = \frac{\mathfrak{F}_0}{\mathfrak{R}_0} \qquad \text{maxwells (1)}$$

If the diaphragm is now caused to vibrate, by reason of independent variations of this magnetic flux due to alternating current in the coils, the reluctance in each airgap of area S sq. cm. will be varied by $-\frac{dx}{S}$ oersteds, if dx is the displacement of the diaphragm from its normal position, towards the pole; so that the total change in reluctance will be $-\frac{2\,dx}{S}$ oersteds.

But differentiating (1)

$$\frac{\partial \Phi_0}{\partial \mathfrak{R}_0} = -\frac{\mathfrak{F}_0}{\mathfrak{R}_0^2} = -\frac{\Phi_0}{\mathfrak{R}_0} \qquad \frac{\text{maxwells}}{\text{oersteds}} \quad (2)$$

or $$\partial \Phi_0 = -\Phi_0 \frac{\partial \mathfrak{R}_0}{\mathfrak{R}_0} \qquad \text{maxwells (3)}$$

but $\partial \mathfrak{R} = -2\,\partial x/S$; so that

$$\partial \Phi_0 = \Phi_0 \cdot \frac{2\,\partial x}{S\,\mathfrak{R}_0} = \mathfrak{B}_0 \cdot \frac{2\,\partial x}{\mathfrak{R}_0} \qquad \text{maxwells (4)}$$

This differential change in the flux through the magnetic circuit is such as would correspond to the action of a certain differential impressed m. m. f. $\partial \mathfrak{F}_0$, such that

$$\frac{\partial \mathfrak{F}_0}{\mathfrak{R}_0} = \partial \Phi_0 \qquad \text{maxwells (5)}$$

Consequently, substituting in (4)

$$\partial \mathfrak{F}_0 = \mathfrak{B}_0 \cdot 2\,\partial x \qquad \text{gilberts (6)}$$

If, then, we know $\mathfrak{B}_0$, the normal mean flux density across the airgaps, an alternating displacement of ∂x cms. r. m. s. towards the poles at reference phase, will generate an equivalent vector m. m. f. according to (6) in phase with ∂x. This is shown in Fig. 4 by the plane vector $\mathfrak{F}_x$. The phase of $\mathfrak{F}_x$ with respect to $\mathfrak{F}_i$ cannot be assigned until we know the phase of the diaphragm displacement ∂x, but means for determining this phase difference will be indicated later on. The locus of $\mathfrak{F}_x$ is indicated in Fig. 4. It is a "displacement-admittance" locus.

At a very low frequency, $\mathfrak{F}_x$ would occupy the plane-vector position $O\,a$. At a very high frequency, it would disappear towards $O\,c$. It would, therefore describe the locus $a\,b\,c$ in the direction of the arrow.

The resultant m. m. f. in the circuit is the planevector sum of $\mathfrak{F}_i$ and $\mathfrak{F}_x$, and is indicated in Fig. 4 by $\mathfrak{F}$. At low frequencies, the size of $\mathfrak{F}$ exceeds the size of $\mathfrak{F}_i$; but towards higher frequencies, the size of $\mathfrak{F}$ falls below that of $\mathfrak{F}_i$. The effect, therefore, of the vibration of the diaphragm is to change the constant impressed a-c. m. m. f. $\mathfrak{F}_i$ to a correspondingly varied m. m. f. following the vector locus $e\,f\,g$, as the frequency is changed.

In Figs. 3 and 4, the vectors represent, to scale, the approxi-

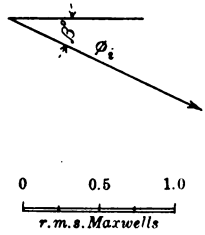

FIG. 5—FLUX DIAGRAM AT 1028 CYCLES PER SEC. — DIAPHRAGM DAMPED

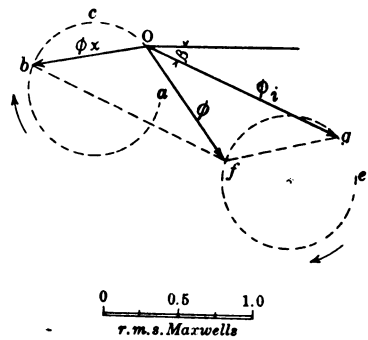

FIG. 6—FLUX DIAGRAM AT 1028 CYCLES PER SEC. — DIAPHRAGM FREE

mate values of $\mathfrak{F}_i$, $\mathfrak{F}_x$ and $\mathfrak{F}$, as derived from experimental tests of the selected instrument.

Magnetic Flux, Damped and Free. In Figs. 5 and 6, the planevector alternating magnetic fluxes are represented with the diaphragm damped and free. When damped, as in Fig. 5, the alternating m. m. f. of $\mathfrak{F}_i$ r. m. s. gilberts at reference phase, produces an alternating magnetic flux of ϕ_i r. m. s. maxwells, lagging in phase $\beta°$ behind the m. m. f. The reason for the lag is partly on account of magnetic hysteresis, and partly on account of magnetic skin effect. This angle $\beta°$ (25.3 deg. in Fig. 5) can be determined from the observed motional-impedance diagram, on the assumption already made that β is half the depression angle of the motional-circle diameter. In certain cases, β is found to exceed 54 deg. although it is, more commonly in the neighborhood of 30 deg.

In Fig. 6, on the assumption already made that the lag $\beta°$ is the same to both $\mathfrak{F}_i$ and $\mathfrak{F}_x$; *i. e.*, that ϕ_x lags $\beta°$ behind $\mathfrak{F}_x$, we obtain the fluxes ϕ_i and ϕ_x with their resultant ϕ, as well as the approximate loci over which they travel under change of impressed frequency, β being taken as substantially constant over that range.

Actual observation shows that the angle of lag β_1 between $\mathfrak{F}_i$ and ϕ_i is not, in general, identical with the angle of lag β_2

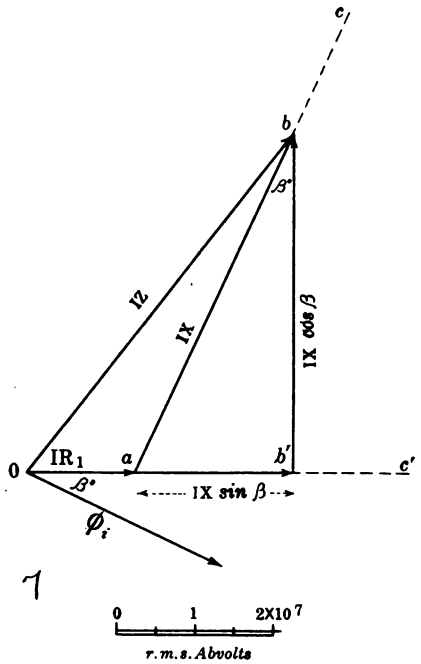

FIG. 7—E. M. F. DIAGRAM AT 1028 CYCLES PER SEC.—DIAPHRAGM DAMPED

between $\mathfrak{F}_x$ and ϕ_x, but their sum is 2 β, and the discrepancy is here neglected.*

Electromotive Forces, Damped and Free. Fig. 7 shows the alternating e. m. f. planevector diagram when the diaphragm is damped. With constant exciting current strength I r. m. s. absamperes, and constant assumed resistance R_1 absohms in the winding, the vector $I R_1$ r. m. s. volts, expended in overcoming the winding resistance, will theoretically remain con-

*Bibliography 18.

stant at all frequencies. The voltage expended in overcoming the reactance of the winding will be $I X$ r. m. s. volts, at a leading slope of $90 - \beta°$; because this voltage must be in leading quadrature to the flux ϕ_i. The resultant voltage $I Z$ is that which must be applied to the terminals of the receiver, in order to maintain in its winding the required constant current strength I. The locus of the impressed voltage $I Z$ on the preceding assumptions, will therefore be the straight line $a\ b\ c$.

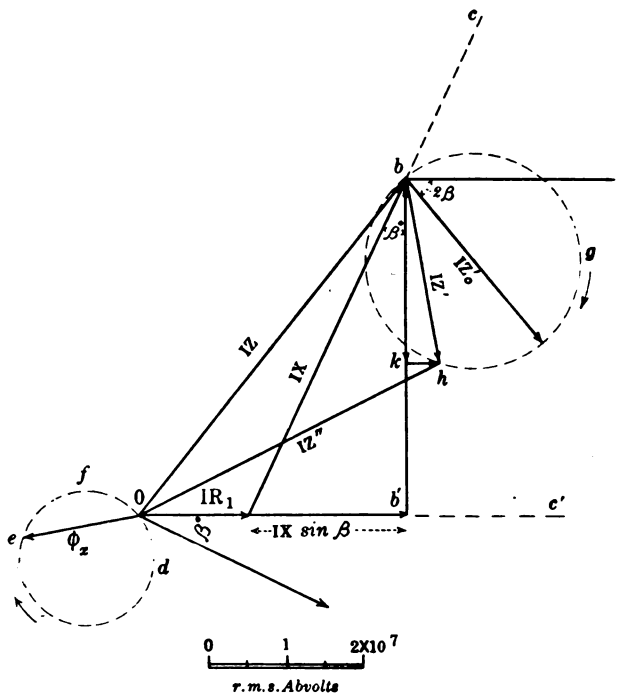

FIG. 8—E. M. F. DIAGRAM AT 1028 CYCLES PER SEC.—DIAPHRAGM FREE

The inductive voltage or voltage expended in overcoming the counter e. m. f. of induction is $a\ b$ on the diagram and is expressed by $j\ I\ \mathfrak{L}\ \omega$ abvolts $\angle$, where $\mathfrak{L}$ is a vector inductance of slope $\sphericalangle\ \beta°$ as defined by the relation

$$\mathfrak{L} = 4\ \pi\ N^2\ \mathfrak{P} \qquad \text{abhenries} \angle \quad (6a)$$

where $\mathfrak{P}$ is a vector permeance expressed in maxwells per gilbert $\angle$, or 1/oersteds $\angle$. The corresponding apparent resistance voltage is $O\ b'$ traversing the locus $a\ b'\ c'$. The

apparent reactance voltage is $b'\,b$. This apparent reactance voltage, as obtained from impedance measurements with damped diaphragm, is

$$I\,|\,X\,|\cos\beta = I\,|\,\mathfrak{L}\,|\,\omega\cos\beta \qquad \text{abvolts (7)}$$

Here the symbol $|\,\mathfrak{L}\,|$ denotes the size of $\mathfrak{L}$ as a scalar.

The apparent inductance $\mathfrak{L}$ of the winding should also remain constant. Actually, observations show that the apparent inductance diminishes as the frequency is increased, owing to the influence of changes in magnetic skin effect, which are assumed to be negligible in the stage of telephone theory here aimed at.

Fig. 8 represents the corresponding planevector e. m. f. diagram, with diaphragm free. In this diagram, the additional periodic flux ϕ_x, taken from Fig. 6, is included, and runs over the locus $d\,e\,f$. The vector impressed voltage $I\,Z''$, travels over the straight line locus $a\,b\,c$, as in Fig. 7; but at its end, there is added an e. m. f. locus due to the time variation of ϕ_x, which is a circle $b\,g\,h$. This circle moves parallel to itself, along the lengthening line $a\,b\,c$. The vector $b\,h$ is in leading quadrature to ϕ_x, in the position $O\,e$, and represents the motional impedance voltage $I\,Z'$ at this frequency, or the voltage expended in overcoming the displacement e. m. f. of the diaphragm considered as a motor element. The e. m. f. $I\,Z''$ which must be impressed at receiver terminals, in order to maintain constant current I, is represented by $O\,h$ abvolts. The component $O\,h'$, is the cophase component of e. m. f. and $b'\,k$ the quadrature or reactive component.

Impedances, Damped, Free and Motional. Figure 7, the damped voltage diagram, might also serve as an impedance diagram, if its various vectors are divided by the constant current I, and if, therefore, these vectors are read off to an appropriate scale of absohms. In Fig. 9, the transition is made, however, to a convenient resistance scale. The apparent resistance is $O\,b = R_1 + |\,X\,|\sin\beta$ absohms, the apparent reactance $b'\,b = |\,X\,|\cos\beta$ absohms, and the impedance with damped diaphragm

$$Z = O\,b = R_1 + |\,X\,|\sin\beta + j\,|\,X\,|\cos\beta = R_1 + X \text{ absohms } \angle \qquad (8)$$

As the impressed frequency increases, the impedance travels over the locus $a\,b\,c$. In Fig. 1 of the paper referred to, (Bibliography 17), the vector damped impedance locus makes an

angle of $\beta = 25.°3$, very nearly, with the reactance axis, between $f = 700 \sim$ and $f = 1500 \sim$.

Fig. 10 shows the corresponding impedance of the instrument with the diaphragm free. The vector $O\,b$ pursues the same path $a\,b\,c$ as in Fig. 9; but at its end, there is added a traveling circular locus $g\,h\,k$. The impedance of the instrument is Z'', and we have the vector relation.

$$Z' = Z'' - Z \qquad \text{absohms} \angle \quad (9)$$

The vector path of Z', plotted separately, is the stationary circle

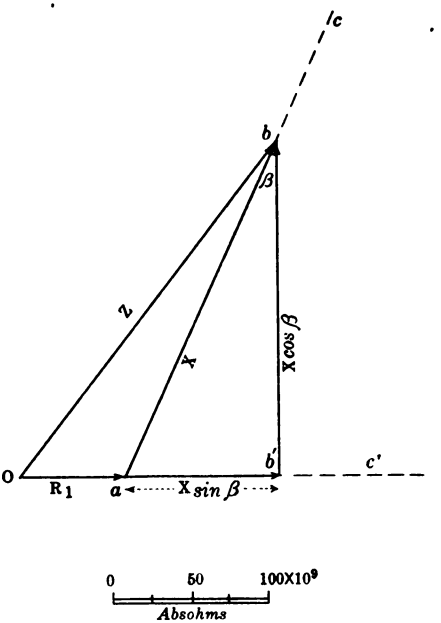

FIG. 9—IMPEDANCE DIAGRAM—DIAPHRAGM DAMPED

$b\,g\,h$, and this circle is obtained from experimental observations at constant current. It passes through the origin of coordinates like the circle of Fig. 27. It has a diametric depression angle, or lag angle, of $2\ \beta$, because the diameter being produced at resonant frequency, the displacement velocity $\dot{x}$ of the diaphragm is then in phase with the flux ϕ_i, which is $\beta°$ behind the current, and the displacement x is then in lagging quadrature with the velocity or $(90° + \beta)$ behind the current. But ϕ_x is $\beta°$ behind the displacement x (Fig. 6) and is therefore $90° + \beta°$ behind the velocity $\dot{x}$ or $90° + 2\ \beta°$ behind I. The e. m. f.

$I\,Z'$, Fig. 8, due to the variation of ϕ_x, being in leading quadrature therewith, is then 2 $\beta°$ behind I, and Z', at resonance, is thus 2 $\beta°$ behind the reference phase, or resistance axis.

Every telephone receiver has its own particular motional impedance circle, which is very sensitive to changes in temperature or in mechanical adjustment. Motional impedance circles differ:

1. In their size, or diametral length.
2. In their depression angle 2 β.
3. In the distribution of frequencies around the circle.

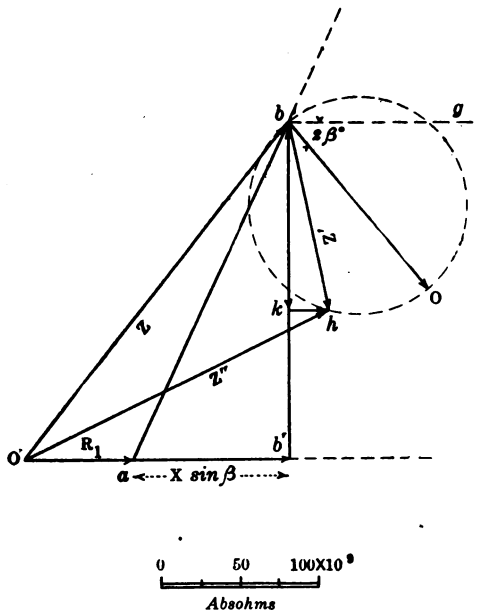

FIG. 10—IMPEDANCE DIAGRAM—DIAPHRAGM FREE

Sharply resonant instruments will pass from the lower quadrantal frequency f_1, to the upper f_2, over half the circle, with a change of only a very few cycles per second. On the other hand, bluntly resonant instruments may require a change in frequency of several hundred cycles per second, to pass over the same range of locus.

Having found by observation the depression angle 2 β of the motional impedance circle, the angle β is known, and the construction of Figs. 9 and 10 may be carried out, with the angle at $b\,b'$ made equal to β. Knowing the apparent resistance $O\,b'$, and the apparent reactance $b'\,b$, at various impressed

frequencies, as well as $\beta°$, we can readily compute R_1 and $\mathfrak{L}$ from (7) and (8). R_1 should theoretically be substantially constant under the assumption that $\mathfrak{L}$ is constant. For the instrument here considered, the following Table gives the values of R_1 as computed from the observed resistances with damped diaphragm, and the angle β assumed constant at resonant value.

Frequency cycles per sec.	Angular Velocity rad. per sec. ω	Measured Resistance absohms at 20 deg. cent. R	Active component of inductive resistance $R_h = \omega \mathfrak{L}_0 \sin \beta$	Reactive component of inductive resistance $X = \omega \mathfrak{L}_0 \cos \beta$	$R_1 = R - R_h$ absohms
0	0	86.7×10^9	0×10^9	0×10^9	86.7×10^9
429	2694	124 "	41.9 "	89 "	82.1 "
702	4420	145 "	68.8 "	146 "	76.2 "
923.4	5801	162 "	90.5 "	191.5 "	71.5 "
*1015	6378	168.4 "	99.5 "	210.5 "	68.6 "
1306	8202	189. "	128 "	270.7 "	61. "
1507	9460	204 "	147.6 "	314.1 "	56.4 "

*Resonant frequency.

The steady apparent fall in the values of R_1 as the frequency was increased, may be attributed to the influence of changes in magnetic skin effect here neglected.

Electric Power, Damped and Free. With the diaphragm damped, the vector diagram of either Fig. 7, or Fig. 9, might serve as a power diagram, if read off to a corresponding scale of abwatts, or ergs per second. The power diagram is repeated, however, in Fig. 11 to a convenient power scale. $O\,a$ is active power, $I^2 R_1$ abwatts, expended in heating the winding. $I^2 X$ is the vector power $a\,b$, expended in the magnetic circuit. It follows the locus $a\,b\,c$, as the frequency is varied. The active component $a\,b' = I^2 \mid X \mid \sin \beta$, is dissipated thermally in the magnetic circuit, in hysteresis and eddy currents. The reactive component $b'\,b = I^2 \mid X \mid \cos \beta$ is utilized in alternately storing and releasing energy in the magnetic circuit.

When the diaphragm is freed, the power conditions are indicated vectorially in Fig. 12. $O\,a$, as before, is the thermal power $I^2 R_1$, dissipated in the winding. The power delivered to the magnetic circuit is $a\,h$, which is in leading quadrature to the resultant flux ϕ, see Fig. 6. The active component $a\,h'$ includes the power expended in hysteresis and eddy currents, and also the active mechanical power delivered from the

magnetic circuit to the diaphragm. The reactive component $h' h$ includes power utilized in storing and releasing magnetic energy in the magnetic circuit, and also power utilized in storing and releasing reactive mechanical energy in the diaphragm.

Mechanical Velocity, Damped and Free. When the diaphragm is damped, the vibrational velocity of displacement must be zero. When, however, the diaphragm is free, the velocity of displacement $\dot{x}$ will have a definite magnitude and phase. If we assume the vibromotive force $f_i = Og$ r. m. s.

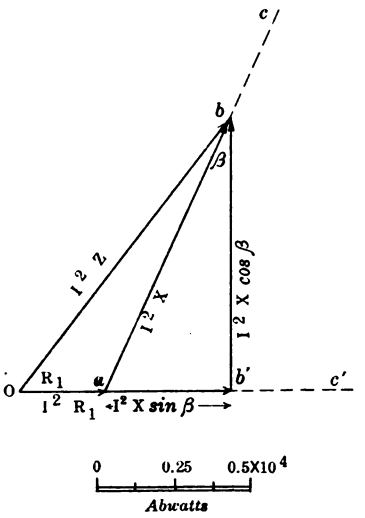

FIG. 11—ELECTRIC POWER DIAGRAM—DIAPHRAGM DAMPED

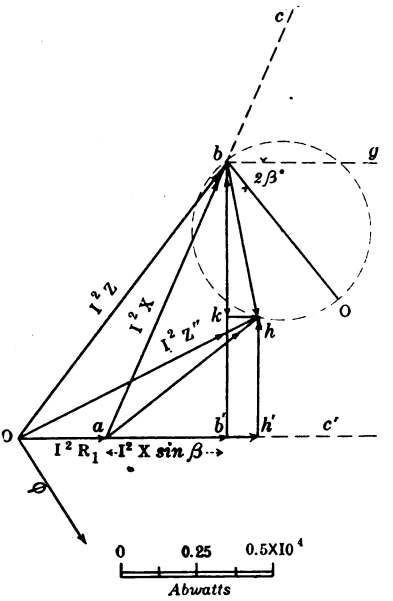

FIG. 12—ELECTRIC POWER DIAGRAM—DIAPHRAGM FREE

dynes, Fig. 13, to remain constant at all frequencies, the locus of the vector velocity $\dot{x}$ will be the circle $O\ a\ b\ c$. This mechanical relation has its complete electric analogy in the simple alternating-current circuit of Fig. 14, where a simple harmonic e. m. f. E, of constant r. m. s. magnitude, and at standard phase, supplies the simple circuit $C\ R\ L$ at successively varied frequencies. All of the resistance of the circuit, assumed constant, is located in the resistor R, all of the inductance in the inductor L, and all the capacitance in the condenser C. At a very low frequency, the impedance of the circuit will

be large and entirely due to the condenser C. The alternating current will be very feeble and will lead the impressed e. m. f. by 90°. As the frequency is raised, the impedance diminishes, both in size and in slope. The current strength will therefore increase in magnitude, and come more nearly into phase with E. As is shown in Fig. 15, when the resonant frequency of the circuit is attained, the current will be a maximum at I_0, and will be in phase with E. Finally, as the frequency becomes very high, the current will disappear, and lag 90° behind E. The locus of the vector current will be the circle $O\ a\ b\ c$, Fig.15.

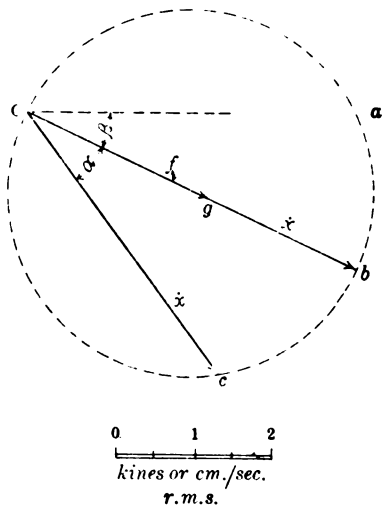

FIG. 13 — VELOCITY DIAGRAM —DIAPHRAGM FREE — CONSTANT V. M. F. AND VARIED FREQUENCY

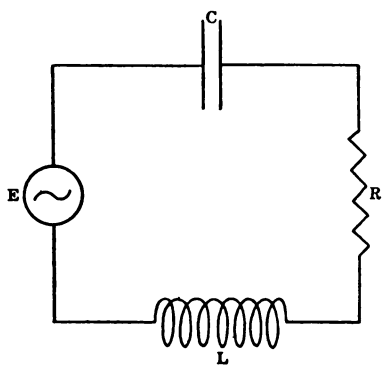

FIG. 14—SIMPLE ALTERNATING-CURRENT CIRCUIT UNDER CONSTANT E. M. F. AND VARIED FREQUENCY

If, in the mechanical system of the diaphragm, the equivalent mass replaces the inductance L, the stiffness s of the diaphragm, replaces $1/C$, and the mechanical resistance to motion r replaces R; also the vibromotive force f_i replaces E; then the vibrational velocity $\dot{x}$ will correspond both in magnitude and phase to the alternating current strength I. The phase lag α of the velocity is then equal to the slope of the mechanical impedance

$$r + j\,(m\,\omega - s/\omega) \qquad \text{mechanical ohms } \angle$$

Mechanical Displacement. The mechanical displacement of the diaphragm at elongation corresponds, in the electrical

system of Fig. 15, to the displacement of electricity at cyclic elongation. It is represented in Fig. 16 by the vector $O\,c$. This vector is in lagging quadrature to the vector $O\,c$ of Fig. 13, at one and the same impressed frequency. The locus of x is the displacement curve $a\,b\,c\,O$.

Force Diagram Damped and Free. If the diaphragm is damped, any single vibromotive force (v. m. f.) f_i, Fig. 17a, will develop a counter v. m. f. f_c, which will make the resultant force zero; so that no displacement results. If, however, the diaphragm is free, there will be four forces called into action, in similarity to those in the corresponding electrical case of Fig. 15; namely, the impressed single v. m. f. f_i, Fig. 17, in phase with

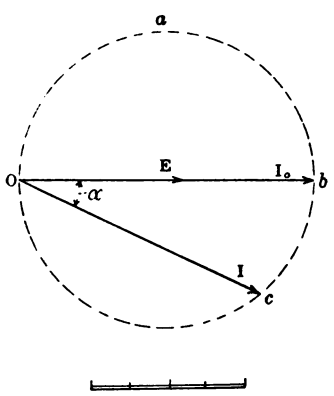

FIG. 15—CURRENT DIAGRAM IN SIMPLE A-C. CIRCUIT, UNDER CONSTANT E. M. F. AND VARIED FREQUENCY

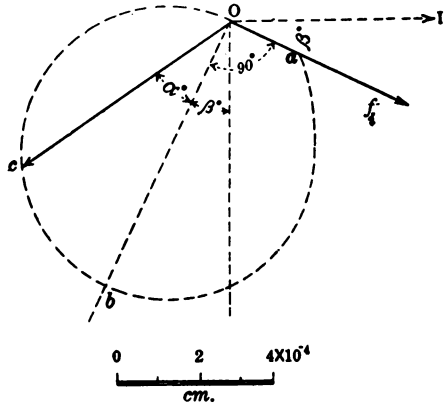

FIG. 16—DISPLACEMENT DIAGRAM—DIAPHRAGM FREE

the flux ϕ_i; the frictional resisting force $-\,r\,\dot{x}$ dynes, the inertia force $-\,j\,\omega\,m\,\dot{x}$ dynes, and the elastic force $j\,\frac{s\,\dot{x}}{\omega}$ dynes. These are represented in Fig. 17 by the vectors $O\,a$, $O\,b$, $O\,c$ and $O\,d$. Since $O\,c$ and $O\,d$ must be mutually opposite, their difference $O\,e$, combined with $O\,b$, must balance the impressed force $O\,a$. This relation determines the position and magnitude of the velocity $\dot{x}$. We have already seen that as the frequency is changed from a small to a large value, the locus of $\dot{x}$ is a circle about O. At mechanical resonance, $\dot{x}$ will have a maximum size and zero slope, or will coincide with f_i in direction. The

displacement x, not indicated in Fig. 17, will always have the direction $o\,c$, 90° lagging behind $\dot{x}$.

The vector force equation is in the rotatable vector diagram of Fig. 17.

$$m\ddot{x} + r\dot{x} + s\,x = f_i \qquad \text{r. m. s. dynes} \angle \quad (10)$$

or since x is a simple harmonic displacement of the type $x_m\,\epsilon^{j\omega t}$,

$$j\,\omega\,m\dot{x} + r\dot{x} + \frac{s\,\dot{x}}{j\omega} - f_i = 0 \qquad \text{r. m. s. dynes} \angle \quad (11)$$

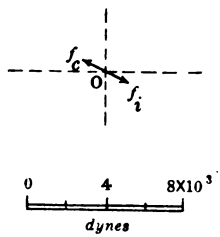

FIG. 17A—FORCE DIAGRAM —DIAPHRAGM DAMPED

FIG. 17—FORCE DIAGRAM FOR THE IDEAL CASE OF A DIAPHRAGM FREE TO VIBRATE UNDER A SINGLE IMPRESSED V. M. F. f_i R. M. S. DYNES

or $-j\,\omega\,m\dot{x} - r\dot{x} + j\dot{x}\,s/\omega + f_i = 0 \qquad$ r. m. s. dynes $\angle$ (12)

whence

$$\dot{x} = \frac{f_i}{r + j\,(m\,\omega - s/\omega)} \qquad \text{r. m. s.} \frac{\text{cm.}}{\text{sec.}} \angle \quad (13)$$

which corresponds completely to Ohm's law in the vector simple alternating-current case.

The specific magnetic force acting at any time on the diaphragm, towards the magnetic poles, is $\frac{\mathfrak{B}^2}{8\,\pi}$ dynes per sq.

cm., where $\mathfrak{B}$ is the total magnetic flux density. This flux density comprises the permanent magnetic flux density $\mathfrak{B}_0$ gausses, and the alternating flux density $\mathfrak{B}$ instantaneous gausses. The total magnetic force is thus

$$\frac{2S}{8\pi}(\mathfrak{B}_0 + \mathfrak{B})^2 = \frac{S}{4\pi}(\mathfrak{B}_0 + \mathfrak{B})^2$$

$$= \frac{S}{4\pi}(\mathfrak{B}_0^2 + 2\,\mathfrak{B}_0\,\mathfrak{B} + \mathfrak{B}^2) \quad \text{instantaneous dynes (14)}$$

Since $\mathfrak{B}^2$ is very small by comparison with $\mathfrak{B}_0^2$, it may be neglected in the summation, and the instantaneous force in the diaphragm is

$$\frac{S}{4\pi}(\mathfrak{B}_0)^2 + \frac{S}{4\pi} \cdot 2\,\mathfrak{B}_0\,\mathfrak{B} \quad \text{instantaneous dynes (15)}$$

The first term is the permanent force which flexes the diaphragm from its plane position, and which plays no material part in the alternating regime here considered. The second term includes the periodic quantity $\mathfrak{B}$, which may be represented vectorially by a vector of size $\mathfrak{B}_i$ r. m. s. gausses, lagging $\beta°$ behind the exciting m. m. f. $\mathfrak{F}_i$. But $S\,\mathfrak{B}_i = \phi_i$ the r. m. s. vector flux in phase with $\mathfrak{B}_i$, so that in the damped condition,

$$\phi_i = \mathfrak{F}_i\,\mathcal{P} = 4\pi N I \mathcal{P} \quad \text{r. m. s. maxwells} \angle \text{ (16)}$$

where I is the r. m. s. exciting current in absamperes, N the total number of turns including both coils, and $\mathcal{P}$ a vector permeance which possesses a lag angle $\beta°$. Consequently from (**15**)

$$f_i = 2\,\mathfrak{B}_0 N \mathcal{P} I = A I \quad \text{r. m. s. dynes} \angle \text{ (17)}$$

or in a bipolar instrument $A = 2\,\mathfrak{B}_0 N \mathcal{P}$ r. m. s. dynes per absampere $\angle$ (**18**)

A is a vector force factor with a lag angle of $\beta°$.

We have thus far supposed that only one periodic force f_i acts on the diaphragm. There is, however, a second periodic force introduced by the flux ϕ_x, due to the displacement m. m. f., the magnitude of which is proportional, by (**6**), to the maximum cyclic value of the displacement, and which has the same phase as that displacement.

We have already shown in (**6**) that the displacement m. m. f. is

$$F_x = 2\,\mathfrak{B}_0\,x \quad \text{r. m. s. gilberts} \angle \text{ (19)}$$

This may be considered as similar to the m. m. f. of current

$$\mathfrak{F}_i = 4\pi N I \qquad \text{r. m. s. gilberts} \angle \quad (20)$$

so that a certain number of turns N' multiplied by the r. m. s. vector displacement, would produce the same m. m. f. as the actual number of turns N multiplied by the corresponding r. m. s. vector current. Consequently, in the case of a bipolar receiver

$$N' = \frac{\mathfrak{B}_0}{2\pi} \qquad \text{equivalent turns} \times \frac{\text{absampere}}{\text{cm.}} \quad (21)$$

If we consider the ratio

$$\frac{N'}{N} = p \qquad \frac{\text{absampere}}{\text{cm.}} \quad (22)$$

which, in the instrument considered, was 0.168,

$$\mathfrak{F}_x = 4\pi N' x \qquad \text{r. m. s. gilberts} \angle \quad (23)$$

and from (17)

$$f_x = p A x = 2 p \mathfrak{B}_0 N \mathcal{P} x \qquad \text{r. m. s. dynes} \angle \quad (24)$$

It may be noted, in passing, that just as in the case of a vector electromagnetic inductance

$$\mathfrak{L} = A/p = 4\pi N^2 \mathcal{P} \qquad \text{abhenries} \angle \text{ or ergs per absamp}^2 \angle \quad (25)$$

so $$p A = 4\pi N'^2 \mathcal{P} \qquad \frac{\text{r. m. s. dynes}}{\text{cm.}} \angle \quad (26)$$

and is a quantity bearing resemblance to an inductance. From (25) and (26)

$$A = 4\pi N N' \mathcal{P} \qquad \frac{\text{r. m. s. dynes}}{\text{absamp}} \angle \quad (27)$$

so that, in this sense, the force factor A bears resemblance to a mutual inductance.

The additional force f_x, due to ϕ_x, may be introduced into the problem either (1) by vector summation with f_i, to form a vector resultant force f, corresponding to ϕ in Fig. 6; or (2), by retaining f_i as the sole active force on the diaphragm, and introducing the action of f_x in the form of a mechanical impedance. For practical purposes, the latter method is to be preferred, just as in the simple alternating-current circuit, the effect of a counter e. m. f. of self induction is usually treated as an impe-

dance, instead of being combined vectorially with the impressed e. m. f. in the numerator of Ohm's law.

The force f_x lags behind the displacement x by the angle $\beta°$, according to the relation

$$f_x = p A x = \frac{p A \dot{x}}{j \omega} = -j p A \frac{\dot{x}}{\omega} \quad \text{r. m. s. dynes} \angle \quad (28)$$

or $90° + \beta°$ behind the phase of the velocity $\dot{x}$.

In Fig. 18, the force f_x is represented in a particular case with the diaphragm free. Here the m. m. f. $\mathfrak{F}_i$ is taken as of reference phase, with f_i lagging $\beta°$ behind it. This force f_i must now equilibrate four forces; namely, the elastic force $O\,d$, the

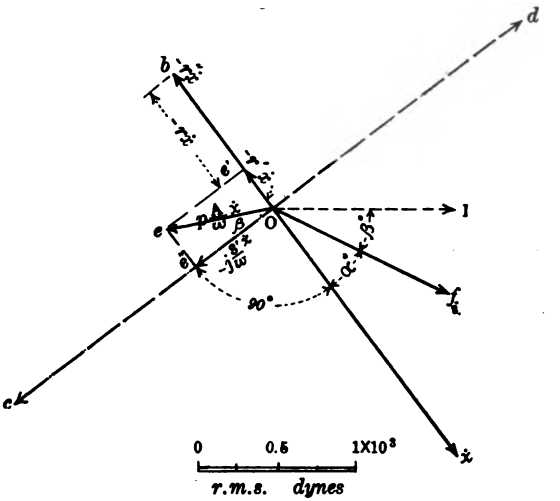

FIG. 18—FORCE DIAGRAM INCLUDING MAGNETIC FORCE DUE TO DISPLACEMENT—DIAPHRAGM FREE ENLARGED SCALE

inertia force $O\,c$, the frictional force $O\,b$, and the new magnetic force $O\,e$, whose components, along the $O\,b$ and $O\,c$ directions, are indicated as $O\,e'$ and $O\,e''$ respectively. With $\mathfrak{F}_i$ at reference phase, the locus of the new force $O\,e$ is a displacement-admittance locus like $a\,b\,c$ in Fig. 4; but considered solely with reference to the velocity $\dot{x}$, $O\,e$ always lags with respect thereto by $90° + \beta°$. The components $O\,e'$ and $O\,e''$ may be defined as $-r'\dot{x}$ and $\frac{-j s' \dot{x}}{\omega}$ respectively; where r' is a virtual frictional resistance, and s' a virtual stiffness coefficient.

The diaphragm therefore behaves as though its frictional resistance were increased by

$$r' = \frac{p\,|A|}{\omega} \sin \beta \qquad \frac{\text{dynes}}{\text{kine}} \qquad (29)$$

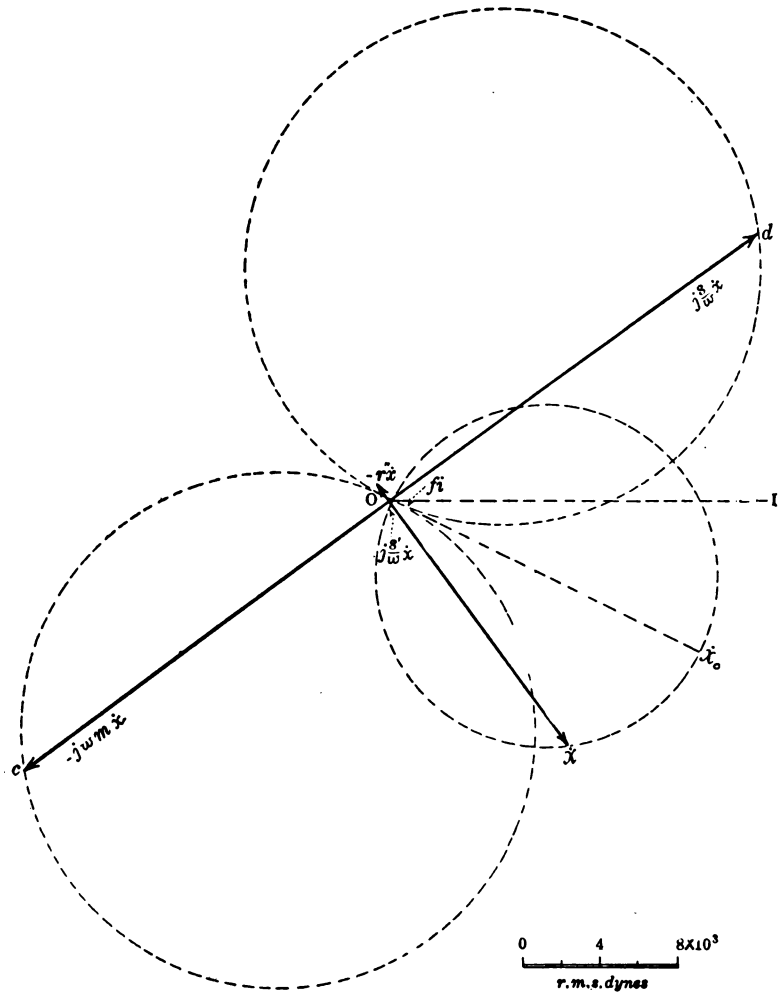

FIG. 19—FORCE DIAGRAM—COMPLETE—INCLUDING MAGNETIC FORCE DUE TO DISPLACEMENT

while the stiffness of the diaphragm is apparently diminished by

$$s' = p\,|A| \cos \beta \qquad \frac{\text{dynes}}{\text{cm.}} \qquad (30)$$

The values of r' and s' can be assigned, when A, β, and p are known. In the instrument considered, at resonance, $r' = 68.8$ dynes per kine and $r = 199$ dynes per kine, r' diminishing, according to our theory, as ω is increased. Also s' is 9.3×10^5 dynes per cm. as against $s = 376 \times 10^5$. According to our theory, s' is thus only about 3 per cent of s, at all frequencies.

In Fig. 19, the loci of the inertia and stiffness forces, $O\,c$ and $O\,d$, are represented to scale, without including therein the components $O\,e'$ and $O\,e''$, Fig. 18, of the added magnetic force f_x. The directions of motion in the loci, with increase of frequency are all clockwise. The locus of $O\,d$ is a displacement-admittance locus, obtained from the circular locus of $\dot{x}$ by time integration; whereas the locus of $O\,c$ is obtained from that of $\dot{x}$ by time differentiation.

The total mechanical impedance of the diaphragm from (**13**) and (**28**) is

$$z' = r + j\,(m\,\omega - s/\omega) + j\,\frac{p\,A}{\omega} \qquad \frac{\text{dynes}}{\text{kine}} \;\angle\; (\mathbf{31})$$

The reciprocal of this quantity, or mechanical admittance y' is

$$y' = 1/z'$$

$$= \frac{1}{\sqrt{r''^2 + (m\,\omega - s''/\omega)^2}} \angle\, \tan^{-1}\left(\frac{m\,\omega - s''/\omega}{r''}\right)$$

$$= \frac{1}{\sqrt{(r + r')^2 + \left(m\,\omega - \dfrac{s - s'}{\omega}\right)^2}}$$

$$\angle\, \tan^{-1}\left(\frac{m\,\omega - \dfrac{s - s'}{\omega}}{r + r'}\right) \qquad \frac{\text{kines}}{\text{dyne}} \;\angle\; (\mathbf{32})$$

The values of r' and s' are to be taken from (**29**) and (**30**). This vector admittance y', multiplied by the constant impressed mechanical force f_i, due to the constant alternating current, gives the mechanical velocity $\dot{x}$, or

$$\dot{x} = f_i\,y' = A\,y'\,I \qquad \text{r. m. s.}\ \frac{\text{cm.}}{\text{sec.}} \;\angle\; (\mathbf{33})$$

and the r. m. s. displacement x by

$$x = -j\,f_i\,y'/\omega = -j\,A\,y'\,I/\omega \qquad \text{r. m. s. cyclic cm.} \;\angle\; (\mathbf{34})$$

The actual maximum cyclic displacement of the diaphragm is then

$$x_m = |x| \sqrt{2} \qquad \text{max. cyclic cm.} \quad (35)$$

Motional Electromotive Force Diagram. Referring to Fig. 16, the vector displacement Oc is determined by equation (34), and the vector velocity Oc in Fig. 13, by equation (33), in terms of the motional constants r, r', m, s and s', as well as A. The displacement flux ϕ_x, Fig. 8, is then obtained through (23) or

$$\phi_x = \frac{p A x}{N'} = 4 \pi N' x \mathcal{P} \qquad \text{maxwells} \angle \quad (36)$$

The e. m. f. produced by ϕ_x in the coils is the motional e. m. f. and is

$$I Z' = j \omega \frac{p A x}{N'} N = j \omega A x$$
$$= A \dot{x} = A^2 y' I \qquad \text{abvolts} \angle \quad (37)$$

It may be noted that since $\dot{x}$ is a velocity in kines, the vector dimensions of A are not only expressed by dynes per absampere, as in (18) or (27), but also by abvolts per kine, as in (37).

The vector motional e. m. f. $I Z'$, Fig. 8, is in leading quadrature to $O e$, the displacement flux. Since in (37), this vector is directly proportional to the velocity $\dot{x}$, which has been shown to travel over a circular locus, when, as in (13), a single periodic force is impressed upon the diaphragm, the motional e. m. f. $I Z'$ must also have a circular locus, as shown in Fig. 8, when the second force f_x is negligible; *i. e.*, when p in (28) may be taken as zero. When p is appreciable, the subsidiary constants r' and s' are introduced into the motional equations (32) and (33). It will be seen that s' merely reduces the stiffness coefficient s of the diaphragm by the same amount at all frequencies; but r' varies with the frequency inversely, as shown by (29). The theoretical effect of r' is therefore to distort the locus of the motional e. m. f. $I Z'$, from a circle, to an extent depending on the magnitude of $p A$, and also upon the range of frequency necessary for the execution of the circle; *i. e.*, upon the bluntness of mechanical resonance. Since in a bipolar instrument

$$p A = \frac{\mathfrak{B}_0^2 \mathcal{P}}{\pi} \qquad \frac{\text{dynes}}{\text{cm.}} \angle \quad (38)$$

an instrument which has a relatively powerful permanent magnetic flux density $\mathfrak{B}_0$ in the airgaps, and also large magnetic-circuit permeance, is one in which the force f_x tends to be greatest, by (**28**). This, with a large value of β and a wide range of ω for executing the circle, would give rise to the largest distortion. In practice, the distortion is usually not sufficiently serious to be very noticeable, probably because the range in ω within which half of the circle is executed, is ordinarily only a few hundreds of radians per second. In the case considered, $\omega_2 - \omega_1 = 305$.

It is evident, moreover, from (**37**) that the lagging displacement of vector $I\,Z'$ with respect to I, is that of $A^2\,y'$, and since, at resonance, the slope of y' vanishes (**32**), it will then be the displacement of A^2, or $-2\,\beta°$, and $A^2 = Z_0'\,r''$.

At resonance, the size of $I\,Z'$, the motional e. m. f. will, by (**37**) be

$$I\,Z_0' = \frac{A^2\,I}{r''} \qquad \text{abvolts} \angle \quad (\mathbf{39})$$

Motional Impedance. Referring to Fig. 10, the motional impedance executes a circular locus similar to that in Fig. 8, neglecting the disturbing influence of r' at different frequencies. At resonance, its size is

$$Z'_0 = A^2/r'' \qquad \text{absohms} \angle \quad (\mathbf{40})$$

and its slope is that of A^2 or $-2\,\beta°$.

From an experimental standpoint, the motional-impedance circle is of primary importance, as, from it, the motional constants may be derived, if the maximum cyclic displacement at resonance

$$x_m = |\,x_0\,|\,\sqrt{2} \qquad \text{cm.} \quad (\mathbf{41})$$

can be measured.

Technique for Deriving the Constants A, m, r'', r', r, s'', s, p and β. (1) The motional-impedance circle is obtained from observations of the apparent resistance and reactance of the instrument, both free and damped, with constant testing current, under adjustably varied frequency. This gives the resonant maximum value Z'_0 and its slope $-2\,\beta°$ at ω_0 the angular velocity of apparent resonance; also the quadrantal

*See technique in Bibliography 17, p. 469.

values ω_1 and ω_2, or their equivalents.* We thus obtain the total damping constant

$$\Delta = \frac{\omega_2 - \omega_1}{2} = \frac{r''}{2m} \qquad \text{hyps per sec. (42)}$$

and

$$\omega_0 = \sqrt{s''/m} \qquad \text{rad. per sec. (43)}$$

(2) The amplitude of displacement x_m over the poles at resonance is measured for the measuring current I. Hence

$$A = \frac{I Z'_0}{j x_0 \omega_0} = \frac{I_m Z'_0}{j x_m \omega_0} = \frac{I Z_0'}{x_0} \qquad \text{abvolts per kine } \angle \text{ (44)}$$

Then from (**40**)

$$r'' = A^2/Z_0' \qquad \text{dynes per kine (45)}$$

Hence by (**42**)

$$m = \frac{r''}{2\Delta} \qquad \text{gm. (46)}$$

Also by (**43**)

$$s'' = m\,\omega_0^2 \qquad \text{dynes per cm. (47)}$$

Having ascertained the value of the vector damped inductance £, at resonant impressed frequency, during the measurements of damped impedance, we find by (**25**)

$$p = A/£ \qquad \text{absamp per cm. (48)}$$

We can then compute the value of the resistance component r' of f_x by (**29**) at resonance

$$r' = \frac{p\,|A|}{\omega_0} \cdot \sin\beta \qquad \text{dynes per kine (49)}$$

and hence r, neglecting changes in r' with frequency,

$$r = r'' - r' \qquad \text{dynes per kine (50)}$$

Next s' can be computed from (**30**) and s found by the relation

$$s = s'' + s' \qquad \frac{\text{dynes}}{\text{cm.}} \quad \text{(51)}$$

The total number of turns N is supposed to be known, from which $\mathfrak{B}_0$ is obtainable through the bipolar relation

$$\mathfrak{B}_0 = 2\pi p N \qquad \text{gausses (52)}$$

The equivalent number of turns N' for computing the displacement m. m. f. is

$$N' = p N \qquad \frac{\text{absamperes}}{\text{cm.}} \qquad (53)$$

assuming that N is a pure numeric. The quantities $p A$, $\mathfrak{F}_i$, ϕ_i and f_i are then easily found.

Motional Power. If a simple periodic m. m. f. of $\mathfrak{F} = 4 \pi N I$ r. m. s. gilberts $\angle$ at the reference phase of I r. m. s. absamperes, acts upon a leackanceless magnetic circuit of vector permeance $\mathcal{P}$ maxwells per gilbert $\angle$, the vector magnetic flux thereby produced, neglecting harmonics, which are powerless, is

$$\phi = \mathfrak{F} \mathcal{P} \qquad \text{r. m. s. maxwells } \angle \qquad (54)$$

The phase of the flux will have the slope $-\beta°$ of $\mathcal{P}$, with respect to the phase of the exciting current and m. m. f. The e. m. f. which will be induced in the coil will be

$$E = -j \omega N \phi = -j \omega N \mathfrak{F} \mathcal{P} \quad \text{r. m. s. abvolts } \angle \qquad (55)$$

The power of this e. m. f., expressed electrically, is

$$P = E I = -j \omega N \phi I \qquad \text{abwatts } \angle \qquad (56)$$

the slope of I being taken as zero.* The real component of P will be active power, expended thermally in the magnetic circuit, and the quadrature component will be reactive power expended in cyclically storing and releasing magnetic energy in the circuit. But (**56**) may be written**

$$P = -j \frac{\omega \mathfrak{F} \phi}{4 \pi} = -j (f/2) \mathfrak{F} \phi \qquad \text{abwatts } \angle \qquad (57)$$

where $\mathfrak{F}$ is taken as at standard phase, and ϕ has the lagging slope of $\beta°$ with respect thereto. The negative sign attached to the expressions in (**56**) and (**57**) indicates that the power is absorbed in the magnetic circuit.

---

*Bibliography 7.

*The power exerted in a magnetic circuit by a simple alternating m. m. f. $\mathfrak{F}$ r. m. s gilberts, at zero slope, on a simple alternating flux ϕ r. m. s. maxwells $\angle$, is, in the C. G. S. system,

$$\dot{P} = \frac{F}{4 \pi} \cdot \frac{d \phi}{d t} \qquad \text{abwatts } \angle \qquad (57a)$$

where the real component is average active power, and the imaginary component max. cyclic reactive power. Here $\frac{d \phi}{d t}$ corresponds to electric current.

In Fig. 20, the vector m. m. f. $\mathfrak{F}_i$ is drawn to the same reference phase as I. The flux ϕ_i, thereby produced, with the diaphragm damped, is indicated as lagging $\beta°$ behind $\mathfrak{F}_i$. The induced e. m. f. E, lags $90° + \beta°$ behind $\mathfrak{F}_i$. The vector power $E\,I$, taken with I as of zero slope, is $O\,a$. Its real component, $O\,b$, is dissipated. The undissipated or reactive component is $b\,a$.

In Fig. 21, the r. m. s. m. m. f. and r. m. s. flux are represented without reference to e. m. fs. Their vector product $\mathfrak{F}_i\,\phi_i$, taking $\mathfrak{F}_i$ as of standard phase, would be along the dotted line $O\,c$. Taking $-f/2$ times this product, as called for in (**57**), we obtain, to a power scale, the vector $O\,d$, Fig. 22.

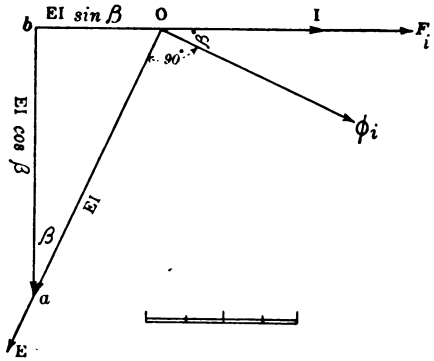

FIG. 20—DIAGRAM OF A R.M.S. M.M.F., THE R. M. S. FLUX THEREBY PRODUCED, THE CONSEQUENT E. M. F. AND THE VECTOR POWER

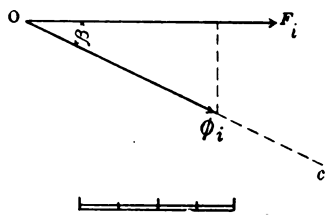

FIG. 21—FUNDAMENTAL RELATIONS OF POWER IN A MAGNETIC CIRCUIT CARRYING A R. M. S. FLUX $\phi\mathfrak{F}_i$, UNDER AN IMPRESSED R. M. S., M. M. F.

The cosine product of $f\ \mathfrak{F}_i/2$ and ϕ_i is reactive magnetic power, and the sine product, or vector product, active power liberated from the magnetic circuit. These conditions are opposite to those in the alternating electric circuit, where the cosine product is active and the sine product reactive electric power. In order to interpret this vector magnetic-circuit power correctly, we may rotate the axis $O\,X$ of reference, through $-90°$, into the position $O\,A$. The component $Oc = -(f/2)\,\mathfrak{F}_i\,|\phi_i|\sin\beta$ is then the average active power, absorbed by the magnetic circuit, and liberated from it, usually as heat; while the reactive component $O\,b = -(f/2)\,\mathfrak{F}_i\,|\phi_i|\cos\beta$ is power absorbed in storing and releasing magnetic energy.

If, however, we consider the vector power delivered by the electric circuit to the magnetic circuit, it will have the opposite sign to $O\,d$, or will be $O\,d$ reversed, and equal to the vector $O\,d'$, whose components are $O\,c' = +\ (f/2)\ \mathfrak{F}_i\ |\phi_i| \sin \beta$, liberated active power and $O\,b' = +\ (f/2)\ \mathfrak{F}_i\ |\phi_i| \cos \beta$ reactive power engaged in storage.

In Fig. 23, we have the vector magnetic power delivered from the electric circuit with the diaphragm damped. The real component is $O\,a'$ and the reactive component $a'\,a$.

When the diaphragm is free, we have the displacement m. m. f. $\mathfrak{F}_x$ and its flux ϕ_x introduced into the magnetic circuit, as shown in Fig. 24. The resultant of these two m. m. fs. is

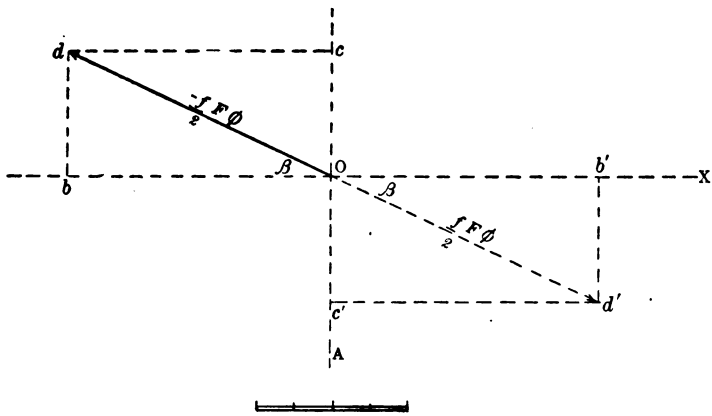

FIG. 22—POWER RECEIVED FROM AND DELIVERED TO A MAGNETIC CIRCUIT CARRYING A R.M.S. FLUX ϕ LAGGING β^0 BEHIND AN IMPRESSED R. M. S. M. M. F. $\mathfrak{F}_i$ AT FREQUENCY f CYCLES PER SEC.

$\mathfrak{F}$, and that of the two corresponding fluxes is ϕ. This magnetic-circuit vector diagram bears a close resemblance to the electric-circuit vector diagram for the simple case of an alternator driving a synchronous motor through the impedance of a connecting circuit. The m. m. fs. of Fig. 24 then correspond to e. m. fs., flux-frequencies to currents, and their respective permeance vector ratios to admittance ratios. We have

$$\mathfrak{F}_i + \mathfrak{F}_x = \mathfrak{F} \qquad \text{r. m. s. gilberts} \angle \quad (\mathbf{58})$$

If we multiply this equation by the vector resultant flux ϕ, considered for that purpose as of standard phase, we obtain

$$(f/2)\ \mathfrak{F}_i\,\phi + (f/2)\ \mathfrak{F}_x\,\phi = (f/2)\ \mathfrak{F}\,\phi \quad \text{abwatts} \angle \quad (\mathbf{59})$$

The first term is here the vector power input P_i'' delivered to the magnetic circuit by the exciting current. The second term, reversed in sign, is the vector power P_m liberated from the magnetic circuit into pure mechanical power of the diaphragm, both active and reactive, and corresponding to vector mechanical power given to a synchronous motor in an electric circuit. The term $(f/2)\mathfrak{F}\,\phi$ is the vector power P_r'' expended thermally within the magnetic circuit in overcoming its reluctance. The equation (**59**) may therefore be written

$$P_i'' - P_m = P_r'' \qquad \text{abwatts} \angle \ (\mathbf{60})$$

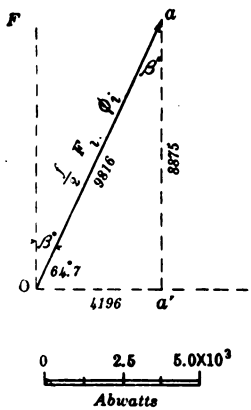

FIG. 23—POWER DELIVERED TO MAGNETIC CIRCUIT AT 1028 CYCLES PER SEC.—DIAPHRAGM DAMPED

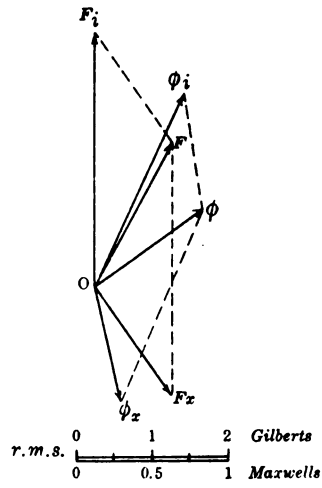

FIG. 24—DIAGRAM OF M. M. F' AND FLUXES IN MAGNETIC CIRCUIT —DIAPHRAGM FREE

In the instrument referred to, these vector values at 1028 ~ were as shown in Fig. 25, where $O\,b$ is the magnetic input of $P_i'' = 6438 \,/\, \underline{36°.8}$ abwatts, with an active component of 5156 abwatts, liberated both in heat and in mechanical power, and a reactive component of 3856 abwatts, engaged in the reactive storage of magnetic energy. P_m or the vector $O\,a$, is the power expended on the diaphragm mechanically, 3349 $\underline{/0.°7}$ abwatts, almost entirely in the active form, nearly 3349 abwatts being developed in vibratory motion $\dot{x}^2\,r$, against mechanical resistance r and 40 abwatts in reactive mechanical power; *i. e.*, power consumed in exchanging potential energy cyclically from the elastic to the inertia type. The vector $a\,b$ or P_r'' is

the power expended in the magnetic conducting circuit by the total flux ϕ in overcoming the vector reluctance $\mathfrak{R}$ of that circuit. At this frequency, it was 4199 $\angle 64°.7$ abwatts, with a real component $a\,b'$ of 1795 abwatts, expended thermally in hysteresis and eddy currents. The reactive component $b'\,b$ of 3797 abwatts is expended in maintaining the activity of cyclically storing and releasing magnetic energy of the type $\frac{\mathfrak{B}^2}{8\pi\mu}$ ergs per cu. cm. in the magnetic conducting circuit.

When the diaphragm is damped, the magnetic circuit conditions are shown in Figs. 21 and 23. Here the magnetic input at 1028 $\sim$ is 9816 $\angle 64°.7$ abwatts, with no counter m. m. f. of

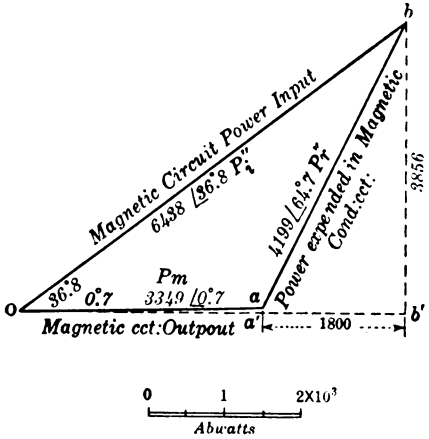

FIG. 25—MAGNETIC CIRCUIT POWER DIAGRAM—DIAPHRAGM FREE

motion. The active component $O\,a'$ is 4196 abwatts, expended entirely in heat leaving the circuit. The reactive component is 8875 abwatts, engaged in maintaining the cyclic storage and release of magnetic energy.

The motional magnetic power diagram is obtained as in Fig. 26 by subtracting the magnetic power input damped P_i, from the magnetic power input free, P_i''. The difference, at the frequency of 1028 $\sim$, is 5108 $\angle$ 79.°2 abwatts, with an active component of 957 abwatts, representing an increase of the power taken from the electric supply circuit and a negative reactive component of 5018 abwatts, representing a diminution in magnetic power of storage.

It should be observed that the active component $O\,c$ = 957

abwatts is much smaller than the power P_m = 3349 abwatts, (Fig. 25) put into the diaphragm. The difference of 2392 active abwatts is diverted from the power previously wasted in the magnetic circuit of 4196, Fig. 23, only 1800 abwatts ($a\ b'$ Fig. 25), being wasted thermally when the diaphragm is freed. Consequently, the motional power diagram does not reveal on its real axis all the power delivered to the diaphragm; but only that part which is supplied from the electric circuit. The

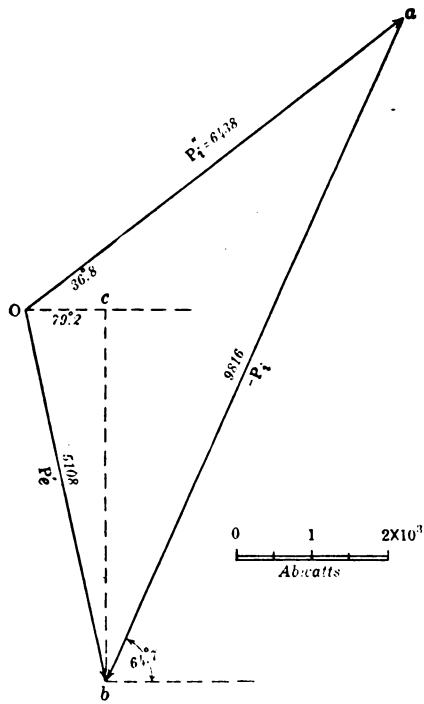

FIG. 26—DIAGRAM OF MOTIONAL POWER IN MAGNETIC CIRCUIT—DIAPHRAGM FREE

remainder has to be made up from power saved in hysteretic and eddy loss, due to the reduction in magnetic flux by the motional counter m. m. f., especially towards higher frequencies.

Turning to Fig. 27, the motional power diagram, the circular locus there represented may be considered as the motional impedance circle of Fig. 10, changed in scale, however, for convenience, in order to permit powers to be read off it. If,

however, a fractional scale of power is accepted, the motional impedance circle may be interpreted directly as a motional power diagram. In Fig. 27, $O\,a$ is the vector corresponding in phase to the motional impedance vector at the frequency considered, in this case 1028 ~. There are three pairs of co-

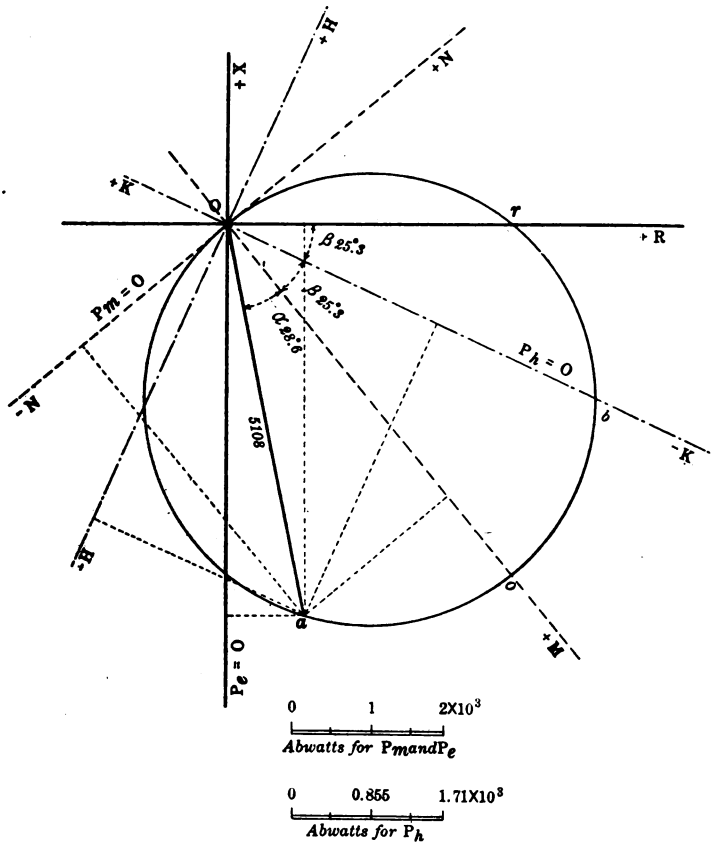

FIG. 27—MOTIONAL POWER DIAGRAM

ordinate axes; namely (1) $O\,R$, at standard phase, for the electric circuit power, and $O\,X$ its perpendicular, (2) $O\,H$, inclined at $-\beta°$ from $O\,X$, and its perpendicular $O\,K$, for components of hysteretic loss in the magnetic circuit, and (3) $O\,M$, at a slope of $-2\,\beta°$ with $O\,R$, and its perpendicular $O\,N$, for mechanical power of vibration in the diaphragm.

At any vector motional power $O\,a$, we have the following vector relation

$$P_m'' = P_e' - P_h' \cdot 2 \sin \beta \qquad \text{abwatts} \angle \quad (61)$$

Or, in language, the vector mechanical power P_m'', as read to coordinates $O\,M$, $O\,N$, is equal to the electrically delivered vector power P_e', read to coordinates $O\,R$, $O\,X$, less the hysteretic power P_h', read to coordinates $O\,H$, $O\,K$, multiplied by the coefficient 2 sin β, which in this case is 0.855: Moreover, this equation is true not only for these quantities as vectors; but also for their respective active components,

$$P_{ma}'' = P_{ea}' - P_{ha}' \cdot 2 \sin \beta \qquad \text{active abwatts} \quad (62)$$

and likewise for the reactive components

$$P_{mr}'' = P_{er}' - P_{hr}' \cdot 2 \sin \beta \qquad \text{reactive abwatts} \quad (63)$$

These propositions, which apply here to the energetics of a telephone receiver, for the particular case of β as the angle separating the systems of coordinates, are true in a general geometric sense for any plane vector, measured to three such sets of coordinates, without restriction of the value of β, and also without restriction as to the locus of the radius vector. This proposition is discussed in the Appendix.

In Fig. 27, we assume a knowledge of Z'_0 absohms $\angle$, as well as I r. m. s. absamperes the testing current strength, at standard phase. The power expended in this impedance will be $I^2\ Z_0'$ abwatts at the same slope as that of Z_0'. In the case considered, $I = 2.04 \times 10^{-4}$ r. m. s. absamperes, and $Z_0' = 140 \times 10^9 \diagdown 50°.6$ absohms. The vector power is therefore $(2.04)^2 \times 1.4 \times 10^3 = 5827 \diagdown 50.°6$ abwatts. This vector $O\,o$ is laid off in Fig. 27, to scale, as the diameter of the motional power circle $O\,r\,o\,a$. At any assigned impressed angular velocity ω, the angle of the corresponding radius vector with respect to the diameter $O\,o$ is

$$\alpha = \tan^{-1}\left(\frac{m\,\omega - s''/\omega}{r''}\right) \qquad \text{degrees lag} \quad (64)$$

In the case considered, with $f = 1028 \sim$, and $\omega = 6460$, $m\,\omega = 5827$, $s''/\omega = 5681$, $r'' = 268$; so that

$$\alpha = \tan^{-1} 0.545 = 28.°6.$$

The vector position $O\,a$, corresponding to $1028 \sim$ can thus be laid down in the circle. Its length is 5108 abwatts. With

respect to the RX coordinates it is $5108 \sphericalangle 79.°2$. It is $5108 \sphericalangle 28.°6$ to MN, and $5108 \sphericalangle 143.°9$ to HK. Here the electrical vector is $5108 \sphericalangle 79.°2$ abwatts, the mechanical vector $5108 \sphericalangle 28.°6$, and the hysteretic vector $P_h = P_h' \cdot 2 \sin \beta$

$$= 5108 \sphericalangle 143.°9 \times 2 \sin 25.°3 = 4369 \sphericalangle 143.°9.$$

The proposition of (**61**) states the mechanical power of $5108 \sphericalangle 28.°6$, is equal to the electrical power of $5108 \sphericalangle 79.°2$, minus the hysteretic power $4369 \sphericalangle 143.°9$. Moreover, the active mechanical power of vibration, $\dot{x}^2 r''$ is the OM component of Oa, or 4484 abwatts. This is made up of the active electric power component $I^2 R'$, as measured on the OR axis, of 957 abwatts, minus the active hysteretic component along the H axis, or $-(-3537) = +3537$ abwatts. The mechanical power is therefore mainly supplied by saving in hysteresis loss, and only partly supplied by assistance from the electric circuit. Similarly, the reactive mechanical power $j\dot{x}^2 (m\omega - s''/\omega)$ is the ON component of Oa, and measures $-j2445$ abwatts. This is equal to the reactive electric component $j I^2 X'$ along OX or $-j5018$ less the hysteretic component measured to its own scale along $OK = -(-j2591) = j2591$ abwatts.

Proceeding in the above manner, the power put into mechanical vibration of the diaphragm can be read off the power circle at any assigned frequency, and its component sources, electrical and hysteretic, determined either graphically or by computation. It will be evident that for frequencies below that of the vector Ob, $\beta°$ behind OR, the hysteretic active power is positive. This means that the hysteretic loss is increased at these frequencies, so that the electric circuit has to supply not only all the mechanical vibration power, but also the extra hysteresis and eddy loss due to increased magnetic flux. At the frequency of Ob, there is no additional hysteretic loss, because the flux in the magnetic circuit has the same size, with the diaphragm either damped or free. At this particular frequency, all the active mechanical power is supplied directly from the electric circuit. At frequencies above that of Ob, the active mechanical power is partly supplied by hysteresis saving. At the vector point c, where the circle cuts the reactance axis, there will be no extra power supplied by the circuit to maintain the mechanical output of the diaphragm; but all of this power will be paid for by saving in hysteresis loss, when the diaphragm is released.

The total active mechanical power developed in the diaphragm will be

$$P_m'' = \dot{x}^2 (r_a + r') = \dot{x}^2 r'' \quad \text{abwatts (65)}$$

and the active power put into vibration

$$P_m = \dot{x}^2 r \quad \text{abwatts (66)}$$

Similarly, the active power put into motional hysteresis loss,

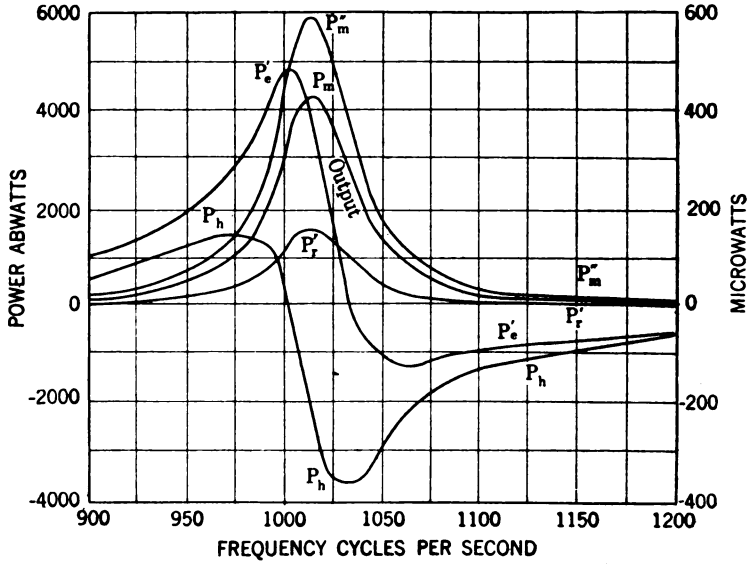

FIG. 28—MAGNETIC CIRCUIT MOTIONAL POWER DISBTRIBUTION AT DIFFERENT FREQUENCIES. P_m'' GROSS MECHANICAL ACTIVE OUTPUT P_e' ACTIVE ELECTRIC POWER INCREASES P_h CHANGE OF HYSTERETIC POWER. P_r' ACTIVE MECHANICAL POWER EXPENDED AGAINST r' IN DISPLACEMENT. P_m NET ACTIVE MECHANICAL OUTPUT FREE. $P_m'' = P_e' - P_h = P_r' + P_m$.

by reason of the vibration of the diaphragm in the magnetic field will be

$$P_r' = \dot{x}^2 r' \quad \text{abwatts (67)}$$

The mechanical efficiency of the diaphragm, as a motor, at resonance, is therefore

$$\eta_0 = \frac{r}{r''} = \frac{r}{r + r'} \quad \text{numeric (68)}$$

In the case considered, $\eta_0 = 0.74$.

Strictly speaking, according to our theory, r' is a function of ω, see (**29**), but unless the resonance is very blunt, the changes in r' and in η, with change in frequency, are not likely to be important.

Fig. 28 shows the distribution of the various active powers, in the instrument considered, over a range of frequency from 900 $\sim$ to 1200 $\sim$. Here $P_m = \dot{x}^2 r$ is the active mechanical power output in sound and in overcoming internal mechanical bending friction of the diaphragm. $P_r' = \dot{x}^2 r'$ is active mechanical power expended in the magnetic circuit in hysteresis and in eddies, by reason of the vibration of the diaphragm in the permanent magnetic field. $P_m'' = \dot{x}^2 r'' = \dot{x}^2 (r + r') = P_m + P_r'$ is the total active mechanical output of the diaphragm. P_e' is the extra active electric power taken from the electric circuit and put into mechanical vibration when the diaphragm is freed. The saving of active damped power put into the magnetic circuit when the diaphragm is freed is $- P_h$. Consequently

$$P_m'' = P_e' - P_h.$$

The following tabular statement gives the computed analysis of the constants of the particular instrument considered, partly taken from the Kennelly-Affel paper of 1915, already referred to, and partly as developed in this analysis:

TABLE OF NUMERICAL DATA CONCERNING ANALYZED RECEIVER

Mechanical	
Area of each pole, cm $\times$ cm.	1.14×0.199
Distance Separating poles, cm.	0.686
External diam. of diaphragm, cm.	5.52
Diameter of clamping circle, cm.	5.0
Thickness of diaphragm over japan cm.	0.031
Weight of diaphragm, gm.	4.397
Number of turns including both spools.	1300
Electrical	
D-c. Res. at 20 deg. cent. absohms R_1	86.7×10^9
Inductance at Resonant Frequency $\mathfrak{L}_0$ abhenries.	3.65×10^7
Current through receiver I r. m. s. absamp.	2.04×10^{-4}
Resonant Frequency apparent, f_0 cycles per sec.	1015
Resonant angular vel: ω_0 radians per sec.	6378
Motional impedance circle diameter Z_0' absohm.	140×10^9
Slope of Permeance at resonant frequency β. degrees	$-25°.3$

Max. amplitude of vibration at resonance x_m cm . 10.35×10^{-4}
Effective cyclic amplitude vibration at resonance x_0 cm. . . . . 7.32×10^{-4}
Max. cyclic velocity at resonance x_0 r. m. s. cm. per sec or kines 4.666
Quadrantal angular velocities ω_1, ω_2 radians/sec. . $\begin{cases} 6227 \\ 6532 \end{cases}$
Total decrement Δ hyps. per sec. 149
Force factor A dynes/absampere or abvolts/kine. $6.12 \times 10^6 \angle 25.^\circ 3$
Total mechanical resistance r'' dynes/kine. 268
Equivalent mass in grams. 0.902
Total stiffness coefficient s'' dynes/cm. . . . . 36.7×10^6

RECOMPUTED ELECTROMAGNETIC DATA

Ratio of numbers of turns p absampere/cm. 0.168
Mechanical resistance of magnetic reaction r' dynes/kine 68.8
Pure mechanical resistance r dynes/kine. 199
Stiffness coefficient of magnetic reaction s' dynes/cm. . . . . 0.928×10^6
Pure mechanical stiffness coefficient s dynes/cm. 37.63×10^6
Equivalent number of turns per cm. displacement N' gilberts/cm. 218
Normal mean polar flux density $\mathfrak{B}_0$ gausses. 1369
Normal total polar flux Φ_0 maxwells/pole 311.0
Equivalent permanent magnetic reluctance $\mathfrak{R}_0$ oersteds . . . . . $0.582 \angle 25.^\circ 3$
Equivalent permanent magnetic permeance $\mathfrak{P}_0$ $(\text{oersteds})^{-1}$ . . . . . $1.718 \angle 25.^\circ 3$
Equivalent permanent m. m. f. gilberts. 181
M. M. F. of testing current (2.04×10^{-4}) r. m. s. gilberts $\mathfrak{F}_i$. . . . . $3.334 \angle 0^\circ$
Flux in magnetic circuit due to current ϕ_i r. m. s. maxwells . . . . . $5.73 \angle 25.^\circ 3$
Mechanical force due to current I f_i, r. m. s. dynes, $v\,m\,f$ . . . . . $1249 \angle 25.^\circ 3$
Magnetic power input at 1028 $\sim$ with current I, P_i abwatts, ... $9816 \angle 64.^\circ 7 = 4196 + j\,8875$
Total mechanical impedance at $f = 1028$, z' dynes/kine . . . . . $305.2 \angle 28.^\circ 6$
Mechanical velocity at $f = 1028$. x. r.m.s. cm/sec. $4.091 \angle 53.^\circ 9$
Cyclic mechanical displacement at $f = 1028$. x r. m. s. cm. . . . . $6.332 \times 10^{-4} \angle 143.^\circ 9$
M. M. F. due to displacement, at $f = 1028$ and for current I, $\mathfrak{F}_x$ r. m. s. gilberts. . . . . $1.735 \angle 143.^\circ 9$
Resultant m. m. f., at $f = 1028$. $\mathfrak{F}$ r. m. s. gilberts . . . . . $2.174 \angle 28^\circ$
Flux due to displacement, at $f = 1028$. ϕ_x r.m.s. maxwells . . . . . $2.980 \angle 169.^\circ 2$

Resultant flux at $f = 1028$. ϕ r. m. s. maxwells. $3.757 \angle 53.°2$

Magnetic input diaphragm free, at $f = 1028$.

P_i'' abwatts ..... $6438 \angle 36.°8$

$= 5156 + j\,3856$

Free magnetic power, or total power absorbed in magnetic circuit, at $f = 1028 \sim$, abwatts $\angle P_r'' = 4199 \angle 64.°7$

$= 1795 + j\,3797$

Mechanical output power of diaphragm, P_m at $1028 \sim$ abwatts $\angle$ ..... $= 3349 \angle 0.°7$

$= 3349 + j\,40$

Total mechanical power of diaphragm at $1028 \sim$

P_m'' abwatts $\angle = 5108 \angle 28.°6 = 4484 - j\,2445$

Motional electric power of diaphragm at $1028 \sim$

P_e' abwatts $\angle = 5108 \angle 79.°2 = 957 - j\,5018$

Hysteretic power at $1028 \sim$ P_h abwatts $\angle$

$= 5108 \times 0.855 = 4369 \angle 143.°9 = -3537 - j\,2591$

Mechanical efficiency of diaphragm at apparent resonance, η_0 numeric $= 0.74$

Net efficiency of receiver, freed, and at apparent resonance numeric, $= 0.4$

Maximum motional impedance per unit of continuous-current resistance Z_0'/R_1 numeric $\angle = 2.04 \angle 50.°6$

Force factor per root of continuous-current res.

$$A/\sqrt{R}\ \frac{\text{dynes } \sqrt{\ } \text{absohms}}{\text{abvolts}} \angle = 23.36 \angle 25.°3$$

Effect of a Changing the Number of Turns in Receiver of given Winding Space. If the windings of a given receiver are allowed to occupy a definite constant volume, and also if the ratio of bare to covered wire diameter is kept constant over the range of wire diameters selected for the winding, so that the same volume and weight of copper will exist no matter what the size of wire; then it is evident that if we reduce the wire diameter one-half, the number of turns N will be quadrupled and the d-c. resistance R_1, at constant temperature, increased sixteen fold. The effect of this will be to increase N, A, $\mathfrak{F}_i$, and ϕ_i, 4 times, leaving $\mathfrak{F}_0$, $\mathfrak{B}_0$, $\mathcal{P}$, and β, unchanged. The quantities $\mathfrak{L}$, Z, Z_0', P_e, and P_{m0}, will be all increased 16 times, (neglecting variations in r') or in direct proportion to the resistance. Consequently the ratio of active mechanical power output $\dot{x}^2\, r/I^2\, R_1$, where R_1 is the d-c. resistance of the instrument, will remain substantially unchanged for all values of R_1 within the range for which the copper in the winding space remains constant. On this theory, changing the winding of a receiver, other things remaining the same, increases the mechanical output at resonance in proportion to the resistance, for a

fixed exciting current strength, but for a given amount of $I^2 R_1$ power loss in the winding, this mechanical power output remains substantially constant.

Since Z_0' the maximum or diametral value of the vector motional impedance increases, according to this theory, directly with the d-c. resistance of the winding, different receivers should have their diametral impedances Z_0' reduced to a common basis of comparison by taking the ratio Z_0'/R_1. The sensitiveness of a receiver is proportionate to this ratio. The ratio is independent of the strength I of the testing current. An instrument of large diametral impedance per unit of d-c. resistance is therefore an instrument of inherently large electromagnetic sensitivity, no matter what the resistance of the winding may be. This ratio calls for no other measurements than that of the motional impedance circle or the essential sector thereof, and the d-c. resistance at normal temperature.

Similarly, the force factor A should be divided by $\sqrt{R_1}$, in order to bring it to a common basis of comparison among various receivers.

It should be observed that the diametral or maximum size of the motional impedance Z_0' is not produced at the frequency of strict mechanical resonance of the diaphragm. True mechanical resonance is produced when the angular velocity is such that the mass reactance $m\ \omega$ is numerically equal to the elastic reactance s/ω. In the motional-impedance circle, however, the apparent resonance and diametral impedance are produced when $m\ \omega = \frac{s''}{\omega} = \frac{s - s'}{\omega}$. The fictitious component s', due to the displacement flux, thus slightly lowers the apparent resonance, or causes the maximum velocity, displacement, and impedance to occur at a frequency a little lower than that of true mechanical resonance. In the case considered, mechanical resonance would be produced at $\omega_0 = \sqrt{s/m} = \sqrt{37.63 \times 10^6/0.902} = 6459$ radians per sec.; corresponding to 1028~; whereas the apparent resonance would be produced at $\omega''_0 = \sqrt{s''/m} = \sqrt{36.7 \times 10^6/0.902} = 6379$, corresponding to 1015~. This displacement of resonance must occur in the motional impedance circle, whatever method of including the effects of the displacement flux φ_x is adopted. Apparent resonance occurs at the frequency of mechanical resonance as modified by magnetic reaction, which acts in such

a manner as to reduce the stiffness coefficient of the diaphragm. The angle of displacement $h\,b\,o$ in the motional impedance circle, Fig. 10, between the vector of true mechanical resonance and apparent resonance, is equal to the angle α between ϕ and ϕ_i at the angular velocity ω_0' of true mechanical resonance; because at ω_0' the velocity $\dot{x}$ is in phase with the resultant flux ϕ.

A bibliography of the subject, without pretensions as to completeness, is appended, in so far as relates to the motional-impedance aspect of telephone-receiver theory.

It may be noted that the maximum mechanical output $\dot{x}_0^2\, r''$ at apparent resonance is entirely active power, and is numerically equal to $I^2\,|Z_0'|$ abwatts or the square of the testing current multiplied by the size of the diametral impedance. This constitutes a simple method of determining the maximum mechanical output of the diaphragm, including frictions and hysteretic loss due to vibration. The gross efficiency of the receiver at apparent resonance is therefore $\frac{I^2\,|Z_0'|}{I^2\,R_0''} = \frac{|Z_0'|}{R_0''}$.

In this case, this efficiency reaches $\frac{140}{257.3} = 0.544$. This must be multiplied by the $\eta_0 = 0.74$ to give the net efficiency of the receiver at apparent resonance of 0.40. This is the ratio of active mechanical output of the diaphragm, including internal frictions and acoustic delivery, to the active electric power consumed at terminals, with the diaphragm free. With the receiver pressed against the ear, the condition is intermediate between damped and free.

Summary of Results

1. The theory presented in the earlier papers mentioned in the bibliography were lacking in not taking into account the m. m. f. and flux, of diaphragm vibratory displacement in the magnetic field.

2. The present theory purports to include the above mentioned elements, under the form of an apparent increment r' in mechanical resistance, and an apparent diminution s' in the stiffness coefficient, the latter being independent of the frequency, but the former varying inversely as the frequency.

3. The effect of r' is to introduce a slight distortion of the motional impedance and power diagrams from the strictly circular locus, assuming the force-factor A and other constants

to remain substantially the same at all frequencies; but the distortion is not serious from a practical standpoint.

4. The m. m. f. of vibratory displacement may be expressed in terms of a coefficient N', a fictitious number of turns. The ratio p of N'/N is a constant of the instrument.

5. The depression of the motional-impedance circle diameter is 2 $\beta°$ where $\beta°$ is the lag angle of the damped magnetic flux behind the exciting current.

6. The power analysis depends directly upon the m. m. f. and flux diagram, without any necessary reference to the e. m. fs. produced. The power in the magnetic circuit is then found to be similar to the power in a simple alternating-current circuit, containing an alternator, a synchronous motor, and a simple connecting impedance.

7. The observed motional impedance circle may be converted into a corresponding motional power circle, by a suitable alteration in scale of linear dimensions. By introducing three sets of coordinate axes, mutually displaced by $\beta°$, the power output P''_m, can be read off in terms of the electric power input P'_e, and the hysteretic power input P_h. The same relation holds for active and for reactive components.

8. At the slope $-\beta°$ in the power circle, the mechanical power is all electric. At the slope $-90°$, it is all hysteretic.

9. The active power mechanically expended in the magnetic circuit by the diaphragm as a motor, against hysteresis and eddy currents $\dot{x}^2 r'$, can be separated from that expended against friction and air resistance $\dot{x}^2 r$. The mechanical efficiency is $\frac{r}{r + r'}$, which varies somewhat with the frequency. It tends to increase slightly with frequency, according to this theory.

10. The behavior of a particular instrument analysed some years ago in a preceding paper is investigated in detail, at a particular frequency, in accordance with the theory.

11. The gross efficiency of a receiver at apparent resonance is $\frac{|Z'_0|}{R''_0}$ or the ratio of the motional impedance diameter to the apparent resistance of the instrument at this frequency with the diaphragm free.

Appendix

Proposition that the Plane Vector

$$|\rho| \angle \alpha = |\rho| 2 \angle \beta + \alpha \qquad - 2 \sin \beta |\rho| \angle 90° + \alpha° + \beta$$

In Fig. 29, $O A$ is a planevector, or geometrical complex quantity of any convenient size ρ, taken at standard phase, or zero slope. It may be denoted by ρ_A · $O B$ is a similar plane vector of the same size, distinguished by the symbol ρ_B. Its slope is $-2\beta°$. $O c$ is a vector denoted by ρ_c of size ρ and drawn perpendicular to $O d$, the bisector of the angle $A O B$.

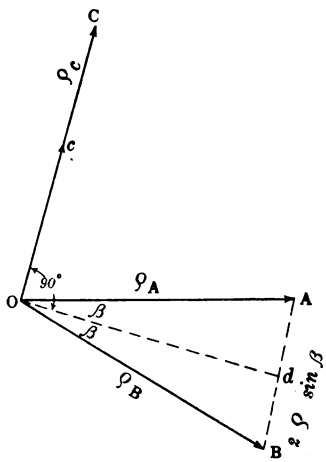

FIG. 29

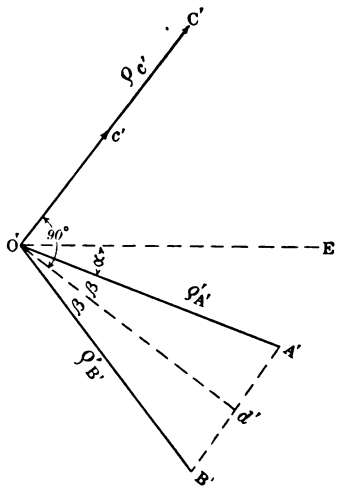

FIG. 30

Then, because $B A$ expressed vectorially is $|\rho| 2 \sin \beta \angle 90° - \beta$ and is equal to the vector $O c$, we have the vector relation

$$\rho_B = \rho_A - 2 \sin \beta \cdot \rho_c \qquad \text{length units} \angle \quad (69)$$

If now, as in Fig. 30, we rotate the whole vector system in the plane of reference through the angle $-\alpha°$ with respect to $O E$, a fixed line of reference, the effect will be the same as though the vector system remained fixed in the plane; but the line of reference, $O E$ was rotated through an angle of $+\alpha$. This rotation of a reference line cannot, however, affect the vector relation expressed in (**69**) when those vectors are taken to the new reference line.

But the three vectors of (**69**) may be regarded as one and the

same vector ρ, Fig. 31, expressed each with respect to three initial lines $O''m$, $O''e$, and $O''h$, and then denoted by ρ_m, ρ_e and ρ_h respectively. Thus in Fig. 32,

$$|\rho_m| \angle \alpha = |\rho_e| \angle 2\beta + \alpha - |\rho_h| 2 \sin \beta \angle 90° + \alpha + \beta \quad \text{length units} \angle \quad (70)$$

Since this relation holds for the vectors themselves, it must also hold for their real components, and for their imaginary components respectively.

The power circle of Fig. 27, corresponds to Fig. 31; while

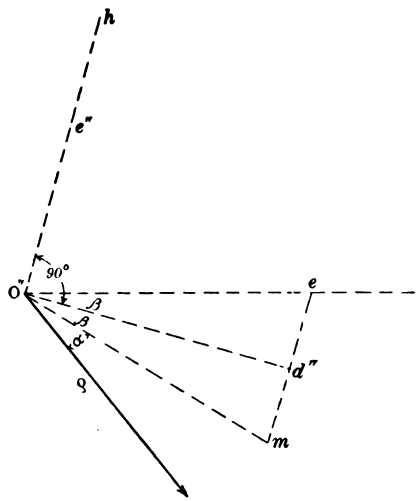

FIG. 31

the interpretation of (62) and (63) are referable to the construction of Fig. 32.

Referring to Fig. 24, in the analogy of a simple a-c. circuit in which a generator of $\mathfrak{F}_i$ r. m. s. abvolts terminal e. m. f. supplies an external circuit of fixed admittance $\mathcal{P}$ mhos $\angle$, with a current of ϕ_i r. m. s. absamperes. To the condition of diaphragm damped, corresponds the analogous condition of zero c. e. m. f. in the synchronous motor. To the condition of diaphragm free, corresponds the analogous condition of e. m. f. $\mathfrak{F}_x$ r. m. s. abvolts in the synchronous motor armature, which would produce the current of ϕ_x r. m. s. absamperes if operating independently in the circuit, at assumed constant frequency.

The vector change in electric power P'_e given by the alternator to the circuit when the diaphragm is suddenly freed, will be the power exerted by the e. m. f. $\mathfrak{F}_i$ on the current ϕ_x. The vector mechanical power P_m'' given to the motor by the current ϕ_i will be the power of ϕ_i on $\mathfrak{F}_x$.

Converting these electric powers into their analogous magnetic powers, and remembering that in the magnetic circuit a vector a-c. m. m. f. $|\mathfrak{F}| \angle \gamma°$ r. m. s. gilberts, producing a vector alternating flux $|\phi| \angle 0°$ r. m. s. maxwells, develops a vector power in the magnetic circuit of $|(f/2)\ \mathfrak{F}\ \phi| \angle 90° - \gamma°$ abwatts, of which the real part is average active power, and the imaginary part is maximum cyclic reactive power, we have

$$P'_e = |(f/2)\ \mathfrak{F}_i\ \phi_x| \angle 90° - (90° + \alpha + 2\ \beta)$$
$$= |(f/2)\ \mathfrak{F}_i\ \phi_x| \sphericalangle \alpha + 2\ \beta = |(f/2)\ \mathfrak{F}_x\ \phi_i| \sphericalangle \alpha + 2\ \beta$$
abwatts $\angle$ (**71**)

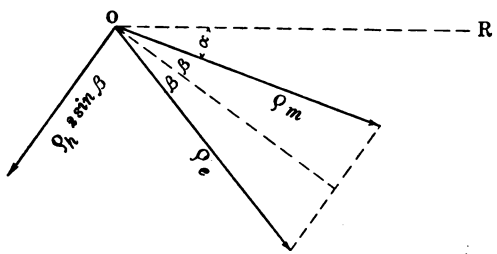

FIG. 32

where $90° + \alpha$ is the angle between ϕ_i and $\mathfrak{F}_x$. This vector power has a circular locus, because $|(f/2)\ \mathfrak{F}_x| \sphericalangle \alpha$ has a circular locus.

Also

$$P_m'' = |(f/2)\mathfrak{F}_x\phi_i| \angle 90° - (90° + \alpha) = |(f/2)\mathfrak{F}_x\phi_i| \sphericalangle \alpha$$
abwatts $\angle$ (**72**)

This vector mechanical power must also have a circular locus under varying frequency.

Consequently,

$$P_e' - P_m'' = |(f/2)\ \mathfrak{F}_x\ \phi_i| \sphericalangle \alpha + 2\ \beta - |(f/2)\ \mathfrak{F}_2\ \phi_i| \sphericalangle \alpha$$
abwatts $\angle$ (**73**)

and this by (**70**) is

$$P_h = |(f/2)\ \mathfrak{F}_x\ \phi_i| \cdot 2 \sin\ \beta \sphericalangle 90° + \alpha + \beta \quad \text{abwatts} \angle \ (\mathbf{74})$$

a vector hysteretic power having also a circular locus.

List of Symbols Employed

For simplicity of numerical treatment and universality of application, the units employed are those of the C. G. S. magnetic system.

A force factor (dynes per absampere $\angle$* or abvolts per kine $\angle$)

α angle of mechanical effective impedance; *i. e.*, mechanical impedance including magnetic displacement reaction (degrees)

$\mathfrak{B}_0$ magnetic flux density in the airgaps due to permanent magnet (gausses)

$\mathfrak{B}_i$ r. m. s. magnetic flux density due to current (r. m. s. gausses $\angle$)

$\mathfrak{B}$ instantaneous alternating flux (gausses)

β mean angle of lag between magnetic flux and m. m. f. (degrees)

C capacitance of a condenser (farads or abfarads)

$\Delta = \frac{r''}{2m}$ total apparent damping constant of a diaphragm (hyp. radians per sec.)

E r. m. s. e. m. f. in a simple alternating-current circuit (volts or abvolts $\angle$)

$E = I Z'$ motional e. m. f. (r. m. s. abvolts $\angle$)

$\eta = r/r''$ mechanical efficiency of diaphragm, corresponding to armature efficiency in a synchronous motor (numeric)

η_0 mechanical efficiency of diaphragm, or friction and acoustic mechanical resistance to total mechanical resistance, at apparent resonance (numeric)

$\mathfrak{F}_i$ m. m. f. due to constant exciting alternating current (r. m. s. gilberts $\angle$)

$\mathfrak{F}_x$ m. m. f. due to vibratory displacement of diaphragm in permanent magnetic field (r. m. s. gilberts $\angle$)

$\mathfrak{F}$ resultant vector m. m. f. in magnetic circuit (r. m. s. gilberts $\angle$)

$\mathfrak{F}_0$ m. m. f. due to permanent magnet (gilberts)

f impressed frequency (cycles per sec.)

*The sign $\angle$ after a unit signifies that the quantity is a plane-vector or complex quantity as distinguished from a scalar or simple numerical quantity.

f_0, impressed frequencies of apparent resonance (cycles per second)

f_c reactive mechanical force of clamping (dynes $\angle$)

f_i vibromotive force on diaphragm due to alternating current I alone (r. m. s. dynes $\angle$)

f_x vibromotive force due to vibratory diaphragm displacement in permanent magnetic field (r. m. s. dynes $\angle$)

I strength of constant small alternating testing current (r. m. s. absamperes)

$j = \sqrt{-1}$

L Self inductance of an electric circuit (abhenries or henries)

$\mathfrak{L}$ Self inductance of a receiver winding with diaphragm damped (abhenries $\angle$)

m Equivalent mass of a diaphragm (grams)

N Number of turns in the winding of a bipolar receiver, including both coils (numeric)

N' Equivalent number of turns for expressing a displacement m. m. f. in cm-turns (absamperes per cm. or gilberts per cm.).

P_e, P_e', P_e'' Electric power supplied to receiver with diaphragm damped, vector change in supplied electric power due to motion with diaphragm free, and total supplied electric power with diaphragm free. (abwatts or ergs per sec. $\angle$)

P_h Increase in magnetic circuit power loss due to motion of diaphragm (abwatts $\angle$)

P_h' Apparent increase in magnetic circuit power loss due to motion of diaphragm, as measured in the motional power circle diagram along the hysteretic axis before applying change in power scale abwatts $\angle$

P_i, P_i'' Damped magnetic power input (abwatts $\angle$), and input power from electric to magnetic circuit with diaphragm free (abwatts $\angle$)

P_m, P_m'' Mechanical output power of diaphragm against pure mechanical res. r (abwatts $\angle$) and total mechanical output power of diaphragm against total resistance of $r'' = r + r'$ (abwatts $\angle$)

P_{ma}, P_{ea}, P_{ha} Active or dissipatory components of mechanical, electric, and hysteretic power (abwatts)

P_{mr}, P_{er}, P_{hr} Reactive or non-dissipatory components of mechanical, electric and hysteretic power (j abwatts)

$P_r' = \dot{x}^2 (r' + j s'/\omega)$ Motional power or power expended against reactive force of diaphragm displacement (abwatts $\angle$)

P_r'' Free magnetic power, or vector power of resultant m. m. f. $\mathfrak{F}$ on resultant magnetic flux ϕ, or total absorbed in magnetic circuit (abwatts $\angle$)

$p = N'/N$ Ratio of equivalent displacement turns to exciting turns (absamperes per cm.)

$\mathcal{P}$ Permeance of magnetic circuit (oersteds^{-1} $\angle$ or maxwells per gilbert $\angle$)

ϕ_i Magnetic flux due to constant exciting current maxwells $\angle$)

ϕ_x Magnetic flux due to displacement x in magnetic field (maxwells $\angle$)

$\phi = \phi_i + \phi_x$ Resultant magnetic flux (maxwells $\angle$)

R_1 Continuous-current resistance of receiver winding (absohms)

R Apparent resistance of receiver to alternating current with diaphragm damped (absohms)

R_h Increment of apparent resistance due to hysteresis and eddy currents, with diaphragm damped (absohms)

R' Resistance component of motional impedance Z' (absohms)

R'' Total apparent resistance of receiver with diaphragm free (absohms)

R''_0 Total apparent resistance of receiver at apparent resonance (absohms)

r Mechanical resistance of diaphragm including internal frictions and acoustic or air resistance (dynes per kine)

r' Hysteretic resistance of magnetic circuit to motion of diaphragm, or apparent increase in friction of diaphragm due to displacement flux losses in magnetic circuit. (dynes per kine.)

$r'' = r + r'$ Total mechanical resistance to motion of diaphragm (dynes per kine)

R_0 Reluctance of magnetic circuit to permanent flux (oersteds)

S Surface area of one pole neglecting magnetic fringe. (sq. cm.)

s Effective stiffness coefficient of diaphragm to vibrational displacement (dynes per cm.)

s' Apparent diminution in stiffness coefficient due to displacement in magnetic field. (dynes per cm.)

$s'' = s - s'$ Total effective stiffness of diaphragm including magnetic displacement (dynes per cm.)

t Time elapsed from a certain epoch (seconds)

X Reactance of a receiver winding with damped diaphragm (absohms $\angle$)

X' Reactive component of motional impedance Z' (j absohms)

X'' Reactive component of receiver impedance Z'' with diaphragm free (j absohms)

x Displacement of diaphragm towards poles from normal flexed position (r. m. s. cm. $\angle$)

x_0 Displacement of diaphragm at apparent resonance (r. m. s. cm. $\angle$)

$x_m = |x_0|\sqrt{2}$ Maximum cyclic displacement of diaphragm at apparent resonance (max. cm.)

$\dot{x}$ Velocity of diaphragm r. m. s. kines $\angle$ or r. m. s. cm. per sec. $\angle$

$\dot{x}_0$ Velocity of diaphragm at apparent resonance (r. m. s. kines $\angle$)

$\ddot{x}$ Acceleration of diaphragm (r. m. s. kines per sec. $\angle$)

$y = 1/z$ Mechanical admittance of a diaphragm when the magnetic reactive force due to displacement is neglected (kines per dyne $\angle$)

y' Apparent mechanical admittance of diaphragm, including magnetic reactive force due to displacement (kines per dyne $\angle$)

Z Impedance of a receiver winding with diaphragm damped (absohms $\angle$)

$Z' = Z'' - Z$ Motional impedance of winding (absohms $\angle$)

Z'' Impedance of winding with diaphragm free (absohms $\angle$)

Z_0' Motional impedance at apparent resonance, and at diametral or maximum size. (absohms $\angle$)

z Mechanical impedance of a diaphragm with reactive magnetic force neglected (dynes per kine $\angle$)

z' Effective mechanical impedance of diaphragm including reactive magnetic force (dynes per kine $\angle$)

$\omega = 2\pi f$ Impressed angular velocity (radians per sec.)

ω_0' Impressed angular velocity at true mechanical resonance (radians-sec.)

ω_0 Impressed angular velocity at apparent mechanical resonance (radians per sec.)

ω_1, ω_2 Lesser and greater quadrantal angular velocities (radians per sec.)

r. m. s. Contraction for root-mean-square.

$|Z|$ Size or mere numerical value of a vector quantity Z.

Bibliography

(1) Lord Rayleigh, "Theory of Sound", 1894, Vol. 1, pp. 366, 473.

(2) Wien, *Annalen, d. Phys.*, Vol. 4, 1901, p. 450.

(3) Henri Abraham, "Rendement Acoustique du Téléphone", *Comptes Rendus, Acad. d. Sc.*, 144, 1907.

(4) Henri Poincaré, "Étude du Récepteur Téléphonique", l'Éclairage Électrique, Vol. 50, Feb. 16, Feb. 23, Mar. 9, Mar. 16, 1907., pp. 221–372.

(5) A. E. Kennelly and Walter L. Upson, "The Humming Telephone". *Proc. Am. Phil. Soc.*, Vol. 47, pp. 329–365, July, 1908 .

(6) John B. Taylor, "Telegraph and Telephone Systems as Affected by Alternating-Current Lines", TRANS. A. I. E. E., Oct., 1909, Vol. 28, Part II, p. 1169–1215.

(7) A. E. Kennelly, "Vector Power in Alternating-Current Circuits", TRANS. A. I. E. E., Vol. 29, pp. 1233–1267, June, 1910.

(8) G. W. Pickard, "Telephone Receiver Efficiency". *Western Electrician*, May 6, 1911, Vol. 56, p. 899.

(9) A. E. Kennelly and G. W. Pierce, "The Impedance of Telephone Receivers as affected by the Motion of their Diaphragms", *Proc. Am. Ac. Arts and Sc.*, Vol. 48, Sept., 1912, pp. 113–151; also *The Electrical World*, N. Y., Sept. 14, 1912; also *British Assoc. Adv. Sc.* Report Dundee Meeting, 1912.

(10) Chas. F. Meyer and J. B. Whitehead, "The Vibrations of Telephone Diaphragms", TRANS. A. I. E. E., Vol. 31, part II, 1912, pp. 1397–1418.

(11) Geo. D. Shepardson, "Equivalent Frequency of Telephone Currents", A thesis in the library of Harvard University, Cambridge, 1912.

(12) H. A. Affel and O. C. Hall, "Telephone Receiver Characteristics", Thesis, *El. Engg. Dept., Mass. Inst. Tech.*, June, 1914.

(13) Augustin Guyau, "Le Téléphone Instrument de Mesure", Paris, *Gauthier-Villars*, 1914.

(14) R. L. Jones, "Simple Vibratory Systems and their Impedance Analysis", Unpublished Memorandum, Engg. Dept., Western El. Co., 1914.

(15) L. Bouthillon and L. Drouet, "Étude Expérimentale du Récepteur, Téléphonique," *Comptes Rendus*, Vol. 158, June 2, 1914, p. 1568, also *La Révue Électrique* Oct. 16, 1914, p. 294-295.

(15a) A. Guyan "The Telephone Receiver" *Journ de Physique*, June, 1914, Vol. 4, pp. 480–492.

(16) A. E. Kennelly and H. O. Taylor, "Explorations over Vibrating Surfaces of Telephonic Diaphragms Under Simple Impressed Tones", *Proc. Am. Phil. Soc.*, April, 1915, pp. 95–136, *Bulletin No. 7, Research Div. El. Engg. Dept., Mass. Inst. Tech.*

(17) A. E. Kennelly and H. A. Affel, "The Mechanics of Telephone-Receiver Diaphragms, as Derived from their Motional Impedance Circles", *Proc. Am. Ac. Arts & Sc.*, Nov., 1915, Vol. 51, pp. 422–482, *Bulletin No. 8, Research Div., El. Engg. Dept., M. I. T.*

(17a) B. S. Cohen and J. G. Hill "Long-Distance and Cable Telephony", *Inst. P. O. Elec. Engrs.* 1916.

(17b) "Notes on the Electromagnetic Theory of the Telephone" by R. L. Wegel, an unpublished memorandum of the Western Electric Co.

(18) A. E. Kennelly and H. O. Taylor, "Some Properties of Vibrating Telephone Diaphragms", *Proc. Am. Phil. Soc.*, April, 1916, Vol. 55, pp. 415–460, *Bulletin No. 11, Research Div., El. Engg. Dept., M. I. T.*

(18a) M. Latour "Theory of Telephone Receiver" *La Lum. Elec.* Vol. 33, June 17th and July 22, 1916.

(19) Geo. D. Shepardson, "Telephone Apparatus", Appleton & Co., 1917.

(19a) B. S. Cohen "Telephonometry" *The Electrician*, Vol. 77, May 26th and June 2nd, 1916, pp., 244–245 and 277–279.

(20) H. O. Taylor, "Motional Impedance Circle of the Telephone Receiver", *Proc. Radio Club of America*, June, 1917.

(21) Henri Tournayre, "Théorie du Téléphone" *L'Industrie Électrique*, July 25, Aug. 10, 1917.

(22) A. E. Kennelly, "Some Experiments on the Effects of Changes in Diaphragm Thickness on the Characteristics of a Telephone Receiver", *Journal of the Franklin Institute*, November, 1917, Vol. 184, pp. 723–726.

(23) John Mills, "Radio Communication", McGraw-Hill Book Co., 1917, pp. 26-35.

(24) W. H. Eccles, "Wireless Telegraphy and Telephony", D. Van Nostrand Co., 1918, pp. 347–350.

(25) Marius Latour, Note sur les Pertes dans les Tôles de Fer aux fréquences élevées. *Révue Gén. de l'Él.* Vol. 3, April 13, 1918, pp. 539–543.

LIST OF RESEARCH BULLETINS

Bulletin Number

*1. The Economical Transportation of Merchandise in Metropolitan Districts. H. Pender and H. F. Thomson; March, 1912.

*2. Notes on the Cost of M
H. F. Thomson; Octo

*3. Observations on Horse
and H. F. Thomson;

4. Relative Fields of Hors
H. F. Thomson; Aug

*5. The Delivery and Hand
Boston Freight Term
and C. P. Eldred; Fe

6. The Delivery System o
H. F. Thomson, H.
tember, 1914.

7. Explorations over th
Diaphragms under
nelly and H. O. Ta

8. The Mechanics of Te
rived from their
Kennelly and H. A

9. Experimental Resear
A. E. Kennelly, F.
ber, 1915.

10. Tractive Resistances
ferent Roads and
and O. R. Schurig;

11. Some Properties of
A. E. Kennelly an

12. Experimental Researc
A. E. Kennelly, F.
1916.

13. Skin-Effect Resistanc
Radio-Frequencies
A. E. Kennelly an

LIST OF RESEARCH BULLETINS — Continued

Bulletin Number

14. Street Railway Fares; their relation to length of haul and cost of service. D. C. Jackson and D. J. McGrath; August, 1917.

15. Apparent Dielectric Strength of Varnished Cambric; A. E. Kennelly and R. J. Wiseman; January, 1918.

16. Magnetic Flux Distribution in Annular Steel Laminae. A. E. Kennelly and P. L. Alger; March, 1918.

17. Electromagnetic Theory of the Telephone Receiver. With Special Reference to Motional Impedance. A. E. Kennelly and H. Nukiyama; March, 1919.

A Rectangular-Component Two-Dimensional Alternating-Current Potentiometer

A. E. KENNELLY and EDY VELANDER

Research Division
Electrical Engineering Department
Massachusetts Institute of Technology
Bulletin No. 18 July, 1919

(Reprinted from the Journal of The Franklin Institute,
July, 1919.)

A RECTANGULAR-COMPONENT TWO-DIMENSIONAL ALTERNATING-CURRENT POTENTIOMETER.*

BY

A. E. KENNELLY, Sc.D.,
Professor of Electrical Engineering: Harvard University, and the Massachusetts Institute of Technology
Member of the Institute.

AND

EDY VELANDER, A.M.

It is here proposed to describe the construction, mode of operation, and use of a special form of alternating-current potentiometer, particularly adapted to telephonic-frequency measurements, and which gives its readings in two rectangular components of the voltage measured.

Brief History.—The name "Electric Potentiometer" was suggested in 1873, by Latimer Clark, for the instrument which he described, as serving to measure continuous-current potential differences, in a paper read in London, January 22, 1873, before the "Society of Telegraph Engineers," the forerunner of "The Institution of Electrical Engineers." This instrument has remained almost unchanged to the present time, and is one of the most valuable measuring instruments which electrical engineering possesses.

An early form of *a-c.* potentiometer was described by Franke in 1891. It employed a small *a-c.* generator with two armature windings mechanically adjustable with respect to a common rotating field; so that both the relative magnitudes and the relative

* Communicated by Dr. Kennelly.

phase of the two induced *emfs.* at one and the same frequency, could be determined.[1]

An improved *a-c.* potentiometer was described by Dr. C. V. Drysdale[2] in 1909. This instrument has come into fairly extensive use. It measures an *a-c.* potential difference in polar coördinates, over the complex plane; *i.e.,* in size and in slope or phase, with respect to a certain phase standard. Its readings are therefore presented in the general form $E \angle \beta°$, such as $1.500 \angle 125.3°$ volts. Its range, without any auxiliary multiplier, is from 0 to 1.8 volts in size, and 0 to 360° in slope. The range in frequency which it claims is from 25 to 1000 ∞. The Drysdale *a-c.* potentiometer has filled a great need for a laboratory instrument capable of measuring planevector[3] voltages. For many such purposes its use is invaluable. When, however, the source of testing current is an oscillator, and not an alternator, there is a difficulty in using this instrument, because the excitation of the necessary phase-shifting transformer requires more than 60 watts. When an oscillator is used as the source of alternating currents, it is necessary to reduce the power absorbed in the measuring instruments to the lowest available limits. The use of oscillators for such purposes is steadily increasing. It then becomes imperative to adopt such a form of *a-c.* potentiometer as will avoid the use of an electromagnetic phase-shifting device.

Prof. A. Larsen described in 1910,[4] a form of two-dimensional potentiometer, the connections of which appear in Fig. 1. It consists of a non-inductive resistance *AB,* in series with the primary winding of an induction coil *BC,* an adjustable portion of the

[1] "Die elektrichen Vorgänge in den Fernsprechleitungen und-Apparaten," by Ad. Franke, Berlin, 1891. Thesis towards the Doctorate at Berlin University.

[2] "The Use of the Potentiometer on Alternating-Current Circuits." *Phil. Mag.,* Vol. 17, p. 402, Mar., 1909; also *Proc. Phys. Soc.,* London, Vol. 21, p. 561, 1909; also *The Electrician,* Vol. 63, p. 8, April 16, 1909; and Vol. 71, pp. 687–690, Aug. 1, 1913.

[3] "A planevector" may be defined as a geometrically directed complex quantity in a plane of reference, and subject to the laws of complex arithmetic, as distinguished from a "vector" which is subject to the laws of vector arithmetic and is not necessarily confined to a plane. In this paper, the term "vector" is used as an abbreviation for "planevector."

[4] A. Larsen: "Der Komplexe Kompensator, ein Apparat zur Messung von Wechselströmen durch Kompensation." *Elek. Zeitschrift,* 13th Oct., 1910, Vol. 31, pp. 1039–1041; also *The Electrical World,* Vol. 56, Nov. 3, 1910, pp. 1085–1088.

secondary winding being connected in series with an adjustable portion of the resistance AB, so that the vector sum of the resistance drop in AB between M_1 and K_1, and the mutual reactance drop between M_2 and K_2, shall be equal to the planevector $p.d.$ to be measured, between leads P_1P_2, as determined by silence in the telephone.

The construction of a resistance-mutual-inductance potentiometer, on the Larsen principle, was taken up in 1916, in the electrical-engineering research laboratories of the Massachusetts Institute of Technology, by Mr. Alfred E. Hanson, in his thesis

FIG. 1.

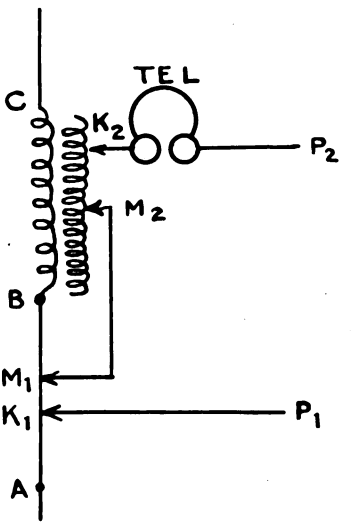

Connections of Larsen potentiometer.

work towards a master's degree. In connection with this thesis,[5] the new type of potentiometer here described was designed.

New Instrument.—The electrical connections of the new instrument are indicated in Fig. 2, and are in all essentials the same as in Fig. 1. The resistance OA contains 50 ohms, in short coils, of *Ia-Ia* wire, wound both anti-inductively and anti-condensively, and also a short length of slide wire of 0.5 ohm. The mutual inductance coil has two equal copper windings, each having 8.8 ohms resistance at 20° C., and 3.9 millihenrys self-inductance.

[5] "The Design and Construction of an Alternating-Current Potentiometer," by Alfred E. Hanson, September, 1916; a Thesis towards the degree of M.S. in Electrical Engineering at the Mass. Inst. of Technology.

The mutual inductance between the two windings is approximately 3.85 millihenrys. The *p.d.* to be measured is connected to the terminals *pp'*. A vibration galvanometer *V.G.* serves as the balance indicator.

FIG. 2.

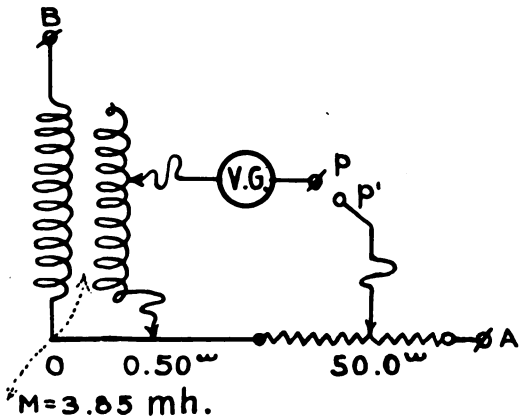

Diagram of connections in new potentiometer.

Fig. 3 shows the general appearance of the Hanson form of potentiometer. The dial switches *A* and *B* control the resistance taps; while the slider *C*, moving over the resistance wire, serves for a fine adjustment of resistance. The dial switches *E*, *F*, and *G*, control secondary taps in the mutual inductor, *E* being for 200 turns per step, *F* 20 turns per step, and *G* 2 turns per step. A fraction of one turn may be added, by turning the handle *f*, as will be described later.

The interior of the mutual inductance box is shown in Fig. 4. The winding is toroidal in form, comprising 41 wooden sectors of suitable taper, as shown in Fig. 5b. The dimensions of one sector appear in Fig. 5a.

Each sector is first wound with a primary winding of 50 turns of No. 21 B. and S. gage double silk-covered copper wire (bare diam. 0.72 mm.) in 2 layers of 25 turns each. Over this primary winding is laid one layer of varnished cambric insulation. Over this insulation is a secondary winding, also 50 turns of the same size wire, in 2 layers of 25 turns each. In some of the bobbins, taps have to be brought out from the secondary winding. The mean diameter of the toroid is 36.8 cm. When all the sectors are assembled, and connected in series, the winding forms a

FIG. 3.

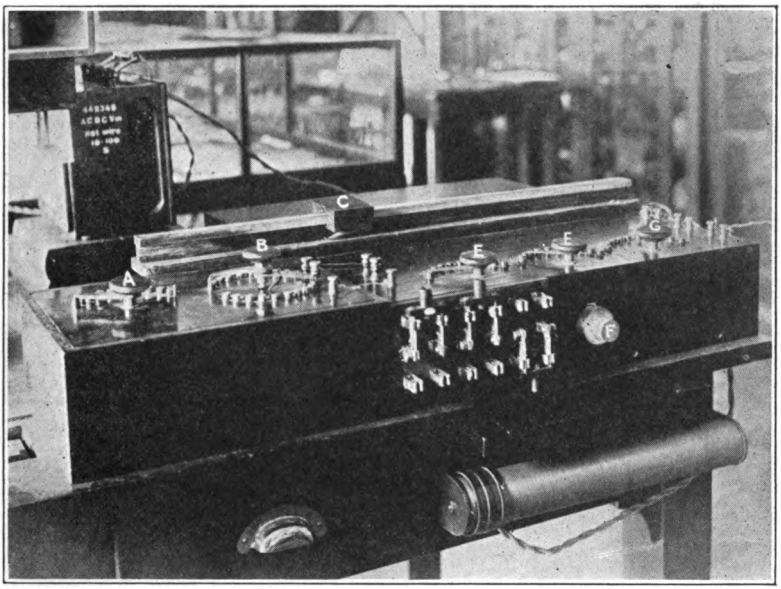

General view of potentiometer.

FIG. 4.

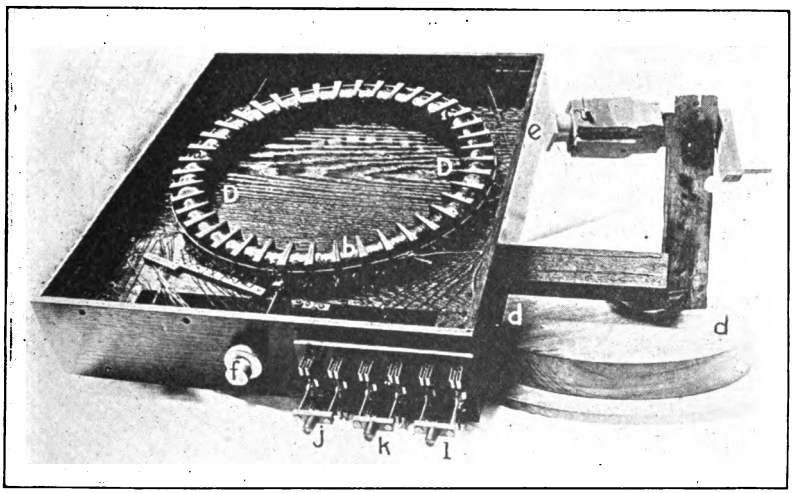

Interior of mutual inductor.

FIG. 5a.

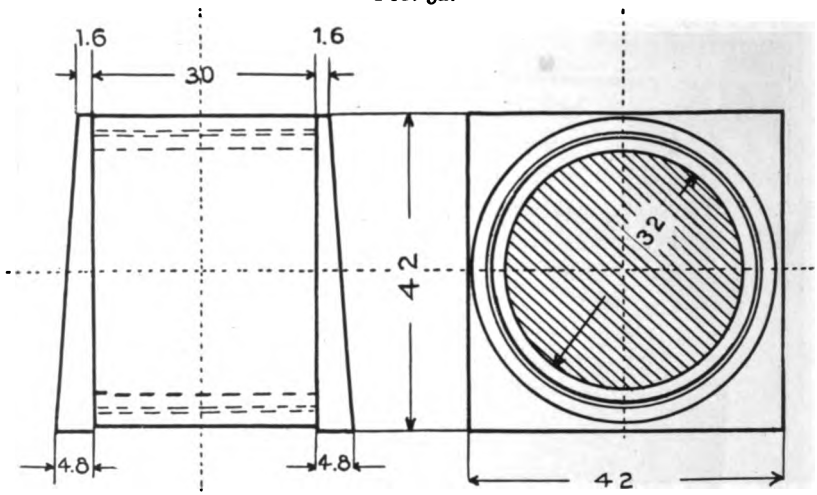

Details of one sector of the mutual inductor. Dimensions in millimeters.

FIG. 5b.

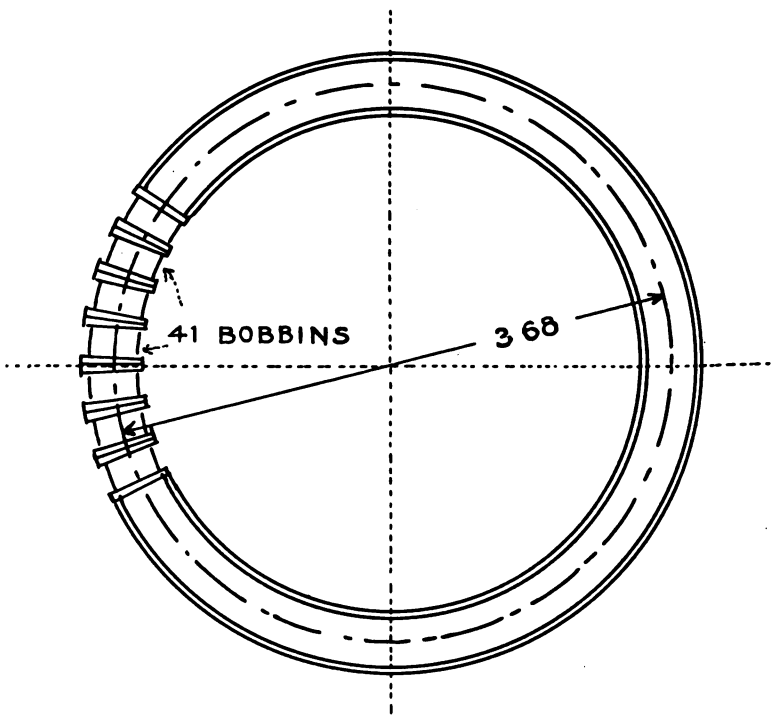

Plan diagram of toroidal mutual inductor. Dimensions in millimeters.

closed circular solenoid with wooden core, devoid of screws or other metallic attachments. A wooden disk *dd*, Fig. 4, serves to support all the individual sectors in their proper places, when glued in position at *DD*. The advantages of the toroidal form of winding are, first, that the external magnetic field is then negligibly small, so that the primary current produces no appreciable stray field in the neighborhood of the apparatus; and second, that with accurate mechanical construction, the mutual inductance between the primary winding and the secondary coils should be proportional to their number of turns. One of the individual wooden

FIG. 6.

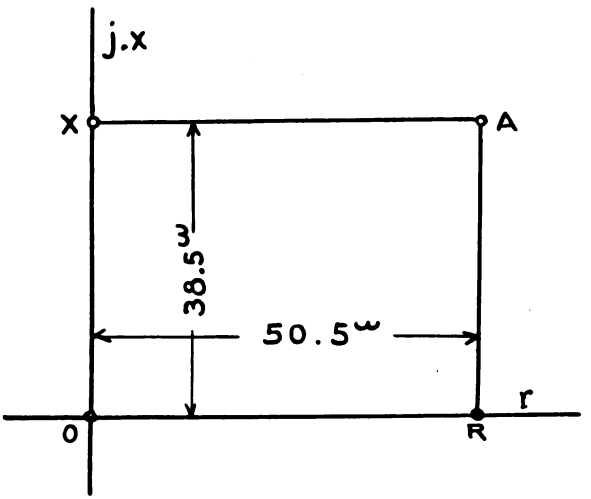

Range of impedance covered by the potentiometer, at $\omega = 10{,}000$ radians per second.

sectors is shown at *e*, held in a winding clamp. The handle *f* connects mechanically, by a spindle, with a single turn of secondary winding, situated in a hollow space at the centre of the core, between two adjacent coil sectors. The range of rotation of *f*, between the limits of $-90°$ and $+90°$, or half a turn, provides the same total change of mutual inductance as one step in the lowest dial.

Rectangular Range of Instrument.—Fig. 6 is a rectangular-coördinate diagram, indicating the range in impedance available with the apparatus for potentiometer measurement. The resistance $OR = 50.5$ ohms, and at $\omega = 10{,}000$ radians per second ($f = 1591$ ∽), $j M\omega = j\ 38.5$ ohms. At any other frequency, the value of the mutual reactance will be varied proportionately.

Any impedance at $\omega = 10{,}000$, within the area *ORAX* on the diagram, can be covered by the simple series connection of resistance and secondary winding shown in Fig. 2.

Fig. 7 is a similar rectangular coördinate diagram, indicating the range in planevector voltage available with the apparatus for potentiometer measurement. If the *r.m.s.* current I_P supplied to the instrument, is 0.1 ampère, or 100 milliampères, taken at standard phase, and also at the frequency of reference ($\omega = 10{,}000$), the voltage that can be covered in the first quadrant is

FIG. 7.

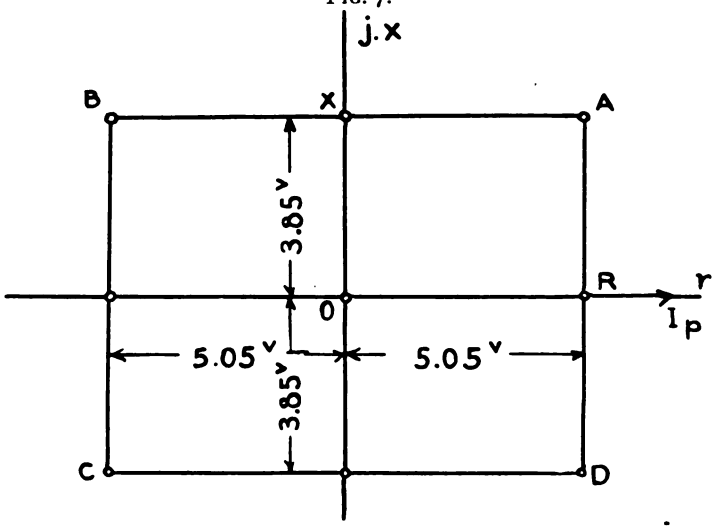

Rectangular range of planevector voltage covered at $\omega = 10{,}000$ and $I_P = 0.1$ ampère.

comprised within the rectangle *ORAX*, and so the maximum *p.d.* within reach of the potentiometer is $5.05 + j\ 3.85$ volts. At any other current strength, the voltage developed in the apparatus will be varied proportionately. Any voltage within the field *ABCD*, Fig. 7, can similarly be covered at $\omega = 10{,}000$, and $I_P = 0.1$ ampère, by suitably reversing either the R or jX components, or both. These reversals are easily made, by means of switches j and k, Fig. 4.

Electrical Connections.—The full connections of the instrument are indicated in Fig. 8. The coil C is the secondary winding of an oscillator of adjustable frequency, which supplies testing current to the apparatus. The resistance R' and the condenser C' are used to adjust the potentiometer current in size and in slope.

The switch j serves to reverse both R and jX. The switch k reverses jX separately. B is a compensating rheostat, so arranged as to keep the total resistance in the circuit constant, while changing the resistance between the tapping points. The unknown *p.d.* is connected to the terminals pp'. The vibration galvanometer, by means of which a balance is secured between the adjusted and unknown vector *p.d.s,* is indicated at *V.G.*

Method of Measurement.—The vibration galvanometer is at first heavily shunted, and is tuned to maximum response for the impressed frequency. The correct quadrant to employ is first found by using switches j and k. Successive adjustments are then made in R and jX, until the vibration galvanometer deflection is a

FIG. 8.

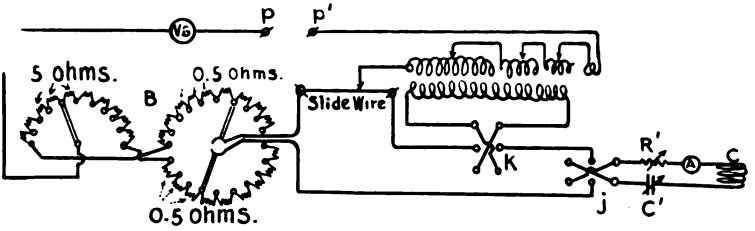

Detailed connections of the potentiometer.

minimum. The galvanometer shunt is now reduced, and the adjustments of R and jX repeated, until a sufficiently satisfactory zero balance has been obtained on the galvanometer.

Absolute and Relative Measurements of P.D.—Two general methods are available for use with potentiometers such as the one here described; namely,

(1) The method of absolute potential differences, secured by passing a measured constant current through the potentiometer, which current is taken as of standard phase.

(2) The method of relative potential differences, secured by passing a constant, but unmeasured current, through the potentiometer, whose readings are then uncalibrated, but which become capable of calibration, by being compared with the reading across a certain impedance which is maintained as a standard of reference.

The first method has the advantage that it enables the potenti-

ometer readings to be stated directly in rectangular-coördinate volts. It has, however, the disadvantage of requiring the measurement of the potentiometer current to an even greater degree of precision than that aimed at in the potentiometer work.

In most laboratory measurements of alternating *p.d.*, relative

FIG. 9.

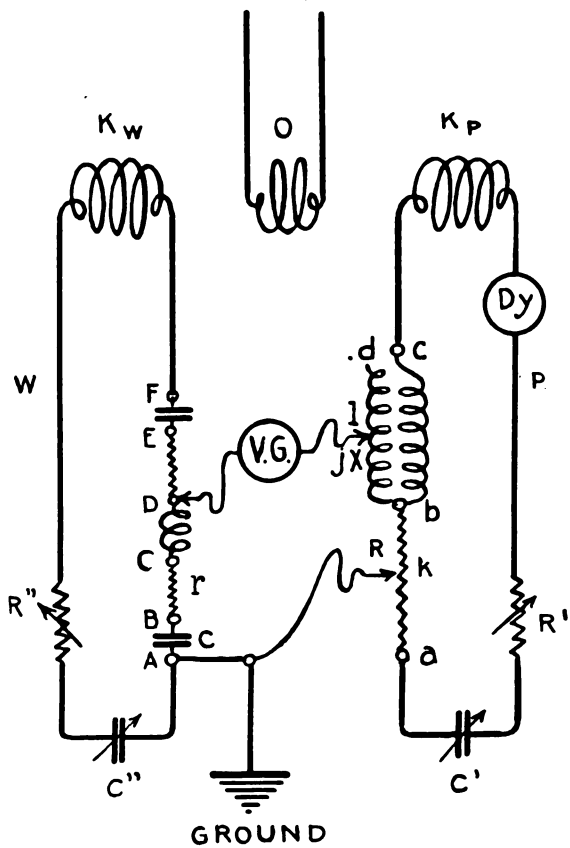

Simplified diagram of connections, showing the rectangular potentiometer *P* arranged for exploration of the potential distribution over the working circuit *W*.

values only are required, and thus it is the ratio of two measured voltages which is of immediate importance. Such ratios can be determined by the relative method, without the necessity of measuring the potentiometer current. The absolute method has, however, to be resorted to, when, as in iron-cored instruments carrying alternating currents, the impedance is a function of the

current strength, and therefore departs from Ohm's law. In all measurements of *p.d.* in circuits which obey Ohm's law, the second or relative method is to be preferred. Both methods of using the new instrument have been tried.[6] In the absolute method, the potentiometer current was measured by a differential dynamometer.[7] This plan was found to work well, although a considerable amount of care was required for the measurement of the potentiometer current. In the progress of the experimental work, however, the relative method was found to be increasingly advantageous.

The essential connections of the second or relative method are presented in Fig. 9. The oscillator coil or source of alternating *emf.* is marked *O*. This coil is inductively connected with each of two circuits; namely (1) the potentiometer circuit *P*, and (2) the tested or working circuit *W*. The *P* circuit contains the tuning condenser *C'*, and the adjustable resistor *R'*, as well as the potentiometer *abc*. The *W* circuit may contain any set of apparatus in which potential differences are to be measured. As shown in the figure, the *p.d.* at the terminals *AD* is being led to the potentiometer through the tuned vibration galvanometer *VG*. In the second or relative method of testing, the drop of potential between terminals *B* and *C* on resistance *r* may be used as the standard *p.d.* Then if the device to be tested in the working circuit is the condenser *c*, the terminals *AB* can be connected immediately afterwards to the potentiometer. As will be shown later, it is important to maintain a ground connection at the point *A*. Consequently, the drop across any single element, such as *BC*, is obtainable as a vector difference between that across *AC* and that across *AB*.

Let r be the standard impedance of known slope (which in the case of a strictly non-inductive resistance would be zero) (ohms $\angle$)

Z be the unknown impedance of the condenser c to be measured (ohms $\angle$)

I_P be the *r.m.s.* current in the potentiometer circuit (ampères $\angle$)

I_W be the *r.m.s.* current in the working circuit (ampères $\angle$)

$R_1 + jX_1$ the reading of the potentiometer across terminals AC.

$R_2 + jX_2$ the reading of the potentiometer across terminals AB.

[6] "Alternating-Current Potentiometry at Telephonic Frequencies," by Edy Velander; a thesis towards the A.M. degree at Harvard University, June, 1918.

[7] "Precise Measurements of Alternating Currents," by C. O. Gibbon, *Electrical World*, May 11, 1918, pp. 979–981.

Then the drop across the standard resistance r will be

$$I_P(R_1 + jX_1) - I_P(R_2 + jX_2) = I_P(R_0 + jX_0) = I_W r \text{ ..volts} \angle \quad (1)$$

In the AB connection, we have

$$I_P(R_2 + jX_2) = I_W Z \text{.....volts} \angle \quad (2)$$

Dividing (2) by (1)

$$\frac{Z}{r} = \frac{R_2 + jX_2}{R_0 + jX_0} \text{.....numeric} \angle \quad (3)$$

This procedure assumes that I_P remains the same in both tests, and also I_W. When, however, a high degree of accuracy is required, this assumption cannot be made. Suppose that in the first test I'_P is the vector potentiometer current, and I'_W the vector working current. Next suppose that when the second measurement is made, both the sizes and the slopes of these currents may have slightly changed, so that I''_P is the new potentiometer current, and I''_W the new working current. Then rewriting (1) and (2) accordingly, we have

$$\frac{Z+r}{r} \cdot \frac{I'_W}{I''_W} = \frac{R_1+jX_1}{R_2+jX_2} \cdot \frac{I'_P}{I''_P} \text{.....numeric} \angle \quad (4)$$

If, however, the potentiometer current and the working current vary together, so that the vector ratios remain equal:

$$\frac{I'_W}{I''_W} = \frac{I'_P}{I''_P} \text{.....numeric} \angle \quad (5)$$

Then equation (3) will still hold. If, then, the mutual inductances between the primary coil, and each of the two secondary coils K_P and K_W remain constant, also the mutual inductance between K_P and K_W; likewise the impedance in each of these circuits; then any variation of current in the primary coil, due to unsteadiness in the oscillator, will not affect the vector ratios of equation (5), and will therefore not affect formula (3). If, however, the frequency impressed by the oscillator varies, then the above reasoning will not hold, and the method will be vitiated. It is therefore necessary that the frequency should be maintained constant within satisfactorily close limits. It should be noted that during *a-c* potentiometer tests, no appreciable change should

be made in the load upon the oscillator; because any change in this load produces some corresponding change in the oscillator frequency.

Frequency Measurements.—It will be evident from the foregoing, that careful measurements of the impressed frequency are necessary in the use of the *a-c* potentiometer.

Probably the simplest device for the measurement of the impressed frequency is the Campbell condenser and mutual inductance branch circuit [8] of Fig. 10. Here a condenser of C farads is shunted by the secondary coil of a mutual inductance of M henrys and a vibration galvanometer VG. One or both of these

FIG. 10.

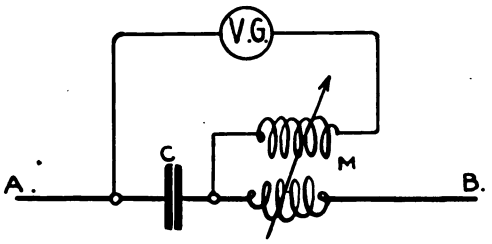

Campbell frequency-measuring arrangement.

elements is varied, until the galvanometer shows no current. We then have, if I is the vector current in the circuit (ampères $\angle$)

$$jM\omega I + I\frac{1}{j\omega C} = 0 \quad \text{volts}\angle \quad (6)$$

whence

$$\omega = \frac{1}{\sqrt{MC}} \quad \text{radians / sec.} \quad (7)$$

Strictly speaking, this zero current in the vibration galvanometer can only be secured if (1) there is no effective resistance in the condenser, and (2) no effective capacitance in the secondary coil. Owing to the great difficulty of securing these conditions, to the necessary degree of precision, a sharp zero balance is hard to obtain. The modification of connections shown in Fig. 11 enables this difficulty to be overcome. A large resistance R, of say 2000 ohms, is connected through an adjustable small inductance l, as a shunt to both the condenser and mutual-inductance primary. The secondary is led through the vibration

[8] A. Campbell. *Phil. Mag.*, May, 1908, Vol. 15, p. 166.

galvanometer to an adjustable tap on the resistance. If the condenser current is represented by I_c *r.m.s.* ampères $\angle$, and the current in the resistance by I_R *r.m.s.* ampères $\angle$, then with V_{AB} *r.m.s.* volts $\angle$ as the *p.d.* between A and B, at balance,

$$I_c = \frac{V_{AB}}{r+j\left(L\omega - \frac{1}{C\omega}\right)} \quad \text{ampères } \angle \quad (8)$$

and

$$I_R = \frac{V_{AB}}{R+jl\omega} \quad \text{ampères } \angle \quad (9)$$

r being the effective resistance of the secondary winding in ohms. The *p.d.* in the galvanometer circuit will be

$$jM\omega I_c + kRI_R = 0 \quad \text{volts } \angle \quad (10)$$

where kR is the resistance included between B and the tapping point. After this zero balance has been obtained, first by assigning k and C, with a final adjustment in M and l, we have

$$\omega = \frac{1}{\sqrt{C\left(L+\frac{M}{k}\right)}} \quad \text{radians / sec.} \quad (11)$$

with the further condition that l has had to be adjusted to

$$l = CRr\left(1+\frac{kL}{M}\right) \quad \text{henrys} \quad (12)$$

This method enables a sharp balance to be obtained at the expense of the additional adjustments. Moreover, since $1/k$ may conveniently be made a large number, C and M can both be kept reasonably small, even at low frequencies.

The same connections are presented in Fig. 12, under the form of a generalized Heaviside bridge. Formulas (8) to (12) apply equally well to this case.

In both Figs. 11 and 12, a ground connection is indicated in the frequency measuring set, at the point B. As will be mentioned in connection with sources of error in the use of the potentiometer, the selection of a proper ground point is vital to the accuracy of the measurements. At frequencies higher than, say, 100 cycles per second, parasitic alternating currents, due to distributed capacitance in the apparatus, play an increasingly prominent part. At very high frequencies, such parasitic currents may even swamp the working current. Either the point A, or the point B may be grounded in Figs. 11 and 12; but prefer-

FIG. 11.

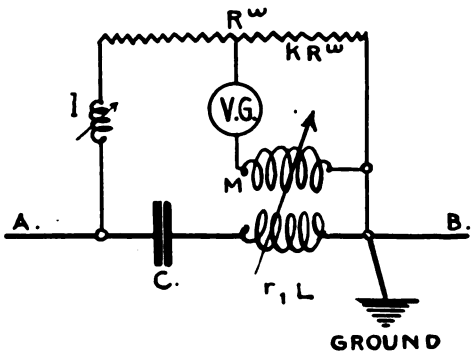

Preferred modification of frequency measurer.

FIG. 12.

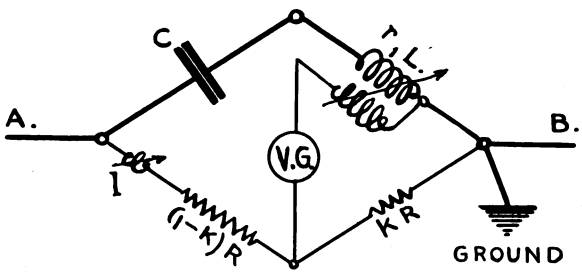

Bridge arrangement of connections in Fig. 11.

FIG. 13.

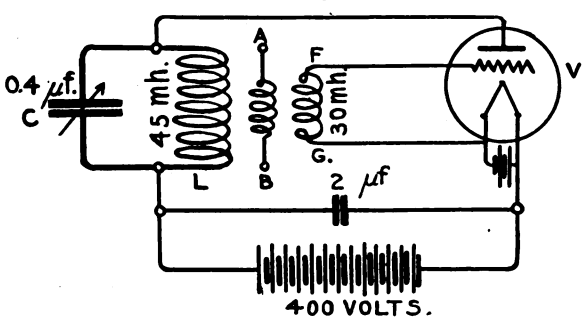

Pliotron connections; skeleton plan of connections.

ably *B*, owing to the preponderating distributed capacitance of the mutual inductor.

Oscillator.—A convenient set of vacuum-tube generator connections appears in Fig. 13. *V* is a 3-electrode vacuum-tube of a pliotron oscillator or similar type, with its plate, grid and filament. The main oscillation circuit consists of the adjustable condenser *C* and inductance *L*. The grid-coil secondary winding *FG* supplies the oscillating excitation to the grid. The secondary

FIG. 14.

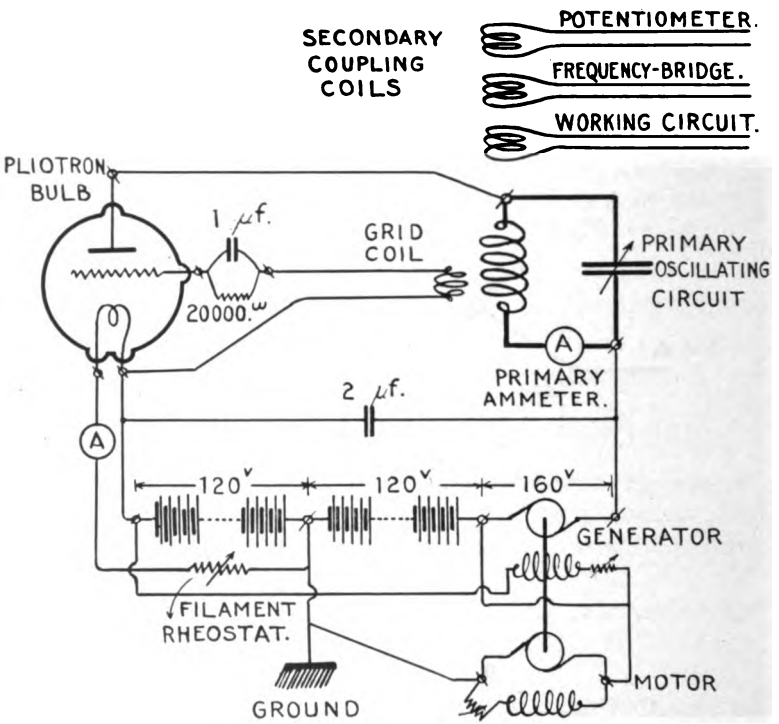

Arrangement of the pliotron as a generator.

winding *AB* may be connected to the potentiometer circuit. Several such secondary coils may be used. The continuous *emf.* may be supplied by a small dynamo generator. If possible, this generator should be driven by a motor actuated by storage battery for steadiness of action. An auxiliary condenser of $2\mu f$ serves as a high-frequency bridge across the inductance of the generator.

A more detailed set of connections, showing an actual arrange-

ment employed, appears in Fig. 14. In this case, 240 volts of continuous plate *emf.* was derived from a storage battery, and 160 volts from a generator which was storage-battery-motor driven.

A Vreeland oscillator was also used in the earlier measurements. This apparatus is too well known to need special description. With the Vreeland oscillator employed, the available range of frequency, without external auxiliary apparatus, was from 400 ∽ to 2500 ∽. With the pliotron oscillator, the available range of frequency was limited only by the capacitances and inductances employed in the oscillation circuit.

Vibration Galvanometer.—In nearly all of the measurements made with the apparatus, a Duddell bifilar vibration galvanometer, adapted for use up to a frequency of 2000 ∽, was employed as the balance detector. This served the purpose satisfactorily when properly tuned to the impressed frequency. When *p.d.* measurements are made upon apparatus of high internal impedance, a detector of greater sensitivity and corresponding impedance would be preferable. A pair of head telephones of suitable impedance were found to work well in such cases. A crystal detector with *d-c.* galvanometer was also used successfully.

Example of the Use of the Instrument in a Simple A-C. Circuit.—As an example of the measurements that may be made with the instrument, we may consider the simple series circuit *ABCDEF* in Fig. 15, consisting of a fixed mica condenser *AB* of 1.0 microfarad, in series with an anti-inductive metallic resistance *BC* of 200 ohms, followed by a non-ferric inductance *CD* of 100 millihenrys and 22.2 ohms, followed again by an anti-inductive resistance *DE* of 200 ohms similar to *BC*, and finally by a second mica condenser *EF* of 1.0 microfarad.

The electrical connections for exploring the potentials along the work series *AF*, Fig. 15, are indicated in Fig. 9. When using the absolute method, the differential dynamometer, *Dy*, measures the *r.m.s.* alternating current strength supplied in the potentiometer circuit, and thus furnishes the voltage scale $E = IR + jIX$, obtained for any reading of R and jX. Fig. 16 shows the results actually obtained in this way, at an impressed frequency of 500 ∽, with a current of 0.020 ampère in the potentiometer circuit. The grounded point *A* was kept fixed, and measurements were made by shifting the lead of the tuned vibration galvanometer along the points *B*. *C*. *D*, *E* and *F* in succession. These vector *p.d.s* are indicated in Fig. 16 by the vectors *AB*, *AC* . . .

AF, respectively. The straight lines connecting the adjoining pairs of points *BC*, *CD*, *DE* and *EF* on the diagram, then become the inferred vector potential drops in the successive elements of the circuit, all presented to the particu'ar phase of the potentiometer current as standard.

It will be observed that the lines *BC* and *DE* are parallel. The direction of these lines shows the phase of the current in the working circuit, assuming that the anti-inductive resistances *BC* and *DE* may be regarded as pure resistances, at the test frequency

FIG. 15.

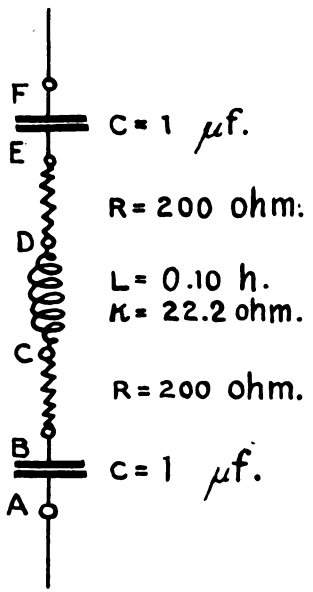

Simple series circuit explored.

of 500∽. The lines *AB* and *EF* on the diagram are also parallel to each other, and are perpendicular to the lines *BC* and *DE*. This shows that the voltages at the terminals of the condensers lag substantially 90° behind the current in the working circuit, according to the regular theory. The line *CD* is the drop in the inductance coil, and may be analyzed into two mutually perpendicular components; namely, *D'D* in phase with the current, due to the presence of resistance, and *CD'* in leading quadrature with the current, due to the inductive reactance of the coil.

If we replot the diagram to working-current standard phase,

as in Fig. 17, we rectify the diagram by a virtual rotation of approximately 65° in the clockwise direction. The various voltage drops are then read off, to rectangular coördinates, in the customary manner.

The diagram of Fig. 17 gives a correct presentation of the voltage drops in each or any series combination of the elements in the working circuit, provided that the potentiometer current I_P has been measured. In order to evaluate the impedance of the

FIG. 16.

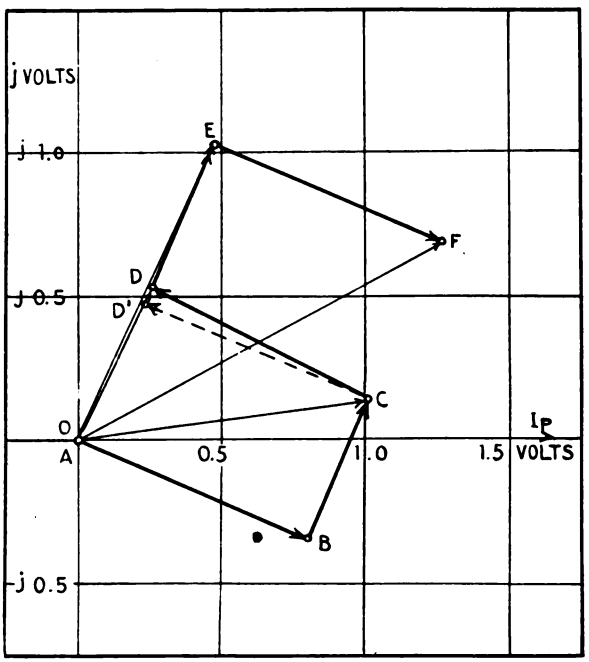

Distribution of planevector voltage along series AF, Fig. 15, at 500 ∽, to potentiometer current standard phase.

corresponding elements, it becomes also necessary to know either the magnitude of I_W, the working current; or, the vector impedance of one of the elements. Thus, if the resistance BC is a standard resistance of 200 ohms, the scale of the entire diagram can be interpreted in ohms. It should be observed that the measurement of I_P, the potentiometer current, with R and jX, is insufficient to determine the impedances of the elements in the working circuit, and that while it would be possible to measure both I_W and I_P, this double operation becomes burdensome and

unnecessary, so that the use of the instrument naturally leads to the relative method of measurement, in which no current strength has to be determined, but a standard impedance—preferably a standard pure resistance—is included in the working circuit. Measured potential drops on unknown impedances are then referred to the measured drop on this standard, as a working unit.

FIG. 17.

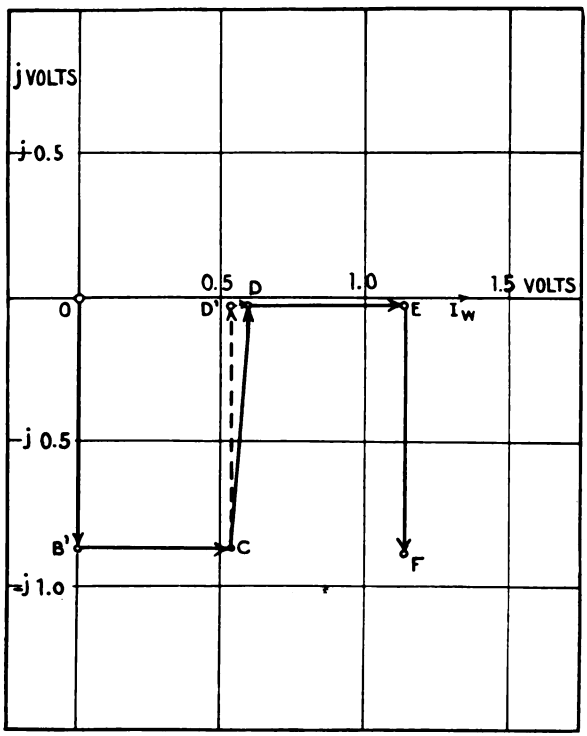

Distribution of planevector voltage in Fig. 16, referred to working current standard phase.

Sources of Error and Their Elimination.—It is impossible to work for any length of time with any *a-c.* potentiometer at a telephonic frequency, without encountering discrepancies in the measurements, which are attributable to the well-known disturbance from parasitic currents in the distributed capacitance of the tested apparatus. The first step in the elimination of these superposed parasitic currents is to ground a suitable point in the working circuit, so as to bring that point to zero potential, and prevent the distributed capacitance in the immediate neigh-

borhood of that point from producing a parasitic condenser current. In general, the ground should be established at one end of the range of the elements in the working circuit to be measured. As an example, Fig. 9 shows a ground established at the point A.

Suppose that the ground is established at the junction B of two impedances AB and BC to be compared, such as Z_1 and Z_2 in Fig. 18, and that I_W is the working current in the absence of distributed capacitance, and therefore equal in the two impe-

FIG. 18.

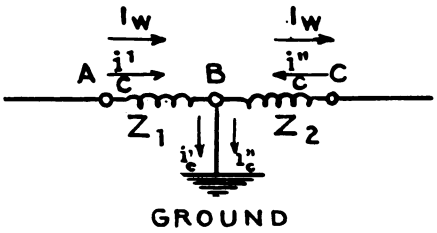

Diagram illustrating the effect of improper grounding.

dances. The current i'_c in Z_1 represents a small parasitic current of a certain magnitude and phase escaping to ground at B, while the current i''_c in Z_2 is a similar small parasitic current which, in general, will have a different magnitude and phase, also escaping to ground at B. The resultant working currents in the two impedances will then be the vector sums $(I_W + i'_c)$ and $(I_W - i''_c)$ ampères, respectively. The ratio of the potential drops in the two impedances will then be

$$\frac{(I_W + i'_c)Z_1}{(I_W - i''_c)Z_2}$$

which, in general, will differ from the required ratio, $\frac{Z_1}{Z_2}$ by an unknown amount.

In cases where the quantity to be determined is a potential difference distribution, rather than an impedance comparison, the importance of a proper grounding point in the working circuit is equally great. It is evident that, as a general rule, during a set of *p.d.* measurements on the same working circuit, the grounded point should not be shifted. This is for the reason that when the ground connection is shifted, the potential of all points along the circuit with respect to the ground is varied, thereby changing the entire distribution of parasitic currents.

An experimental example of the effect of shifting the ground connection in a working circuit appears in Fig. 19. Here a standard resistance box of 100,000 ohms, in 10 series coils of 10,000 ohms each, was inserted in the working circuit, as shown in Figs. 20a and 20b. In Fig. 20b, the vibration galvanometer connection to the potentiometer is carried permanently to the end *B* of the resistance box. Since it is manifestly inadmissible to establish a ground connection on this lead, as it would bring parasitic current directly through the galvanometer, the ground has to be established at *t*, the travelling lead to the potentiometer.

FIG. 19.

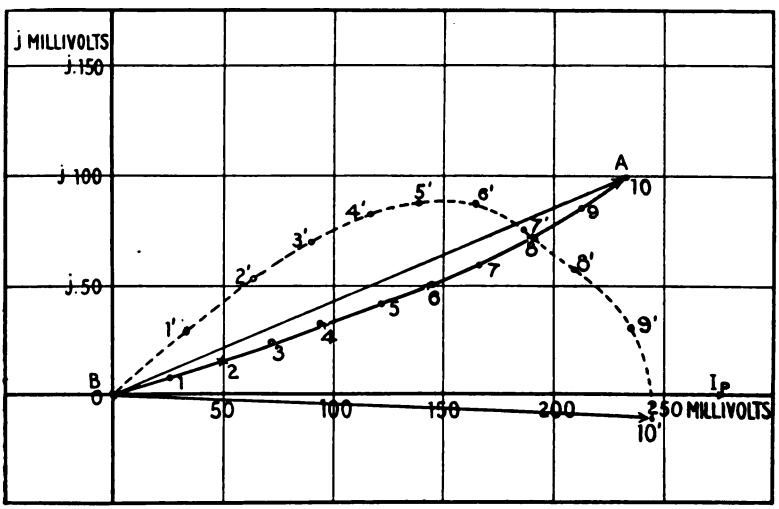

Distribution of planevector voltage along 100,000-ohm resistance box. Small circles indicate observed values, crosses indicate computed values, assuming that each section of the box subtends a hyperbolic angle of 0.08 $\angle 45°$ hyp. radian.

This involves, however, a change in the distribution of potential and capacitance current at each change in the position of *T*. The result is shown in the broken curve 1′, 2′, 3′ of Fig. 19. The curve of *p.d.* between *A* and *B*, Fig. 20, should evidently be a uniform straight line *O*10′ in Fig. 19. The presence of the changing parasitic current distribution appears to have been responsible for the erratic curve shown. Assuming that the *p.d.* across the entire resistance box is correctly represented by the vector *O*10′, Fig. 19, then all of the intermediate *p.d.s* should be

situated along this straight line; whereas the actually measured *p.d.s* from *O* to the successive points 1, 2, 3, etc., Fig. 20b, follow the bending line 1′, 2′, 3′ . . ., etc.

The connections were then changed to those of Fig. 20a, in which the ground connection is kept fixed at *B*, and the travelling

FIG. 20a.

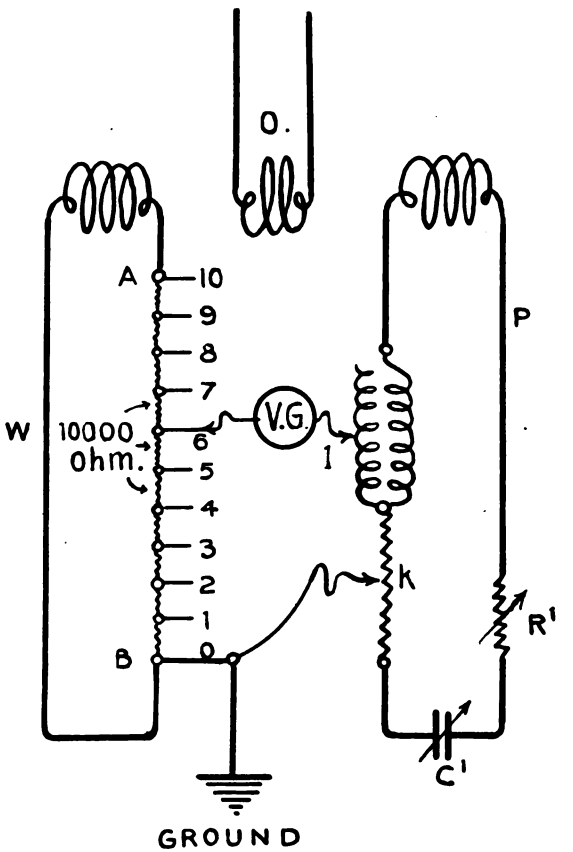

Exploration by means of the potentiometer *P*, of the voltage drop along a high-resistance box *A B*, of 100,000 ohms. Note correct position of ground-connection at *B*.

lead contains the vibration galvanometer. The corresponding vector curve of *p.ds* is shown at 1, 2, 3, 4, Fig. 19, and is a much closer approximation to a straight-line vector *OA*, representing the *p.d.* over the entire resistance. This curve resembles in form that presented by an artificial cable when an alternating *emf.*,

such as *OA* Fig. 19, is impressed on the sending end, while the distant end is grounded. The curve indicates that each section of the box subtends a small hyperbolic angle.

Applications of the New Form of A-C. Potentiometer.—A large field of experimental investigation in the laboratory lies

FIG. 20b.

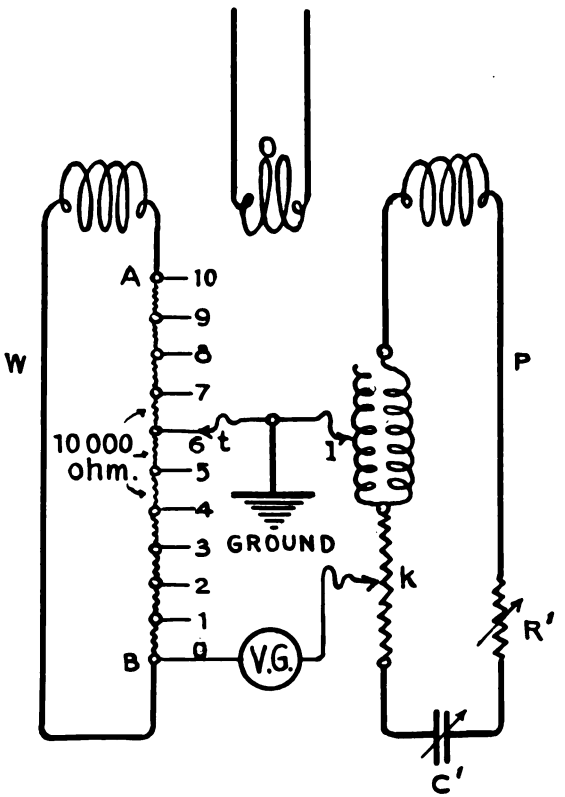

Incorrect arrangement of ground-connection giving rise to the erroneous results 1', 2', 3' . . . . . in Fig. 19.

open to the *a-c.* rectangular potentiometer. The power it consumes is a fraction of 1 watt, while its range of voltage is extensive. It enables the vector *p.d.* on different parts of an alternating-current instrument, or on different sections of an alternating-current line, to be measured conveniently. The results are also of considerable educational value to the student. It is pro-

posed to communicate in another paper a number of the results obtained experimentally at various telephonic frequencies.[9]

It should be pointed out that the degree of precision obtainable with the instrument, although very satisfactory from an alternating-current standpoint, is not to be compared with that readily obtainable from the *d-c.* potentiometer. This relatively low precision is attributable to parasitic currents from distributed capacitance, and also to stray alternating magnetic fields. If these two sources of error could be eliminated, the precision of the instrument might be of the same order as that of the *d-c.* potentiometer.

Suggestions for Improvements in Construction.—A weak point in the design of the new instrument is the relatively high internal capacitance between the primary and secondary windings of the mutual inductor, which, at high frequencies, tends to produce impurity in the vector mutual reactance jX. This defect could be reduced by increasing the insulating spacing between the concentric primary and secondary windings on the toroid. At 2000∿, the discrepancy due to this mutual capacitance appears by measurement, in this instrument, to be $(0.25 + j1.2)$ per cent. in voltage, but rapidly diminishes as the frequency is reduced. There is also a weak point in the toroidal form of mutual inductor, that although there is negligibly small stray alternating field produced in the apparatus by an exciting primary current, yet the secondary winding is not exempt from the influence of stray magnetic fields from external sources at testing frequency. Precautions should therefore be taken to remove the apparatus from the vicinity of alternating magnetic fields.

SUMMARY.

(1) The principle of the *a-c.* rectangular potentiometer here described is not new, but the form of the instrument appears to be new.

(2) By the use of this instrument, alternating *p.d.s* can be measured, to rectangular coördinates, up to at least 2000∿, with only a small expenditure of power.

(3) The use of the instrument shows the marked influence of distributed capacitance in *a-c.* apparatus, and the importance of reducing this disturbing effect when measurements are made.

[9] *Proc. American Philosophical Society*, 1919.

(4) The importance of a proper ground connection in the working circuit is emphasized.

(5) The *a-c.* rectangular potentiometer escapes the necessity of measuring the strength of alternating current in either the potentiometer circuit, or the working circuit, provided that the relative method is used, and that the impressed frequency is maintained constant.

(6) Owing to the effects of distributed capacitance, the voltage distribution in a simple series resistance box, carrying alternating currents, fails to follow a vector straight-line law. The deviation tends to increase with the impressed frequency.

(7) The importance of reducing the mutual capacitance between the concentric primary and secondary windings of the toroidal induction coil, at high frequencies, is emphasized as the result of experimental tests.

LIST OF RESEARCH BULLETINS

Bulletin Number

*1. The Economical Transportation of Merchandise in Metropolitan Districts. H. Pender and H. F. Thomson; March, 1912.

2. Notes on the Cost of Motor Trucking. H. Pender and H. F. Thomson; October, 1912.

*3. Observations on Horse and Motor Trucking. H. Pender and H. F. Thomson; March, 1913.

4. Relative Fields of Horse, Electric and Gasoline Trucks. H. F. Thomson; August, 1914.

*5. The Delivery and Handling of Miscellaneous Freight at the Boston Freight Terminals. H. Pender, H. F. Thomson, and C. P. Eldred; February, 1914.

6. The Delivery System of R. H. Macy & Co. of New York. H. F. Thomson, H. L. Manley, and A. L. Pashek; September, 1914.

7. Explorations over the Vibrating Surfaces of Telephonic Diaphragms under Simple Impressed Tones. A. E. Kennelly and H. O. Taylor; April, 1915.

8. The Mechanics of Telephone-Receiver Diaphragms as Derived from their Motional-Impedance Circles. A. E. Kennelly and H. A. Affel; November, 1915.

9. Experimental Researches on Skin Effect in Conductors. A. E. Kennelly, F. A. Laws, and P. H. Pierce; September, 1915.

10. Tractive Resistances to a Motor Delivery Wagon on Different Roads and at Different Speeds. A. E. Kennelly and O. R. Schurig; June, 1916.

11. Some Properties of Vibrating Telephone Diaphragms. A. E. Kennelly and H. O. Taylor; April, 1916.

12. Experimental Researches on the Skin Effect in Steel Rails. A. E. Kennelly, F. H. Achard, and A. S. Dana; August, 1916.

13. Skin-Effect Resistance Measurements of Conductors at Radio-Frequencies up to 100,000 Cycles per Second. A. E. Kennelly and H. A. Affel; December, 1916.

*Out of print.

LIST OF RESEARCH BULLETINS—Continued

Bulletin Number

14. Street Railway Fares; their relation to length of haul and cost of service. D. C. Jackson and D. J. McGrath; August, 1917.

15. Apparent Dielectric Strength of Varnished Cambric. A. E. Kennelly and R. J. Wiseman; January, 1918.

16. Magnetic Flux Distribution in Annular Steel Laminæ. A. E. Kennelly and P. L. Alger; March, 1918.

17. Electromagnetic Theory of the Telephone Receiver, with Special Reference to Motional Impedance. A. E. Kennelly and H. Nukiyama; March, 1919.

18. A Rectangular-Component Two-Dimensional Alternating-Current Potentiometer. A. E. Kennelly and Edy Velander; July, 1919.

Current Distribution in Armature Conductors

WALDO V. LYON

Research Division
Electrical Engineering Department
Massachusetts Institute of Technology
Bulletin No. 19 July, 1919

Current Distribution in Armature Conductors

By
WALDO V. LYON
Assistant Professor of Electrical Engineering, Massachusetts Institute of Technology

Reprinted from
ELECTRICAL WORLD
July 12, 1919

Current Distribution in Armature Conductors

Equations Are Derived Showing How Alternating—Current Resistance Depends Upon Depth of Slot—Calculations of Deep-Slot Induction Motors with High Torque May Thus Be Investigated—Condensed Formulas Proposed by Dr. Kennelly

BY WALDO V. LYON
Assistant Professor of Electrical Engineering, Massachusetts Institute of Technology

A MATHEMATICAL investigation of current distribution in armature conductors in open slots reveals the fact that, beyond a certain depth, the alternating-current resistance varies directly as the slot depth. The relations thus derived have an important application in the design calculations of high-torque induction motors such as those used for the propulsion of the new battleships of the United States Navy. It is also shown that the assumption of uniform current distribution, in the calculation of leakage reactance, leads to serious errors, especially in the case of deep slots. In order to reduce the problem of alternating-current distribution in armature conductors to its simplest and most workable form, it is assumed that the conductors are of rectangular cross-section and are embedded in slots which have parallel sides and are not wholly closed. Fig. 2 is a cross-section showing a typical arrangement of this sort. When this conductor carries current, there is established about it a magnetic field as indicated by the flux lines *a*, *b* and *c*. Elements of the conductor near the bottom link more flux than those near the top and will therefore have a greater inductance. The true resistance of all elements is of course the same. Since the voltage drop through a given length of each element is the same, it follows that the current density will be least at the

bottom and greatest at the top of the conductor when the current is an alternating one. This phenomenon is very frequently described as "skin effect." In calculating the distribution of current it will be assumed, as is usually done, that the reluctance of the iron portion of the magnetic circuit is negligible compared with the reluctance of the space within the slot. This is, of course, equivalent to neglecting the eddy currents and hysteresis due to this so-called leakage flux, although they often account for an important loss in the machine.

The flux is assumed to cross the slot in parallel lines. Whenever this assumption is permissible, the current densities in elements cut by the same flux line are equal, no matter what the shape of the cross-section of the conductor may be. Furthermore, the relative current densities at points within the conductor below any flux line are not affected by flux that may exist above this line. That is to say, the conductor may be divided longitudinally by a surface in which the flux density is constant and the upper portion of the conductor removed without affecting the relative current densities in the lower portion of the conductor. For example, referring to Fig. 2, the current densities at the points u, y and z on the flux line b are equal. Also the portion of the conductor above this flux line may be removed without changing the relative current densities at any points in the lower or cross-hatched section of the conductor. The only flux that modifies the current within a given cross-section of a conductor is that within the cross-section. If there are two conductors in a slot, one above the other, the upper conductor has no appreciable effect in modifying the distribution of current within the lower conductor, although the current in the lower conductor influences the current distribution in the upper one. These statements are true no matter what the shape of the cross-section may be. They depend only upon the assumption that the flux lines through the conductor are parallel, as they are nearly, if the slot is not wholly closed.

The fundamental equation used in determining the current density is

$$e = \rho c + d\phi/dt + d\Phi/dt \text{ c.g.s. electromagnetic units} \quad (1)$$

e is the voltage between cross-sections of the conductor 1 cm. apart; c is the current density at any point in

the conductor; ρ is the resistivity of the conductor; ϕ is flux within the conductor linking the element of current considered; Φ is flux outside the conductor. The flux within the conductor linking a given element of current is equal to

$$\phi = \int_x^d \frac{4\pi}{s} i_x dx \qquad c.\ g.\ s.\ lines$$

in which i_x is the current in the conductor below the element considered, and s is the width of the slot. If this value for ϕ is substituted in equation (1) and the equation is differentiated twice with respect to x, it becomes

$$0 = \rho \frac{\delta^2 c}{\delta x^2} - \frac{4\pi w}{s} \frac{\delta c}{\delta t} \qquad c.\ g.\ s. \qquad (2)$$

Differential equations of this same form are used in solving other important physical problems; for example, the flow of heat, the distribution of magnetic flux in laminations,[1] and the distribution of electric current in very wide conductors of rectangular cross-section[2].

If the current varies sinusoidally with the time, the general solution for the current density is

$$\begin{aligned} c = {} & K_1 \varepsilon^{mx} (\cos mx \sin (\omega t + \alpha) \\ & + \sin mx \cos (\omega t + \alpha)) \\ & + K_2 \varepsilon^{-mx} (\cos mx \sin (\omega t + \alpha_2) \\ & - \sin mx \cos (\omega t + \alpha_2)) \end{aligned} \qquad (3)$$

The constants of integration are K_1, K_2, α_1 and α_2. $m = 2\pi \sqrt{\frac{fw}{s\rho}}$. In this particular case the solution can be written in a much simpler form, since $K_1 = K_2$ and $\alpha_1 = \alpha_2$ so that the equation becomes, expressed in practical units;

$$\begin{aligned} c = {} & K (\cosh mx \cos mx \sin \omega t \\ & + \sinh mx \sin mx \cos \omega t) \text{ amp./cm.} \end{aligned} \qquad (4)$$

Since $i = \int^d wc dx$, the constant of integration is

$$K = \frac{2\sqrt{2}\, I}{w \sqrt{\cosh 2md - \cos 2md}} \text{ amp/cm}^2$$

I is the current in amperes in the entire conductor, and w is the width of the conductor. The instantaneous

[1] See Alexander Russell, "Alternating Currents," Vol. 1, page 353.
[2] See A. E. Kennelly and H. A. Affel, "Skin-Effect Resistance Measurement of Conductors," *Proceedings Institute of Radio Engineers*, May, 1916; Appendix III.

value of the current in the conductor is found by integrating the current density from zero to d. When written in complex notation it is

$$\dot{I} = \frac{w K}{2 m}\left[\begin{matrix}(\cosh mx \sin mx + \sinh mx \cos mx) \\ +j\,(\cosh mx \sin mx - \sinh mx \cos mx)\end{matrix}\right] \text{amp.} \quad (5)$$

The instantaneous voltage drop per centimeter in the

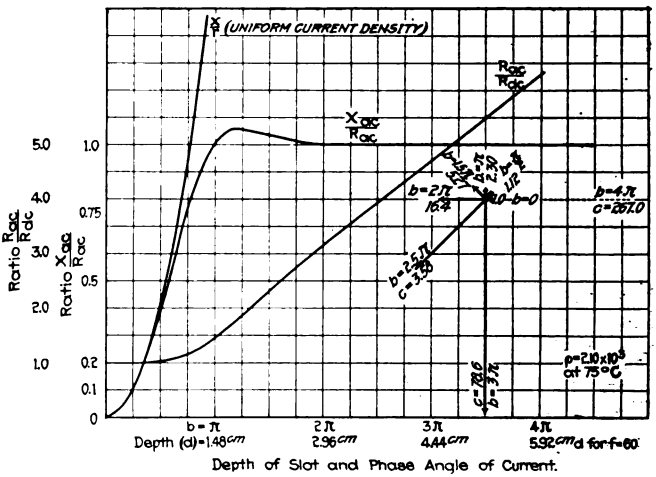

FIG. 1—VARIATION OF ALTERNATING-CURRENT RESISTANCE WITH SLOT DEPTH AND EFFECT OF ASSUMPTION THAT CURRENT DENSITY IS UNIFORM

conductor due to its resistance and to the flux within the conductor, equals the product of the specific resistance and the current density in the uppermost layer. This voltage, when written in complex notation, is

$$\dot{V} = \rho K\,[\cosh md \cos md + j \sinh md \sin md] \text{ volts} \quad (6)$$

The leakage impedance in complex form is

$$\dot{Z} = \frac{b\,\rho}{2a}\left[\frac{\sinh b + \sin b}{\cosh b - \cos b} + j\,\frac{\sinh b - \sin b}{\cosh b - \cos b}\right] \text{ohms} \quad (7)$$

$$b = 4\,\pi\,d\sqrt{\frac{f\,w}{s\,\rho}} \text{ radians,}$$

in which b is the phase angle of the current and $a = wd$ = cross-section area, sq.cm.

The resistance of such a conductor to alternating current is thus

$$R_{ac} = \frac{b\,\rho}{2a}\,\frac{\sinh b + \sin b}{\cosh b - \cos b} \text{ ohms.}$$

The resistance to direct current is $R_{dc} = \frac{\rho}{a}$ ohms

The ratio of alternating to direct current resistance is therefore

$$\frac{R_{ac}}{R_{dc}} = \frac{b}{2} \frac{\sinh b + \sin b}{\cosh b - \cos b} \tag{8}$$

The ratio of leakage reactance due to flux within the conductor to the alternating resistance is

$$\frac{X}{R_{ac}} = \frac{\sinh b - \sin b}{\sinh b + \sin b} \tag{9}$$

Ordinarily the reactance of such a conductor is calculated on the assumption that the current density is uniform. In this case the ratio of reactance to resistance is $\frac{x}{r} = \frac{b^2}{6}$.

Fig. 1 shows the manner in which the current density and the resistance and reactance vary in such a conductor. These curves are plotted for the case in which the conductor completely fills the slot. w is then equal to s, and the angle b which appears in the various formulas equals 4π times the depth of the conductor in centimeters times the square root of the frequency in cycles per second divided by the specific resistance in c.g.s. units; *i.e.*, the specific resistance in ohms per centimeter cube multiplied by 10^9. As shown by the scales of abscissas, the angle b equals π when the depth of the conductor is 1.48 centimeters for a frequency of 60 cycles and a specific resistance of 2.10 microhms per centimeter cube. This angle b determines the manner in which the current density, the ratio of alternating current to direct current resistance and the ratio of reactance to resistance vary. If, for example, the current density at the bottom of such a conductor is taken as unity, at a point above this corresponding to an angle of π the current density will be 2.3 times as great and will lead by an angle of 90 deg. At double this distance from the bottom the current density is 16.4 times as great and is in exact opposition. That is to say, the current will be flowing in opposite directions in the conductor at the same moment at these two points.

If the conductor is of a depth corresponding to an angle $b = 4\pi$, the current density in the upper layer will be 267 times as great as the current density in

the bottom layer and will be in time phase with it. This fact, that the current may be flowing in opposite directions at different points in a conductor at the same time, has long been known. It is interesting to note that the locus of the vector representing the current density is practically a logarithmic spiral for angles, b, greater than 3π.

Dependence of Alternating-Current Resistance on Slot Depth

The ratio of alternating to direct resistance is practically unity for conductors less than 0.75 cm. deep at a frequency of 60 cycles. For conductors deeper than about 1.5 cm. the ratio of alternating to direct resistance

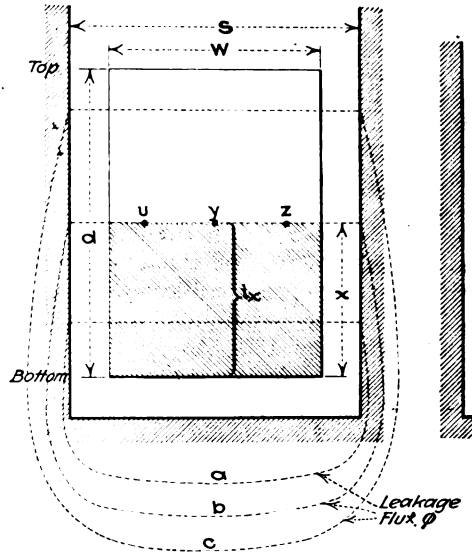

Fig. 2

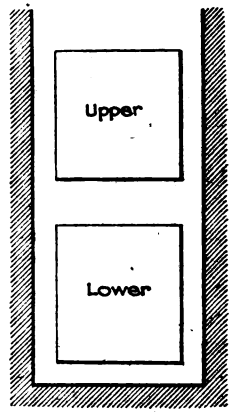

Fig. 3

FIG. 2—FLUX IS ASSUMED TO CROSS SLOT IN PARALLEL LINES
FIG. 3—COMMON ARRANGEMENT OF CONDUCTORS IN A SLOT

is practically proportional to the depth of the conductor. The ratio of reactance to resistance is interesting. It reaches a maximum value of about 106 per cent for a conductor of 1.70 cm. deep at a frequency of 60 cycles and a resistivity of 2.1 microhms per centimeter cube, but if the conductor is more than 3 cm. deep under these conditions the reactance and resistance are equal. The ratio of reactance to resistance on the assumption of

uniform current density is correct only for very shallow conductors. If the depth of the conductor is such that the angle b is not more than $\pi/2$, the current is practically uniformly distributed over the cross-section of the conductor, the alternating and direct current resistances are equal, and the reactance may be calculated in the usual way. b varies directly with the depth of the conductor, directly as the square root of the frequency, and inversely as the square root of the resistivity. Thus at 25 cycles rather than at 60 the conductor would need to be 55 per cent deeper in order that the skin effect should be the same. A conductor of high resistance material would likewise need to be much deeper in order that the skin effect should be the same. Thus one which had a resistivity sixteen times that of copper would need to be four times as deep to have the same skin effect.

The fact that the skin effect varies in the manner shown with the depth of the conductor and the frequency is quite important in the design of squirrel-cage induction motors and the damper windings of synchronous machines. With an induction machine a high efficiency necessitates a low rotor resistance, whereas if the starting torque is to be large, the rotor resistance must be high. Since under running conditions the frequency of the rotor currents is very low, the skin effect is negligible, while at starting, when the rotor current is of the rated frequency, the skin effect may be quite considerable, especially if the rotor conductors are deep. If, for example, rotor conductors 2 cm. by 2 cm. in cross-section are replaced by others that are 1 cm. by 4 cm; the starting torque is more than twice as great for the same current, although the efficiency is not changed. The deeper conductors, however, would probably require a rotor of larger diameter in order that the rotor core may have the proper cross-section back of the teeth. In order that a damper winding may be efficient in limiting hunting in a synchronous machine, its resistance must be low. The frequency of the current set up in the damper due to hunting, however, is so small that the skin effect is negligible. If the damper is used to increase the starting torque, it is more effective if its conductors are as deep as practicable. Again in the latter case, the field poles would need to be some-

what longer in order to accommodate the same field winding back of the damper.

Another problem, although one much more difficult to solve, is the case of two rectangular conductors, one above the other in the same slot, as shown in Fig. 3. The distribution of current in the lower conductor is independent of the current in the upper one, but the equation for the current density in the upper conductor must now be written in its general form (see equation 3). The introduction of four constants of integration makes the computations much more difficult—so much more so, in fact, that they will not be attempted here.

[Dr. A. E. Kennelly, who has done much to develop the application of hyperbolic functions of complex angles to the solution of such problems, adds the following discussion.—EDITOR.]

APPLICATION OF HYPERBOLIC FUNCTIONS OF COMPLEX ANGLES

In the foregoing discussion the author made use of complex numbers, but has not used complex angles. If one avails himself of complex angles the formulas can be shortened and condensed as follows:

Starting with the differential equation (2), its solution may be written in the form

$$\frac{c_x}{c_d} = \frac{\cosh \alpha x}{\cosh \alpha d} \qquad \text{numeric } \angle$$

where $\alpha = \sqrt{j\, 4\pi \left(y \frac{w}{s}\right) \mu\omega} = \sqrt{j\, 2\, m^2} = m + j\, m =$

$m\ \sqrt{2}\ \angle\ 45°$, y being the actual conductivity of the copper and $(w/s)y$ the effective conductivity in view of the insulating wall between the copper and the magnetic polar surfaces of the slot. The angular velocity $\omega = 2\pi f$ radians per second. The hyperbolic angles αx and αd are both semi-imaginary.

The average current density over the whole cross section of the bar is

$$c_q = \frac{I}{wd} = \frac{1}{d}\int_o^d c_x\, dx = \frac{1}{d}\frac{c_d}{\cosh \alpha d}\int_o^d \cosh \alpha x\, dx =$$

$$\frac{1}{\alpha d}\frac{c_d}{\cosh \alpha d}\sinh \alpha d = c_d \frac{\tanh \alpha d}{\alpha d}, \text{ amp. per sq. cm.}$$

The skin effect impedance ratio Z/R_{dc} is:

$$\frac{Z}{R_{dc}} = \frac{c_d}{c_q} = \frac{\alpha d}{\tanh \alpha d} = \frac{dm\sqrt{2}\angle 45°}{\tanh (dm\sqrt{2}\angle 45°)} \quad \text{numeric } \angle$$

The real part of this ratio is R_{ac}/R_{dc}, the skin effect resistance ratio.

For any given value of $dm\sqrt{2}$, tanh $(dm\sqrt{2}\angle 45°)$ can be found from published charts and tables. When dm exceeds 4, tanh $(dm\sqrt{2}\angle 45°)$ is practically unity, so that then

$$Z/R_{dc} = dm\sqrt{2}\angle 45° = \alpha d \quad \text{numeric } \angle$$
$$\text{and } R_{ac}/R_{dc} = dm \quad \text{numeric } \angle$$

The equivalent skin depth of alternating-current penetration is then also 1/m *cm*.

From the standpoint of skin-effect theory the case considered in this article of a rectangular copper bar mounted at the base of a rectangular slot in laminated steel is of particular interest, because it presents a case of a copper strip devoid of edge effect and subject only to skin effect on one face. Rayleigh[3] first published in 1886, the formula for the skin effect in an indefinitely wide conductive strip, and therefore for a strip of copper devoid of edge effect because the magnetic flux paths are all parallel to the strip surfaces. It has only been found possible to realize such a condition by placing two such similar strips *A* and *B* parallel, *A* say immediately over *B*, the two being separated by a thin uniform layer of insulator, and making *A* the going and *B* the returning conductor; so that the flux in the insulating layer between them will be sensibly parallel to the strip surfaces except near the edges. Such pairs of strips have been tested and found to have very small edge effect.[4] A single flat strip has been found, however, to have a greatly increased effective resistance, owing to edge effect, since the magnetic flux intersects the strip at all parts except at the center of its width.[5]

In the dynamo armature bar conductor here considered, however, neglecting magnetic lag and losses in the iron, the bar is subject to the pure skin effect of an infinitely wide strip even in very narrow specimens, owing to the parallelism of the flux to the bar's surface.

---

[3]Rayleigh, *Phil. Mag.*, 1886; *Scientific Papers*, Vol. 2, pp. 486-495.

[4]Kennelly, Laws and Pierce, "Experimental Researches on Skin Effect in Conductors," *Proceedings A. I. E. E.*, September, 1915.

Current in Armature Conductors

IN the design of large induction motors it is desirable to secure a relatively large secondary resistance during the operation of starting, because the magnitude of the starting torque depends directly upon this resistance. External starting resistances are commonly resorted to for the purpose of increasing the secondary circuit resistances by auxiliary means. On the other hand, it is also desirable that the secondary resistances should be relatively low during full-speed operation, because the speed regulation and the efficiency are thus improved. If an induction motor is operated from 60-cycle mains, the frequency of the currents in the secondary windings will be 60 cycles per second at standstill but will diminish to mere slip frequency at full speed. This condition is utilized in some designs by employing secondary conductors in which considerable extra resistance from skin effect will be set up at starting frequencies, but this extra resistance will practically all disappear at running frequencies. Consequently, it becomes important to study the phenomena of skin effect in large copper conductors, in order the more effectively to utilize this principle in the design of induction motors.

The article by Prof. Waldo V. Lyon in our last issue bears strongly on the principles of skin effect in rectangular copper conductors embedded in the open slots of laminated-steel armature bodies. In such cases the magnetic flux may be regarded, at least to a first approximation, as passing straight across from one wall of the slot to the other, through the substance of the copper bar. The density of this flux, due to alternating currents in the bar, naturally attains a maximum at the outer surface of the bar, and reaches zero at the bottom of the bar, in the lowest parts of the slot. The return flux is supposed to be all carried by the walls of the slot, with inappreciable leakage and also relatively small hysteretic lag or loss. Under these conditions, the formulas controlling skin-effect extra resistance, at any given frequency, become relatively easily managed. They are developed in the article. If, however, the same bar is surrounded by air or other non-magnetic material, the flux paths through the copper deviate considerably from straight

lines, and edge effect presents itself, with greatly increased mathematical difficulties.

In the case considered the conductor, if sufficiently massive, virtually behaves as though its depth were reduced from the actual dimension to a certain equivalent skin depth, which varies inversely as the square root of the frequency of the currents carried, so that the virtual depth of the conductor at 60 cycles is only half of that at 15 cycles.

Although the extra resistance of skin effect is much easier to compute when edge effect is absent, yet the presence of edge effect adds considerably to the extra resistance. For that reason a strip or strap of copper supported in air on insulators is apt to develop a very appreciable extra resistance from edge effect when in large sizes, even at frequencies as low as 25 cycles per second.

LIST OF RESEARCH BULLETINS

Bulletin Number

*1. The Economical Transportation of Merchandise in Metropolitan Districts. H. Pender and H. F. Thomson; March, 1912.

2. Notes on the Cost of Motor Trucking. H. Pender and H. F. Thomson; October, 1912.

*3. Observations on Horse and Motor Trucking. H. Pender and H. F. Thomson; March, 1913.

4. Relative Fields of Horse, Electric and Gasoline Trucks. H. F. Thomson; August, 1914.

*5. The Delivery and Handling of Miscellaneous Freight at the Boston Freight Terminals. H. Pender, H. F. Thomson, and C. P. Eldred; February, 1914.

6. The Delivery System of R. H. Macy & Co. of New York. H. F. Thomson, H. L. Manley, and A. L. Pashek; September, 1914.

7. Explorations over the Vibrating Surfaces of Telephonic Diaphragms under Simple Impressed Tones. A. E. Kennelly and H. O. Taylor; April, 1915.

8. The Mechanics of Telephone-Receiver Diaphragms as Derived from their Motional-Impedance Circles. A. E. Kennelly and H. A. Affel; November, 1915.

9. Experimental Researches on Skin Effect in Conductors. A. E. Kennelly, F. A. Laws, and P. H. Pierce; September, 1915.

10. Tractive Resistances to a Motor Delivery Wagon on Different Roads and at Different Speeds. A. E. Kennelly and O. R. Schurig; June, 1916.

11. Some Properties of Vibrating Telephone Diaphragms. A. E. Kennelly and H. O. Taylor; April, 1916.

12. Experimental Researches on the Skin Effect in Steel Rails. A. E. Kennelly, F. H. Achard, and A. S. Dana; August, 1916.

13. Skin-Effect Resistance Measurements of Conductors at Radio-Frequencies up to 100,000 Cycles per Second. A. E. Kennelly and H. A. Affel; December, 1916.

*Out of print.

LIS

Bulletin Number

14. Stre
c
A

15. App
K

16. Mag
A

17. Elec
Sp
ne

18. A F
Cu
Ve

19. Curr
Ly

ed

aul and
cGrath;

8-21-77

9-5-77

. A. E.

aminæ.

r, with
. Ken-

nating-
Edy

ldo V.